SECURITY CLASSIFICATION OF THIS PAGE

UMENTATION PAGE

Form Approved
OMB No. 0704-0188

AD-A213 644

1b. RESTRICTIVE MARKINGS
NONE

3. DISTRIBUTION/AVAILABILITY OF REPORT
APPROVED FOR PUBLIC RELEASE;
DISTRIBUTION UNLIMITED.

2b. DECLASSIFICATION/DOWNGRADING SCHEDULE

4. PERFORMING ORGANIZATION REPORT NUMBER(S)

5. MONITORING ORGANIZATION REPORT NUMBER(S)
AFIT/CI/CIA- 88-229

6a. NAME OF PERFORMING ORGANIZATION
AFIT STUDENT AT
NORTH CAROLINA STATE UNIVERSITY

6b. OFFICE SYMBOL (If applicable)

7a. NAME OF MONITORING ORGANIZATION
AFIT/CIA

6c. ADDRESS (City, State, and ZIP Code)

7b. ADDRESS (City, State, and ZIP Code)
Wright-Patterson AFB OH 45433-6583

8a. NAME OF FUNDING/SPONSORING ORGANIZATION

8b. OFFICE SYMBOL (If applicable)

9. PROCUREMENT INSTRUMENT IDENTIFICATION NUMBER

8c. ADDRESS (City, State, and ZIP Code)

10. SOURCE OF FUNDING NUMBERS

PROGRAM ELEMENT NO.	PROJECT NO.	TASK NO	WORK UNIT ACCESSION NO

11. TITLE (Include Security Classification) (UNCLASSIFIED)
PRECIPITATION DISTRIBUTIONS ASSOCIATED WITH CYCLONES ORIGINATING OVER THE GULF OF MEXICO AND SURROUNDING COASTAL REGIONS

12. PERSONAL AUTHOR(S)
DAVID I KNAPP

13a. TYPE OF REPORT	13b. TIME COVERED	14. DATE OF REPORT (Year, Month, Day)	15. PAGE COUNT
THESIS/~~DISSERTATION~~	FROM _____ TO _____	1988	107

16. SUPPLEMENTARY NOTATION
APPROVED FOR PUBLIC RELEASE IAW AFR 190-1
ERNEST A. HAYGOOD, 1st Lt, USAF
Executive Officer, Civilian Institution Programs

17. COSATI CODES		
FIELD	GROUP	SUB-GROUP

18. SUBJECT TERMS (Continue on reverse if necessary and identify by block number)

19. ABSTRACT (Continue on reverse if necessary and identify by block number)

DTIC
ELECTE
OCT 25 1989
S B D

89 10 24 157

20. DISTRIBUTION/AVAILABILITY OF ABSTRACT
☒ UNCLASSIFIED/UNLIMITED ☐ SAME AS RPT. ☐ DTIC USERS

21. ABSTRACT SECURITY CLASSIFICATION
UNCLASSIFIED

22a. NAME OF RESPONSIBLE INDIVIDUAL	22b. TELEPHONE (Include Area Code)	22c. OFFICE SYMBOL
ERNEST A. HAYGOOD, 1st Lt, USAF	(513) 255-2259	AFIT/CI

DD Form 1473, JUN 86

Precipitation Distributions Associated with Cyclones Originating Over the Gulf of Mexico and Surrounding Coastal Regions

by

David I Knapp

A thesis submitted to the Graduate Faculty of
North Carolina State University
in partial fulfillment of the
requirements for the Degree of
Master of Science

Department of Marine, Earth, and Atmospheric Sciences

Raleigh
1988

Approved By:

_____

_____ _____

Co-Chairman of Advisory Committee Co-Chairman of Advisory Committee

Abstract

KNAPP, DAVID I. Precipitation Distributions Associated with Cyclones Originating Over the Gulf of Mexico and Surrounding Coastal Regions. (Under the direction of Steven Businger and Gerald Watson.)

An investigation of the evolution of precipitation patterns associated with intensity and movement of winter surface lows across the southeast United States was undertaken. A 24-year climatology (1960-1983) of the 66 storms producing wide areas of precipitation totals in excess of 25 mm revealed three dominant storm tracks. Six-hour totals of hourly precipitation data were objectively analyzed and contoured. Grid point values were extracted from the contour charts and compiled for all storms plotted along each track. Mean precipitation distribution charts and frequency of occurrence charts (for specified amounts) revealed the evolving precipitation fields surrounding storms in each track.

Precipitation maxima for storms tracking from the Gulf of Mexico to the Ohio Valley were found to extend across the Appalachians to the Atlantic coast, best explained by Miller's (1946) Type B cyclones and found to have occurred in 5 of the 12 cyclones following this inland track. Precipitation patterns for storms tracking along the Gulf coast across the Florida panhandle to the Atlantic coast suggest that the Atlantic Ocean joins the Gulf of Mexico as a second moisture source. The central Gulf coast area tended to receive the brunt of the precipitation from these lows.

Multiple linear regression equations revealed the importance of storm longitude, surface geostrophic relative vorticity, and surface central pressure for forecasting various precipitation parameters.

A case study focused on a cyclone event during the GALE field project (10-11 February 1986) when a surface low developed over the Gulf coastal states and traveled rapidly east-northeastward into North Carolina. Conveyor belt theory was applied to this case and shown to explain the advection of moisture into this system. Heavy precipitation totals remained well south of the storm center throughout its duration. Analysis of the 300°K isentropic surface revealed the existence of a low-level jet or warm conveyor belt in excess of $35 ms^{-1}$ originating at 900-mb over the Gulf of Mexico and rising to 750-mb along the North Carolina coast. This Gulf Conveyor Belt (GCB) forced relatively higher mixing ratios into the Carolinas along its axis. Vertical cross-sections revealed the presence of a potentially unstable layer within the GCB, however, a significantly drier layer needed to enhance convection (Marks and Austin, 1979, and Bosart, 1973) was not evident.

Acknowledgements

The author expresses sincere appreciation to Dr. Steven Businger, Dr. Gerald Watson, and Dr. Sastry Pantula for their assistance and patience during the preparation of this thesis. Thanks also to Mary McVicker for her steady drafting hand responsible for most of the figures in this thesis, Jeff Medlin for his number-crunching enthusiasm in calculating surface vorticity values for the climatology, Dr. Alan McNab for his input as precipitation data were compiled, Mr. Kermit Keeter for his opinions and expertise from the forecaster's perspective, and to the United States Air Force for the opportunity to pursue this advanced degree.

Particular appreciation must be expressed to fellow Air Force Captains Steve Seabaugh and Ken Carey for their constant tutoring and encouragement. Also, their ability to make the author laugh when it seemed hard to do so made the worst of times go by much faster.

Finally, the author wishes to express his most heartfelt appreciation to his wife, Libby, and son, Peter, for their constant prayers, support, encouragement, and patience. Thanks also to my parents who have always provided encouragement to keep going forward throughout my life.

Table of Contents

1. INTRODUCTION

A particular challenge to local weather forecasters are accurate 24-hour precipitation forecasts. For the general public, most disruptive and dangerous weather events are commonly associated with heavy showers, thunderstorms, and hurricanes occurring during the spring, summer, and fall seasons. However, winter precipitation, especially that produced from surface cyclones traveling across the southeast United States, usually contributes more to the total annual precipitation than the precipitation recorded during each of the three warmer seasons. Examples from four cities display this tendency (Table 1).

TABLE 1

Selected Precipitation Totals By Quarter.

	% of Annual Precipitation				
City	Jan-Mar	Apr-Jun	Jul-Sep	Oct-Dec	Totals (mm)
Atlanta, GA	30	25	24	21	1228
Jackson, MS	30	25	22	23	1249
Montgomery, AL	29	24	26	21	1266
Nashville, TN	31	25	22	22	1168

(Data taken from Local Climatological Data; Annual Summaries. 1981. NOAA, Environmental Data and Information Service.)

In the past, case studies have categorized precipitation according to intensity and location with respect to frontal features surrounding surface low pressure systems. There are also several climatologies of cyclone evolution. However, few climatological studies have attempted to relate precipitation patterns to the movement of low pressure centers. From the few that have been published (Tasaka, 1980 and Jorgensen, 1967 are examples), typical relationships between the storm system and its precipitation distribution become evident.

Surface cyclone types, frequencies, and tracks over North America have been summarized to explain general tendencies of formation, demise, and movement. Miller

(1946) classified cyclones originating in the Atlantic coastal region into two categories for 208 cases (October - April) over a period of ten years. The Type A cyclone is common along the Atlantic coast when cold outbreaks occur. These cyclones originate near or over the ocean and move in a northeasterly direction. Type B cyclones originate near the Atlantic coast line to the southeast of an older cyclone. The older cyclone is usually found in the vicinity of the Great Lakes when Type B cyclogenesis occurs along a warm front extending eastward from the older storm. Miller concludes that it is sometimes possible to anticipate the type of cyclogenesis two or three days in advance on the basis of characteristic synoptic features. Type B cyclones occur more frequently from December to April than do Type A cyclones.

Winter cyclones over the eastern United States tend to avoid the Appalachian mountains as evidenced by a distinct frequency minimum shown, for example, by Colucci (1976). This author further found that there is a concentration of winter storms in a band from Cape Hatteras to New England over the northern edge of the Gulf Stream. Deepening is favored over the southern Appalachians, the North and South Carolina coasts, and along the northern edge of the Gulf Stream. The northeastern Gulf of Mexico is a poor region for cyclone deepening.

Zishka and Smith (1980) found the same minimum of winter cyclones over the Appalachians as Colucci. Their study of January and July surface cyclones from 1950 to 1977 also concluded that storms are more numerous, more intense, and displaced farther south in January than in July. Cyclogenesis occurs most often along the east coast of the United States and in the lee of the Rocky Mountains. Minimum surface pressure at the cyclone center was used as an indicator of intensity to show trends in storm strength with respect to time. From 1950 to 1977, while the number of January cyclones is shown to decrease, however, their average intensity increased. Whittaker and Horn (1981) and Reitan (1979) also noted this same statistically significant decline in the frequency of North American cyclogenesis in recent years.

Cyclone activity studies confirm Colucci's findings. Langs (1986) used sea-level geostrophic relative vorticity calculated at NMC grid points to define surface cyclones over a ten year period from 1973 to 1982. Major cyclone activity was found to occur in the lee of the Rockies and along the east coast of North America in all seasons. These regions are most prominent in winter and migrate eastward and northward in summer. Martin (1986) similarly used the same vorticity calculations to conclude that the preferred region of cyclone activity over North America is from the Rocky Mountains to the Mid-Atlantic Ocean.

Detailed research studies on precipitation distribution and rates surrounding surface lows have addressed the responsible physical processes on a wide range of scales from synoptic to mesoscale to convective scale (wavelengths from 2000 to 20 km). Miller (1955) concludes that the horizontal transport of potentially colder air over warmer and more moist air (or any vertical variation of the horizontal transport of heat and humidity which decreases vertical stability of an air column) results in intensification of precipitation. This vertical instability from differential advection can cause precipitation rates to vary markedly from time to time and place to place on the synoptic scale.

Eddy fluxes of latent and sensible heat, radiative heat fluxes, and dissipation of kinetic energy are the key ingredients for cyclone-scale precipitation development over the North Atlantic Ocean. Over the North American continent, these heat and cold sources can add to cyclone development when a marked upper cold trough with strong positive vorticity advection on its forward side approaches a low-level frontal zone (Petterssen, et al., 1962).

The observed structure of precipitation distribution around surface lows has been attributed to dynamically-induced, large-scale (baroclinic) ascent, to small-scale overturning (convective ascent) associated with vertical instability, and to topography-induced ascent. Two or more of these effects often interact at the same time (Browning and Harrold, 1969; Harrold, 1974). Harrold goes on to conclude that precipitation on the mesoscale is often in narrow bands, with local topography markedly influencing the precipitation structure of surface lows. For example, the influence of underlying topography on precipitation distribution can extend up to several hundred kilometers downstream of mountains. In widespread baroclinic precipitation, topography can also influence precipitation intensity and distribution on more than one scale.

Austin and Houze (1972) analyzed 17 fully developed surface cyclones crossing New England and found that precipitation areas are organized on four subsynoptic scales. Synoptic areas are defined as those larger than 100,000 km^2 and have a lifetime of one to several days. Large mesoscale areas range from 10,000 to 100,000 km^2 and last several hours. Small mesoscale areas cover 100 to 400 km^2 and last about an hour. The smallest areas cover roughly 10 km^2 and often last only a few minutes.

Bosart (1973) shows the importance of convective motions in terms of precipitation distribution within what appears to be routine, steady precipitation areas. For a large percentage of Atlantic coastal storms, the equivalent melted precipitation will range from one to two inches in 12 to 24 hours (over an area of 50,000 km^2). Bosart concludes that the bulk of such rainfall may occur on time scales of just several hours. In several cases, one to two inch convective rainfalls occur in less than one hour during winter storms and

can be compared with precipitation rates typical of more intense summer thunderstorms. Convective rainbands in winter storms responsible for these higher precipitation rates often contain small mesoscale elements (110 to 500 km^2 in area) of maximum rainfall intensity. These can often be found in concentrations of one to three per 1000 km^2. These areas routinely move with the winds located between 850- and 700-mb (Houze, et al., 1976).

Research concerning precipitation in extratropical cyclones has focused on the conceptual model of conveyor belts in transporting moisture and energy towards the surface low (Harrold, 1973, and Browning and Pardoe, 1973). The warm conveyor belt is defined by Harrold (1973) as a low-level jet typically a few hundred kilometers wide, a few kilometers deep, and flowing parallel to and immediately ahead of the surface cold front. Most precipitation forms within this well-defined belt which also transports westerly momentum, heat, and moisture poleward. Surface frontal precipitation results from condensation within the ascending portion of the conveyor belt. Ascent starts in the warm sector and wraps around the surface low center. The surface distribution of precipitation is better related to conveyor belt configuration than to frontal position. Harrold goes on to define the vertical dimensions of the conveyor belt. It is bounded at the top by air of different origin advecting over the cold front, on the west side by the cold front itself, and on the east side by the edge of significant northward flow of air.

Browning and Pardoe (1973) discuss warm conveyor belts and low-level jets ahead of mid-latitude cold fronts. Fronts with active convection lines often contain a low-level jet found in the convective boundary layer on the forward side of the front. This jet attains maximum speeds of 25 to 30 ms^{-1} at levels from 900- to 850-mb located just ahead of the surface cold front. There may often be more than one low-level jet (more often in the horizontal than the vertical), each approximately 200 km in width, and often thousands of kilometers long.

Warm and cold conveyor belts within cyclones are further defined and modeled by Carlson (1980). The warm conveyor belt generally flows parallel to the surface cold front and ascends while turning anticyclonically above the warm front. The cold conveyor belt originates as descending air approaching the surface low center from the east. Then the parcels rapidly rise as they move westward while underneath the warm conveyor belt. Air parcels within the western edge of the warm conveyor belt (just ahead of the surface cold front) possess the highest moisture content and experience the greatest vertical displacement (region of maximum upward vertical velocity). This region of maximum vertical displacement occurs in conjunction with highest wind speeds in the warm conveyor belt, and also the area of maximum (convective) precipitation around the surface low.

Blevins (1985) reviews the relationship of divergence and vorticity aloft to the wind field for United States' east coast surface lows. Any changes in the winds corresponds to changes in divergence and vorticity. Thus, changes in the orientation of the precipitation pattern around a surface low are proportional to changes in the orientation of the kinematic forcing patterns (seen as changes in vertical velocities aloft, etc.). Finally, changes in the easily recognizable conveyor belt patterns imply changes in the dynamic forcing patterns at the surface and aloft associated with surface lows.

A series of detailed research papers were published during the mid-1960s dealt with the synoptic climatology of precipitation patterns around lows over the plateau states of the western United States (Jorgensen, et al., 1967; Jorgensen, 1967; and Klein, et al., 1968). Jorgensen, Klein, and Korte (1967) studied precipitation distributions for 645 upper-air closed lows in winter. 12-hour cumulative precipitation totals were calculated for 280 stations. The area of maximum precipitation is found just to the southeast of the centers of intense 700-mb lows (intensity is defined here as the departure from the normal mean 700-mb height for each low). Precipitation is found to vary in areal extent relative to the low pressure centers and also quantitatively with cyclone intensities. The effect of upper-air lows in producing precipitation generally varies directly with their intensity and inversely with altitude. Winter precipitation appears to be more closely related to the circulation at the surface than at any upper level (Klein et al., 1968).

Jorgensen (1967) attempts to determine precipitation distribution around lows in terms of mean values, frequencies of occurrence, and other climatological statistics. Precipitation variation from storm to storm is well known, but the amount of fluctuation within a given storm from one 6-hour period to the next may be large. Jorgensen's synoptic climatology gives the average precipitation in a storm area and frequencies of occurrence in percent of amounts in various ranges for winter lows in the central United States (from the Great Plains eastward to the western Appalachians). Twenty-nine storms are studied using 6-hour cumulative precipitation amounts (for the subsequent hours after observation time) from an observing network of 400 stations across the eastern two-thirds of the United States. For the average storm, the center of maximum precipitation is located about 450 km to the northeast of the storm center, whereas the center of maximum frequency of precipitation occurrence is about 300 km north of the center. Tasaka (1980) found a strong relationship between the location of a low and the distribution of precipitation and its amount as related to local topography. The distribution and amount changes systematically with the progression of lows across a geographic region.

The major purpose of this research is to relate the intensity and movement of winter surface lows originating in the Gulf of Mexico coastal regions to the evolution of their precipitation patterns as the storms move across the southeast United States. Only those storms producing the heaviest and most widespread precipitation during the three-month period of January, February, and March from 1960 to 1983 comprise the climatology. An objective analysis technique is used to smooth the raw data from Hourly Precipitation Data (HPD) observation stations onto an equally-spaced grid. All storms in selected geographical regions are composited, and a storm-following precipitation climatology developed. It is hoped that the roles of the Gulf (of Mexico) and Atlantic (Ocean) moisture sources feeding these storms may be revealed as storms travel along respective tracks.

Another objective of the present study is to examine the mesoscale precipitation distribution around one winter storm (10-11 February 1986). This is accomplished through a detailed case study of one of the few lows originating in the Gulf coast states and moving northeastward through the Carolinas during the Genesis of Atlantic Lows Experiment (GALE). The evolution of precipitation is related to conveyor belt concepts and kinematic fields associated with the cyclone by employing the special observation networks during GALE.

2. Climatological Study

2.1 Criteria for Case Selection

To be considered in the climatology, winter storms tracking across the southeast United States must have passed through the area east of 95W and south of 38N as outlined in Fig. 2.1a. Geographic regions of cyclogenesis for these storms are defined in Fig. 2.1b. The Atlantic Coast and Gulf Coast Regions are outlined as two common regions of cyclogenesis. The Midwest region encompasses the continental United States beyond the boundaries of the two coastal regions west of 85W. Cyclone track charts contained within the Climatological Data, National Summary and Mariners Weather Log were used to categorize 453 winter lows traveling across the regions from January to March 1960 to 1983. Only those low pressure centers which could be identified for 24 hours or more were included on these charts.

Table 2.1 reveals that most of the winter storms originated in the Atlantic Coast Region, followed by the Gulf Coast, and the Midwest Regions.

Table 2.1

Origin of Winter Lows (January-March, 1960-1983)

Origin of Low	Number of Occurrences	% of Total
Midwest	126	28
Gulf Coast	146	32
Atlantic Coast	181	40
Totals	453	

In order to narrow down the scope of research, only those storms producing the heaviest precipitation are included. These lows were responsible for generating at least 25 mm (or one inch) of precipitation over 24 hours at a minimum of three reporting stations encompassing at least a two state area along the storm tracks. National Oceanographic and

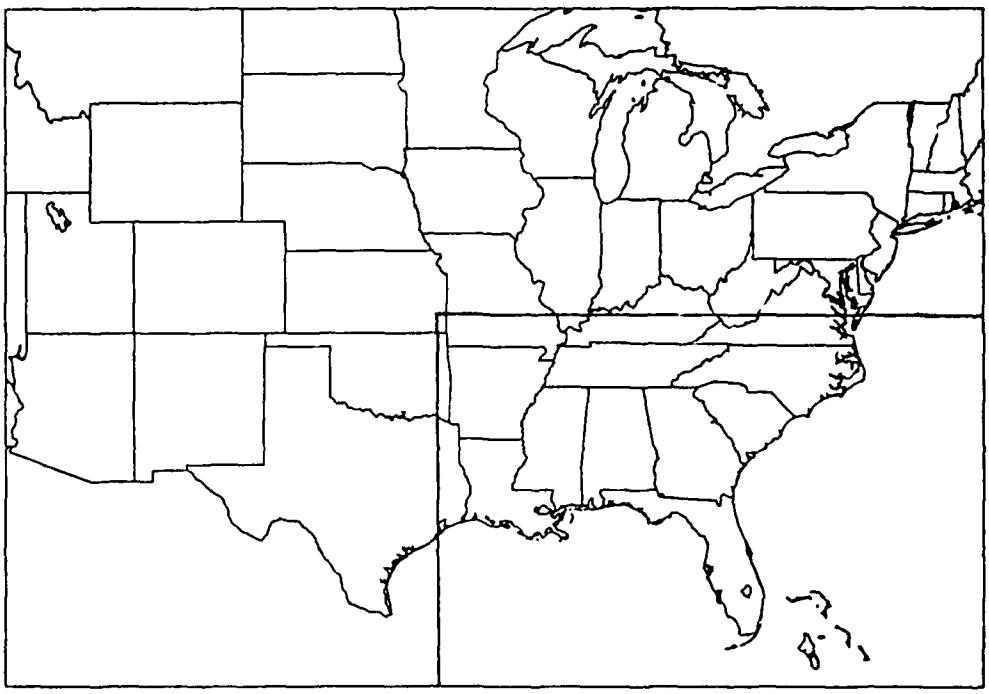

a

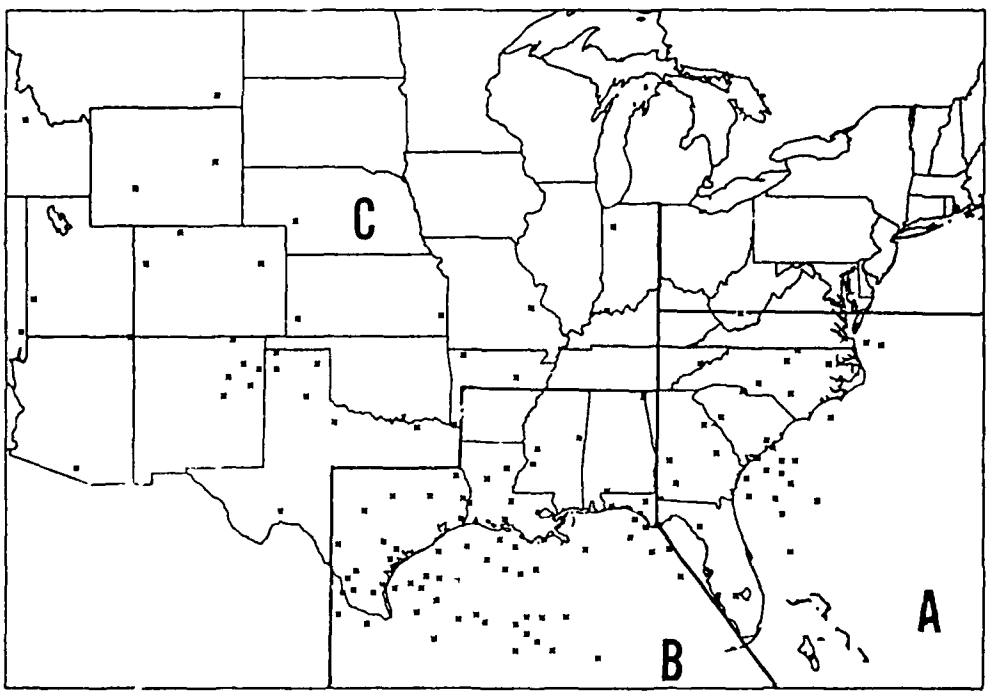

b

Figure 2.1 (a) Outlined area through which surface lows must pass to be included in the climatology. (b) Geographic regions of cyclogenesis with points where lows were first analyzed on surface charts. Regions A, B, and C defined as Atlantic Coast, Gulf Coast, and Midwest respectively.

Atmospheric Administration's Daily Weather Maps (Weekly Series), Precipitation Summary Charts, were reviewed for the days when the 453 winter lows occurred. Of these lows, 130 (29%) were found to be significant precipitation producers. Most develop along the coasts of Texas and Louisiana and the northwest Gulf of Mexico. The dots in Fig. 2.1b show the location of cyclone development for the 130 lows as they relate to cyclogenesis regions. The northeastern Gulf of Mexico is found to be a sparse region of cyclogenesis, a finding which confirms Colucci's (1976) conclusion that this area is not conducive to storm deepening. The Atlantic Coast and Midwest Regions also display areas of cyclogenesis for these heavier precipitation producing storms. Of special note are the pockets of cyclogenesis around north-central Texas, northeastern New Mexico, and the coastal waters off South Carolina and Georgia. The Appalachians contain only three locations of cyclogenesis of the 130 plotted. This is similar to another of Colucci's (1976) and Zishka and Smith's (1980) findings that winter storms tend to bypass the Appalachians.

Contrary to the statistics for all lows in Table 2.1, Atlantic Coast storms were responsible for just 31 of the 130 storms producing precipitation amounts of at least 25 mm (Table 2.2). The Gulf Coast spawned one half (66) of the storms producing heavy precipitation. Since this is twice as many heavy precipitation storms compared to those originating in the Midwest and Atlantic Coast Regions, only these 66 Gulf Coast lows are submitted for further climatological summary.

Table 2.2

Origin of Significant Precipitation Producing Lows
(January-March, 1960-1983)

Origin of Low	Number With Precipitation ≥ 25 mm	% of All Lows w/Precip ≥ 25 mm	% of Total Lows
Midwest	33	25	7
Gulf Coast	66	51	15
Atlantic	31	24	7
Total	130		

2.2 Storm Track Climatology

Changes in the precipitation distribution surrounding the surface lows of interest are documented in a Lagrangian climatology. The goal is to describe the evolution of precipitation distribution around the lows as they move from the Gulf Coast region northward and eastward. The first step in the study is to determine if there are any major tracks that these lows tend to follow. If preferred tracks exist, determining average precipitation rates for the lows as they travel from region to region would give a picture of the evolution of the precipitation patterns surrounding the lows.

Geographic regions are defined across the southeast United States to assist in tracking each storm center (Fig. 2.2a). Centers passing through Regions 1 and 2 represent those storms in which moisture originating over the Gulf of Mexico makes a major contribution to the precipitation distribution. Regions 3 and 5 would contain lows likely to draw on Atlantic Ocean moisture to spread precipitation northward and westward over land. Region 4 may experience storms drawing on Gulf and Atlantic moisture with the Appalachians significantly influencing precipitation to the east of the surface low center.

Specific variables were recorded at certain times for the tracks of each of the 66 low pressure centers. Time, latitude and longitude (to the nearest half degree), central surface pressure, and surface geostrophic relative vorticity values were recorded for the one time that each low passed closest to the midpoint of a particular geographic region. The first four variables were read directly off the North American Surface Charts (archived in three-hour intervals) and interpolated to the desired observation time if this time differed from the surface chart analysis time. Vorticity was calculated similar to Langs' (1986) method as follows. The North American Surface Charts were produced on a polar stereographic projection. Vorticity at the cyclone center is calculated from a superimposed square grid with a spacing of 381 km at standard latitude (60^{o}N). The grid spacing, E, at any other latitude is

$$E = 381.0/K$$

where K is the map scale factor given by

$$K = (1 + \text{SIN } 60^{o})/(1 + \text{SIN } \phi)$$

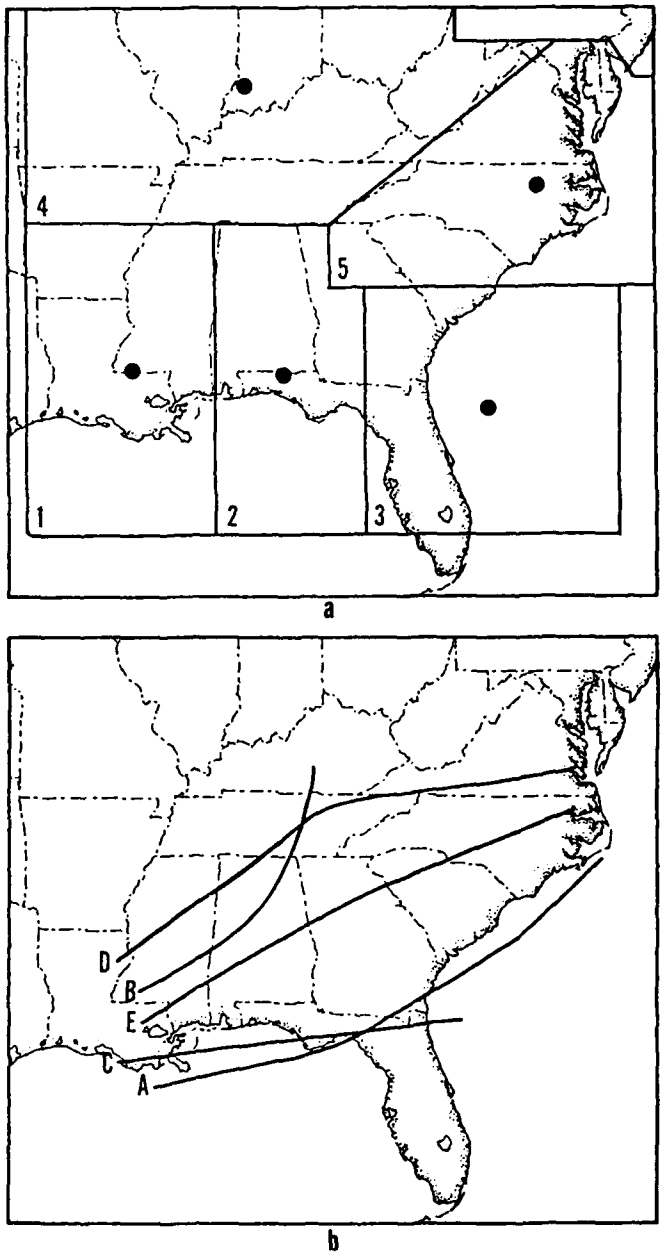

Figure 2.2 (a) Geographic regions derived to assist in tracking storm centers. Midpoint of each region indicated by ●. (b) Composite storm tracks for the 66 lows studied.

and defined as the ratio of the actual earth distance at latitude (ϕ) of the low pressure center to the grid distance at the true latitude of the map projection.

Geostrophic relative vorticity, q, was calculated from the equation:

$$q = (1/\rho f)\nabla^2 p$$

where ρ is the air density (1.225 kgm^{-3}), f is the Coriolis parameter (dependent on latitude), and p is the sea level pressure. The Laplacian of the pressure field, $\nabla^2 p$, is defined by the centered finite-difference formula:

$$\nabla^2 p = \{[\, p(1) + p(2) + p(3) + p(4)] - 4p(0)\} / E^2.$$

Fig. 2.3 illustrates the grid point configuration for this computation. The p(1)-p(3) axis was always oriented north-south through the cyclone center. Cyclonic vorticity is positive and its magnitude is a measure of the storm's circulation intensity.

Each low pressure system was categorized according to the geographic regions it passed through. Using the locations (latitude/longitude) recorded at the one time each low was recorded passing through a region, composite storm tracks were compiled (Fig. 2.2b). Tracks A, B, and C were the most frequently traveled mean tracks accounting for 52% (34), 18% (12), and 14% (9) of the 66 storm tracks, respectively. Tracks D and E account for 7% (5) and 9% (6), respectively. From Figs. 2.2a and b, the geographic regions which the lows in each track passed through can be determined; thus orographic and moisture source influences can be implied from the compiled precipitation distributions. It can be surmised which geographic features should influence the precipitation associated with each storm track. The Gulf of Mexico provides the moisture source at the initial positions of all the tracks. The Appalachians will orographically enhance precipitation amounts for Tracks B, D, and E when storms are west of the mountains, and perhaps decrease amounts when storms track east of the mountains. Tracks A and C have the advantage of the Atlantic Ocean as another moisture source as storms cross the Florida panhandle. The Appalachians' influence on precipitation distributions for these lows should be much less than for the previous tracks mentioned.

For this research, further statistical and analytical investigation has been accomplished for lows in Tracks A, B, and C. The smaller number of lows in Tracks D

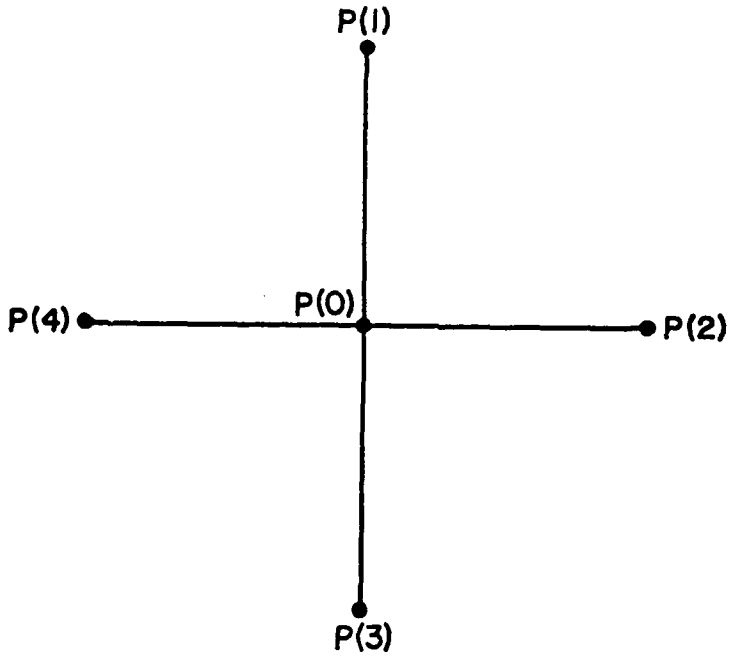

Figure 2.3 Grid point configuration for calculation of the Lapalcian of pressure.

and E would make similar results questionable and inconclusive, so these two tracks are not considered.

Table 2.3 lists speed, central pressure, and vorticity changes accompanying cyclones following Tracks A, B, and C for each segment depicted in Fig. 2.4. The segment or leg numbers correspond to the regions shown in Fig. 2.2a. Lows in Leg 2 of Track A experience the highest mean speed with deepening ($dp/dt < 0$) yet also experiencing weakening ($dq/dt < 0$). Maximum deepening occurs in Leg 1 of Track B. Comparatively slow storm speed and no intensification also characterize this leg. The region of strongest intensification occurs along Leg 3 of Track A which is also an area well-known for cyclogenesis. Note also that storms tend to weaken along Tracks A and C as they move from the Gulf of Mexico to the Florida peninsula.

2.3 Precipitation Data Acquisition and Manipulation

With the tracks established and variables recorded for the lows as they tracked through each geographic region, the next step was to calculate precipitation totals for selected observation stations. Past climatological studies (Tasaka, 1982; Korte, et al., 1972: Klein, et al., 1968; and Jorgensen, et al., 1967) based their findings on 12- or 24-hour precipitation totals for each low. Jorgensen's 1967 study based its findings on precipitation totals from the six hours following the synoptic time at which a storm center was plotted. One of the objectives of the current research is to relate observed changes in the synoptic scale precipitation patterns to moisture sources and topographic factors as these lows progress. Therefore, six-hour precipitation totals are calculated centered at the observation time for each low in each geographic region. This time period is long enough to reveal the overall precipitation pattern, but short enough to see major evolutionary changes.

2.3.1 Hourly Precipitation Data Archives

Raw data for the climatology consists of Hourly Precipitation Data (HPD) compiled by observers at principal (primary) stations, secondary stations, and cooperative observer stations operated by the National Weather Service and the Federal Aviation Administration. The Fischer Porter precipitation guage and the Universal Rain Guage are the primary instruments used to create the historical HPD files at the National Climatic Data Center (NCDC), Asheville, North Carolina. The Fischer Porter guages store precipitation

TABLE 2.3

Track Statistics

TRACK		Leg 1	Leg 2	Leg 3
A	SPEED	48	76	55
	dp/dt	-.28	-.26	-.44
	dq/dt	-.39	-.15	1.05
B	SPEED	23	58	
	dp/dt	-.56	-.32	
	dq/dt	-.01	.21	
C	SPEED	45	52	
	dp/dt	-.24	-.33	
	dq/dt	.16	-.31	

SPEED = Distance traveled divided by time taken to travel from mean locations in successive geographic regions (as defined in Fig. 2.4) in km/hr.

dp/dt = change in pressure (mb/hr).

dq/dt = change in surface geostrophic relative vorticity (x 10^{-5} s^{-1}/hr)

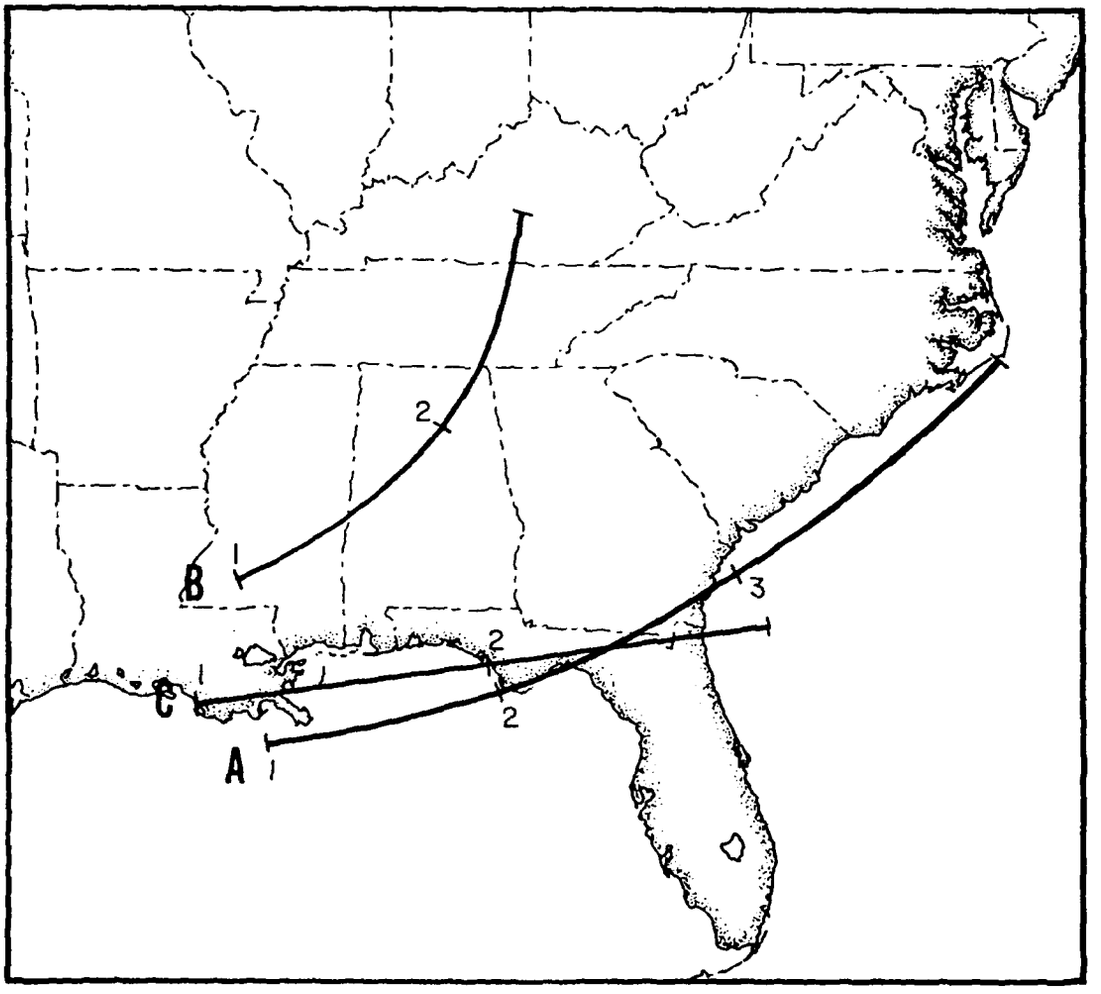

Figure 2.4 Regional legs for Tracks A, B, and C.

amounts in hundredths of inches, but usually report to tenths only. For this study, amounts recorded in hundredths of inches are rounded to the nearest tenth of an inch. The Universal guages also report in tenths of inches.

Stations with the most continuous record of HPD observations from 1960-1983 were desired for the data source. The Hourly Precipitation Station Inventory (by state) lists the number of days each month when a station was unable to report HPD values (for whole or part of each day). This inventory was used to determine which stations would be the most reliable. Certain criteria had to be met in order to include a station in the study and to assume that no reporting of precipitation during a certain hour meant that the station was indeed open and operating (but no rain or snow had fallen). Stations were deleted from the climatology data base based on the percentage of time they were listed as closed on the Station Inventory. If a station was closed for more than 15 days from January to March of a particular year (or 20% of the time), and this occurred for five years or more from 1960 to 1983, then that particular station was eliminated from the study. The locations of the final 316 stations considered as being "open" for the climatological study are plotted in Fig. 2.5a.

The HPD raw data tape received from NCDC had to be edited and manipulated to conform to a program written to compile and plot precipitation totals by station location (latitude/longitude). Stations were listed by two-digit state codes, followed by a four-digit station identifier. The 316 stations' data (January to March, 1960 to 1983) were extracted from the original NCDC source tape and loaded onto a new tape. Less than 1% of the HPD observations consisted of cumulative totals (of greater than one hour) for a particular station, and these observations were deleted from the source data. HPD was recorded in local time at each station, not Greenwich Mean Time (GMT), and 143 of the stations were located in the Central Standard Time zone while 173 were in the Eastern Standard Time Zone. The precipitation-totaling program ensured that all stations conformed to the same GMT time periods of interest.

2.3.2 Objective Analysis Scheme

Non-uniformity in the HPD were reduced as much as possible by using data from only those stations with the most consistent station histories and by editing the raw data for cumulative precipitation totals, as discussed above. However, data-sparse regions existed in Louisiana, Alabama, Kentucky, West Virginia, and parts of Virginia, the Carolinas, and southeastern Georgia. This was also compounded by the fact that it would have been very

tedious and time consuming to determine when and if a station was non-operational for a period of time during a particular 6-hour interval of interest. The final format of the HPD tape dictated that a station might well have been reporting no precipitation when it was actually closed during a precipitation event. To compensate for this, and to depict an accurate precipitation distribution picture around the surface lows, an objective analysis computer software scheme was employed to smooth and contour the data.

Six-hour precipitation totals for each station in Fig. 2.5a were assigned corresponding latitude/longitude locations in an output file for future use. These totals were calculated at all 316 stations for each time period a low was tracked through a particular region. Locations and precipitation totals in the output file were then loaded into the Dataplotting Services, Inc. software package RGRID for each time period. RGRID is a software system that generates a regular distribution of grid values in 2-dimensions (x,y or LAT,LON for this climatology) from original data (in the HPD output file) sampled at random or scattered locations on the plane. The data is interpolated onto a network or grid whose grid point density is computer-determined depending on the density and number of raw data points from the HPD output file for each time period. Numerous gridding parameters in RGRID were adjustable according to the user's preference. Search radius (the radius of the circle surrounding a grid point in which original data values lie) was held constant to guarantee that at least one data value would be found in at least five octants around each grid point. Interpolation options allowed for determining which data values found in the search radius would be used to calculate the grid point value. The option which used all data values within the radius was employed. This allowed for large-scale features of the precipitation distribution to be emphasized, rather than local details.

The final parameter specified is the order of the weighting function. For the precipitation data, order 2 was chosen which defined each grid point value as a weighted average of the data values selected surrounding the grid points. The values were weighted by the inverse square of their distance from the grid point.

Once the 6-hour totals were gridded, another Dataplotting software package called CONTOUR was used to generate contour lines (at user-defined intervals) drawn through contiguous points on the gridded data surface with the same values. An example of this with actual HPD reporting totals for the chosen 6-hour period appears in Fig. 2.6. From these contour charts, 1^{o} latitude by 1^{o} longitude intersection point values (Fig. 2.5b) were manually extracted for future use in compiling the precipitation climatology. For example, 6-hour HPD grid point totals were calculated for all Track A storms at the times they passed

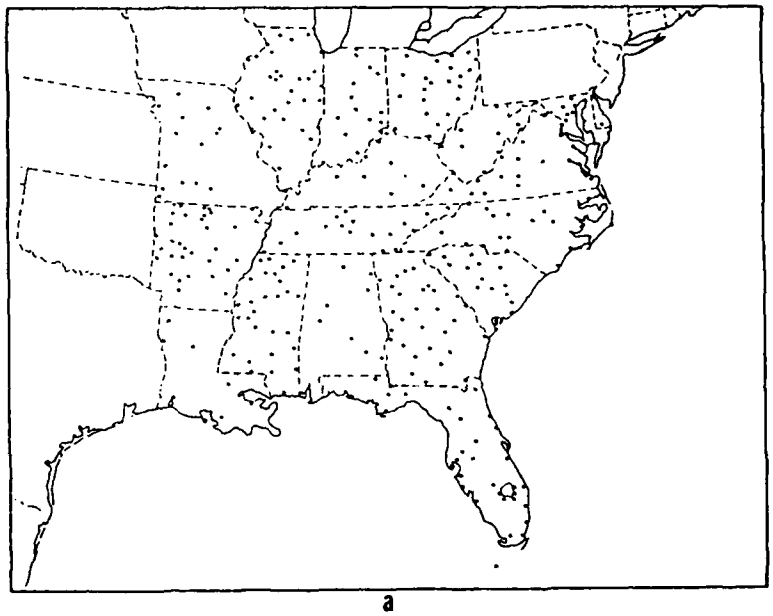

a

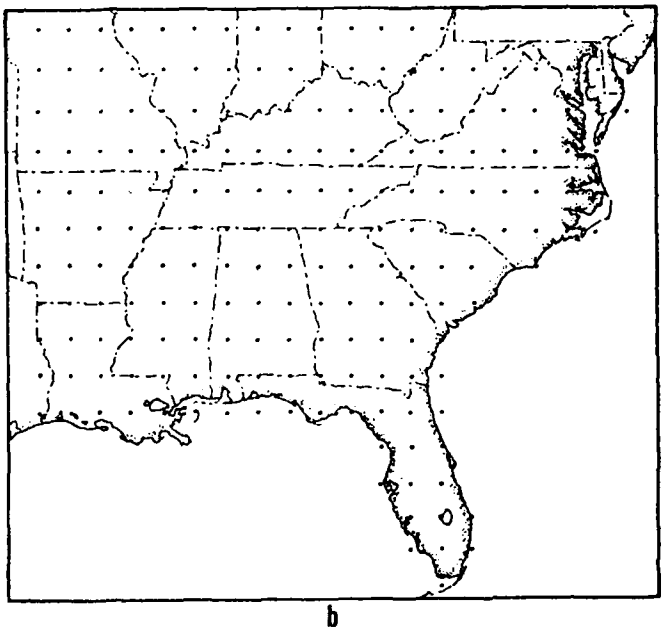

b

Figure 2.5 (a) Hourly Precipitation Data stations. (b) Grid point system for extracting totals from contoured precipitation charts.

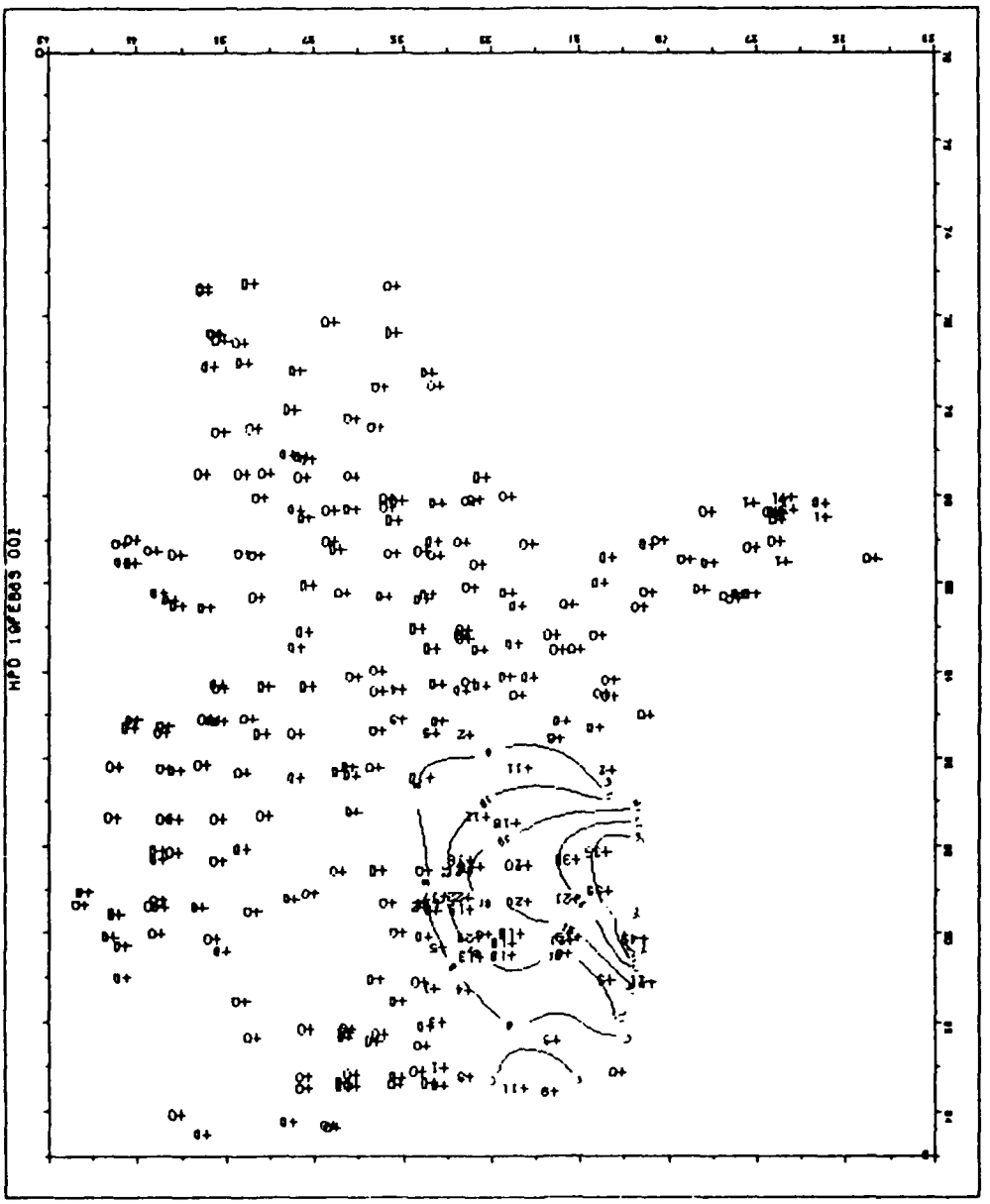

Figure 2.6 Example of objectively analyzed and contoured precipitation totals for the 6-hour period centered at 0000 GMT 19 February 1963. Longitude and Latitude depicted along abscissa and ordinate axes, respectively. Actual (uninterpolated) reporting stations' totals included.

through Region 1. After all totals were extracted from the contour charts for each storm, grid point totals were averaged to provide a picture of the mean precipitation distribution for all lows in Track A passing through Region 1. Synoptic scale mean precipitation distribution charts were thus compiled to determine the evolution of the precipitation field surrounding the lows as they progressed along each track from one geographic region to another. Frequency of occurrence charts for specified precipitation amounts were similarly compiled.

2.4 Results of the Precipitation Climatology

2.4.1 Storm Track Analyses

For each of the three tracks studied, the average distribution of precipitation surrounding the mean location of the lows in each geographic region are compiled. Figs. 2.7a-d depict the evolution of the distribution pattern around storms in Track A. As the lows cross the Gulf Coast region, precipitation amounts maximize at 13 mm in Region 2. Here the Gulf of Mexico has been continuously feeding moisture into the warm sector of the storms. The double maximum of precipitation in Fig. 2.7b may indicate that the Atlantic joins as a second moisture source as the storms cross the Florida panhandle in Region 3. It seems likely that moisture feeding into the storms from the Gulf of Mexico is cut off by the time they reach the North Carolina coast. Precipitation amounts drop off to 7 mm in six hours just north of the low in Fig. 2.7d.

The frequency of precipitation occurrence (percent) contour patterns (Figs. 2.8 to 2.10) are similar to those of precipitation amount for Track A. The frequency charts are divided into three categories: light (1 mm or more in 6 hours), moderate (10 mm or more), and heavy (20 mm or more). The three categories for Track A storms all exhibit a growth in areal extent of the maximum frequency of occurrence areas from Regions 1 to 2, followed by a gradual decrease as storms cross to the Atlantic in Region 3 and northeastward in Region 5. Nearly the entire southeast United States experiences light precipitation at least 10% of the time when the Gulf of Mexico is the major moisture source (Figs. 2.8a and b). As storms travel through Regions 3 and 5, the extent of light precipitation west of the Appalachians decreases by the time lows reach the North Carolina coast (Fig. 2.8d). Frequency of moderate to heavy precipitation is generally highest to the northeast of the storm centers. The chance of moderate precipitation is always less than

60%, while heavy precipitation occurs less than 30% of the time at a given location (Figs. 2.9 and 2.10).

Track B storms seem to be predominantly influenced by Gulf of Mexico moisture. Mean precipitation patterns (Fig. 2.11) display maximum values decreasing from 15 mm to 9 mm as lows track from Region 1 through 2 and into 4, yet the general area of precipitation of at least 1 mm continues to cover virtually the entire map area. This is also evidenced on the frequency of light precipitation occurrence charts in Fig. 2.12. Moderate precipitation occurs at least 50% of the time across a wide area north and east of the lows in Regions 1 and 2 (Fig. 2.13). This area decreases to 30% in Region 4. The frequency of heavy precipitation maximizes in Region 2 (Fig. 2.14), with some interesting local patterns over and to the lee side of the Appalachians when lows move into Region 4. Warm, moist Gulf of Mexico airflow may explain the widespread precipitation distributions and frequencies for Regions 1 and 2. Precipitation induced by upslope flow west of the Appalachians should act as a drying mechanism as saturated air is lifted, cooled, and condensation results in precipitation. The result should be a relative minima of precipitation to the lee of the mountains. This, however, is not the case. The 9 mm precipitation maximum (Fig. 2.11c) and the frequency of occurrence maxima for all three precipitation categories (Figs. 2.12c, 2.13c, and 2.14c) all appear to the lee side of the Appalachians where relative minimas would be expected. One possible explanation for this is that once these more intense storms reach Region 4, they tend to spawn Miller's (1946) Type B cyclones along the Atlantic coast. A check of the 12 storms categorized in Track B revealed that 5 (or 42%) of them tracking into Region 4 spawned secondary lows along the Atlantic coast. Secondary cyclogenesis occurring from South Carolina to Virginia would tend to force moist flow from the Atlantic north and westward towards the Appalachians, thus explaining this anomaly.

Storms in Track C tend to mimic the precipitation patterns of those in Track A for Regions 1 and 2, though Track C precipitation amounts and frequencies of occurrence tend to be slightly greater (Figs. 2.15-2.18). Mean precipitation values were 15 mm and 13 mm, respectively, as lows track through Regions 1 and 2, (Fig. 2.15). By the time these storms reach Region 3 and continue eastward, they are too far south and moving away from the Atlantic coast to produce significant precipitation totals over land (Fig. 2.15c). Local maxima in 6-hour precipitation totals and frequencies of occurrence appear only along the coasts of Georgia and the Carolinas. Southern Mississippi, southern and central Alabama, and the Florida panhandle tend to receive the brunt of the heavy precipitation from these storms.

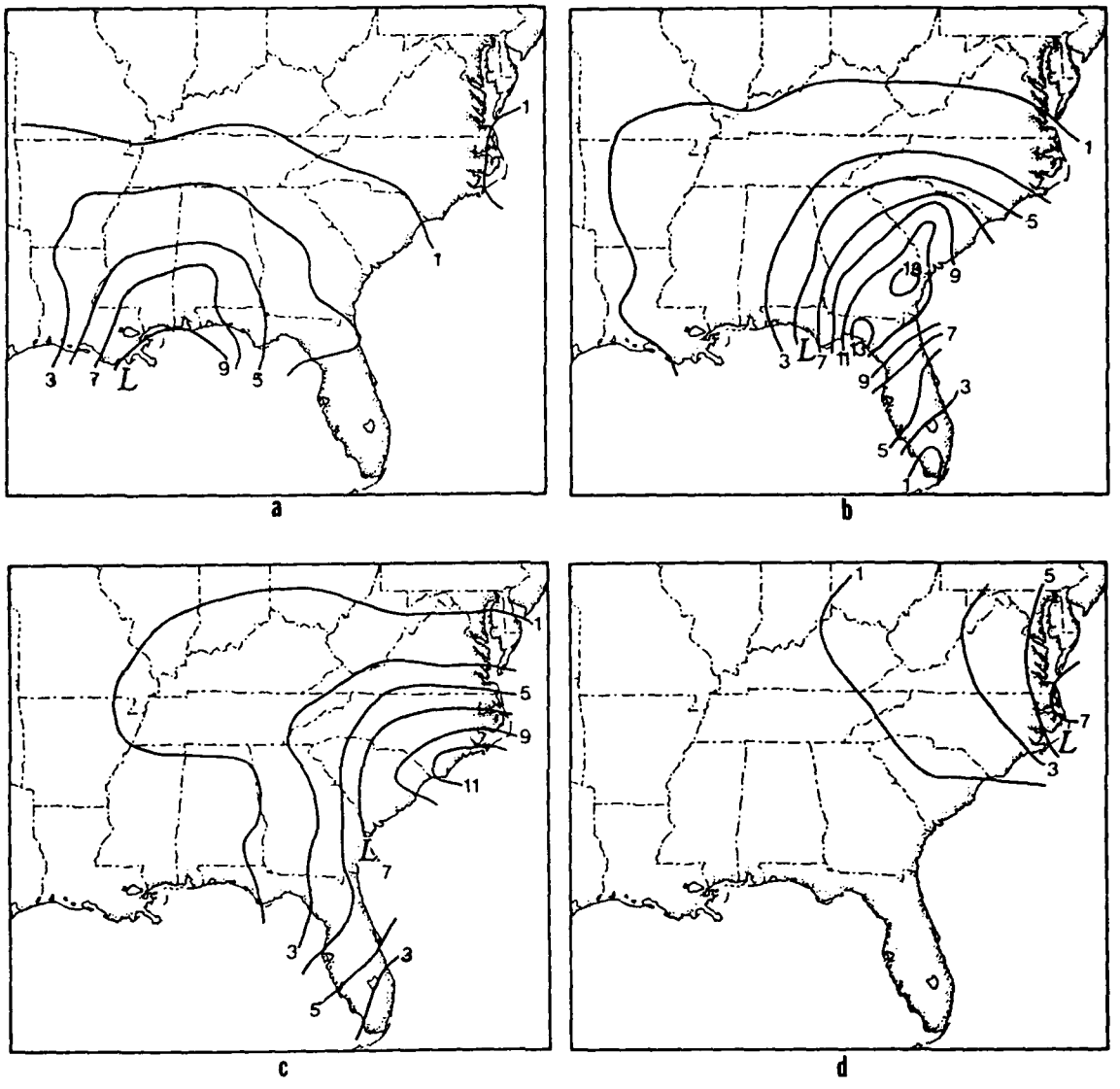

Figure 2.7 (a-d) Mean 6-hour precipitation totals (mm) for lows in Track A compiled for mean location of lows (indicated by the "L") passing through regions 1, 2, 3, and 5, respectively (from Fig. 2.2a).

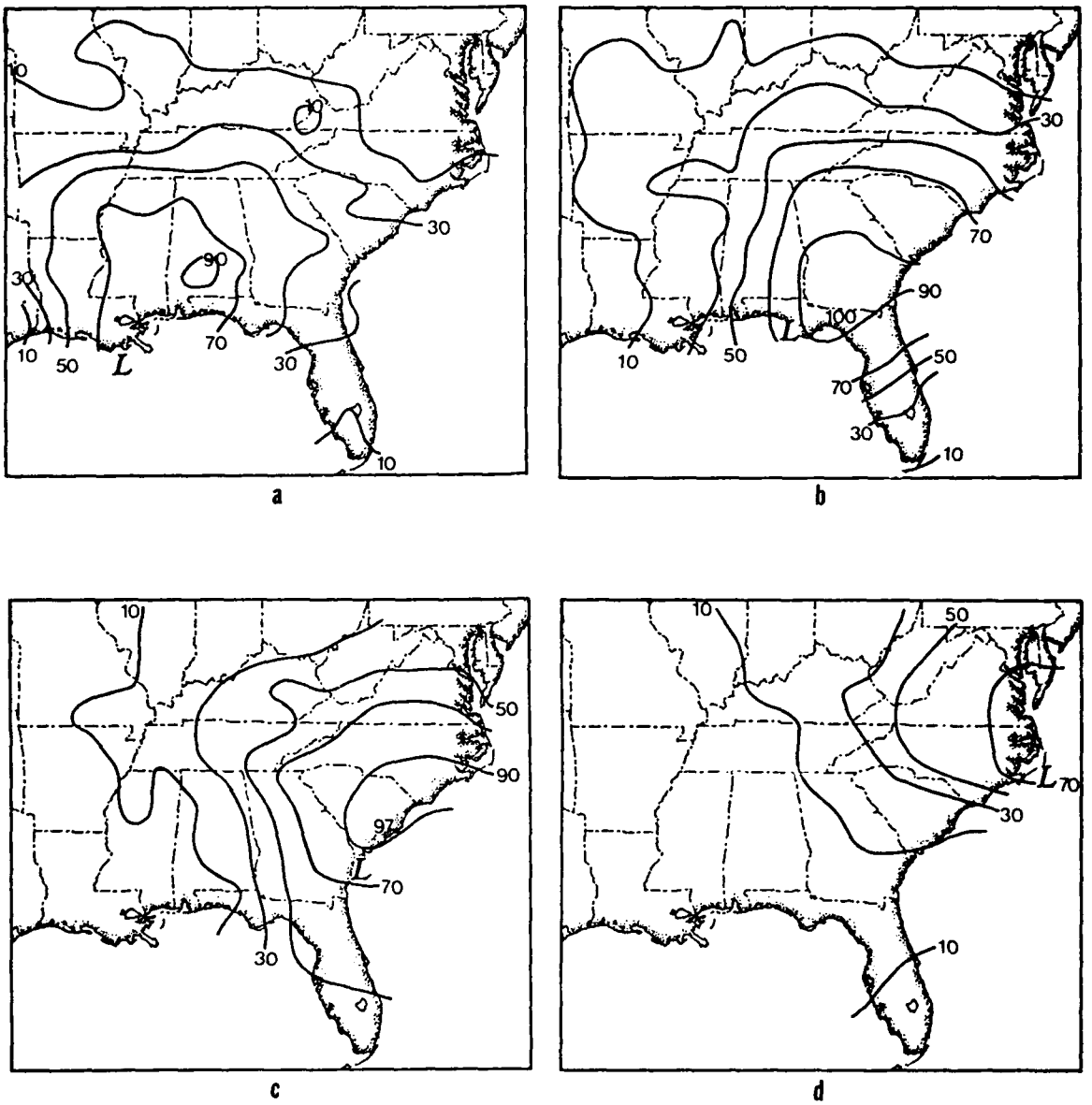

Figure 2.8 (a-d) Same as Fig. 2.7a-d, except contours are values of percent frequency of occurrence for precipitation totals ≥ 1 mm. Highest percentages indicated if greater than maximum contour value.

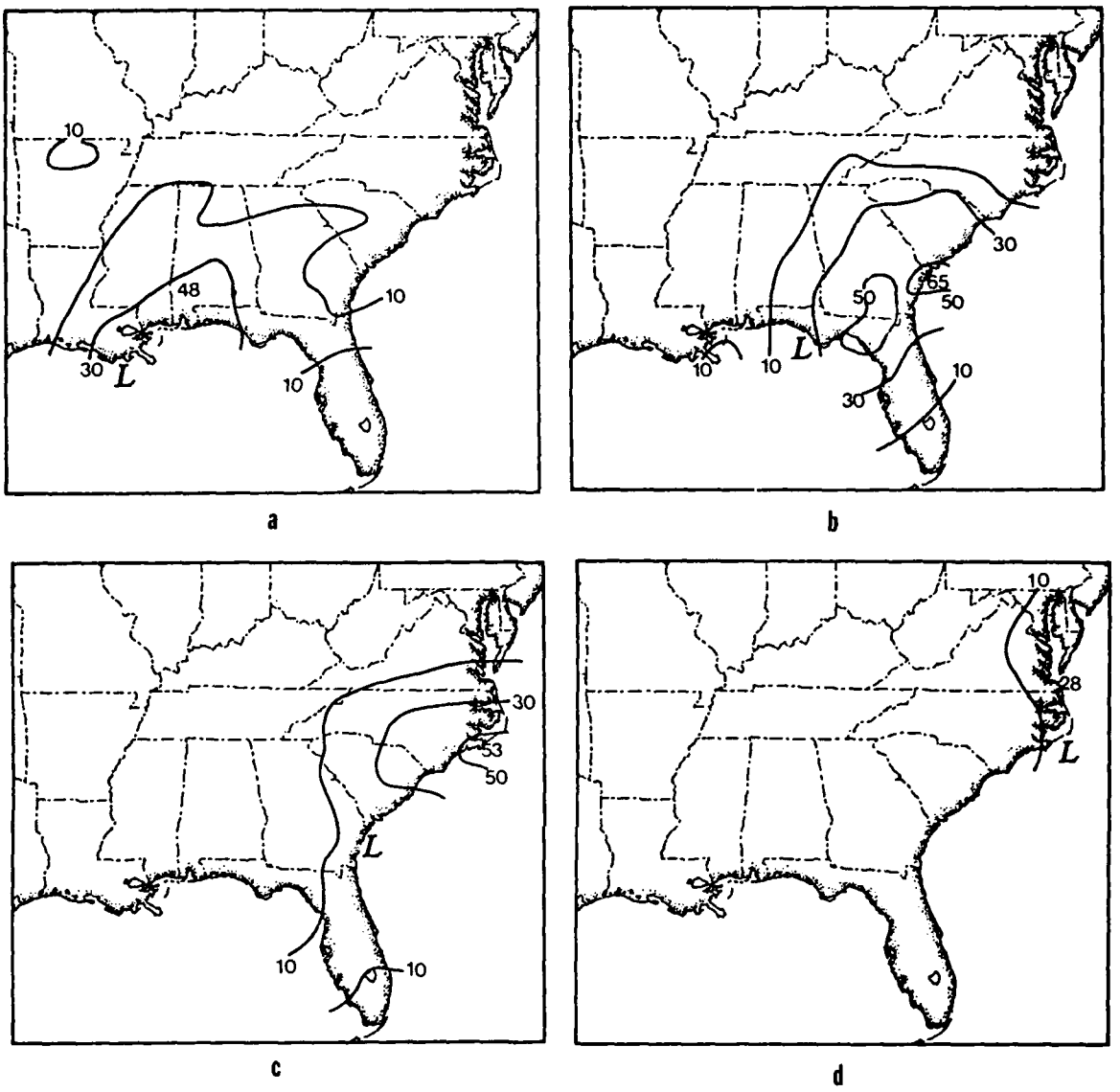

Figure 2.9 (a-d) Same as Fig. 2.8a-d for precipitation totals ≥ 10 mm.

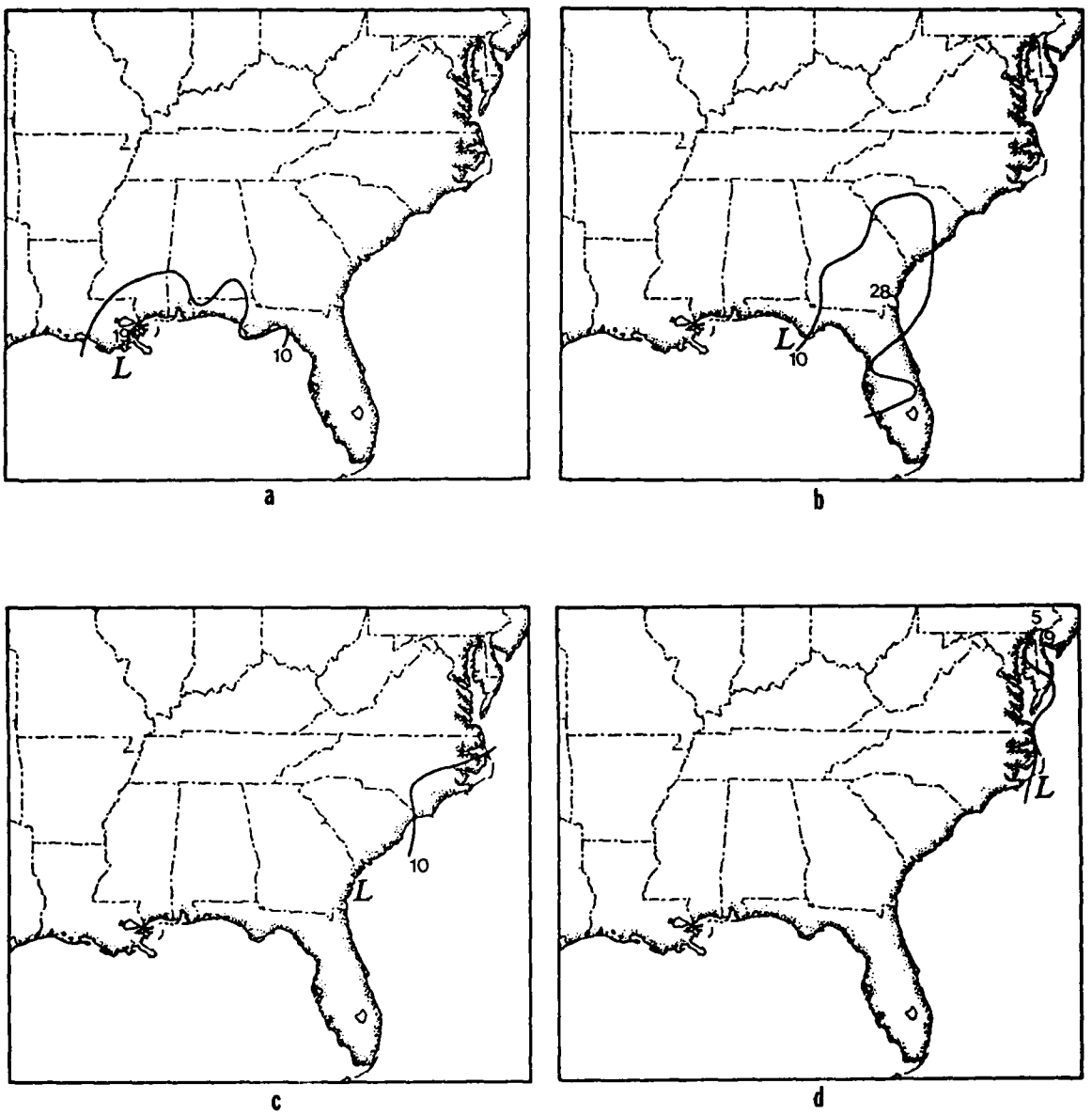

Figure 2.10 (a-d) Same as Fig. 2.8a-d for precipitation totals ≥ 20 mm.

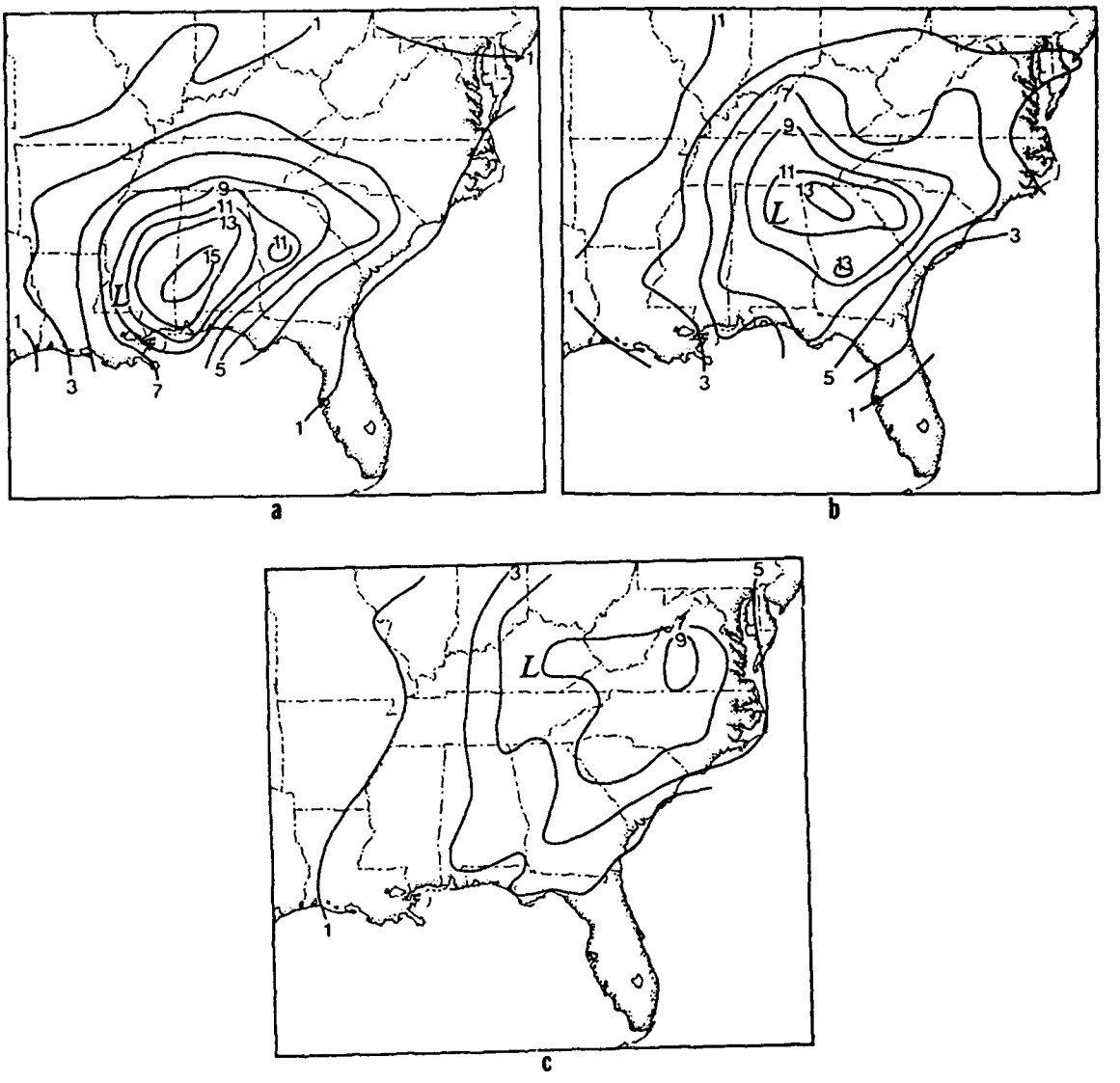

Figure 2.11 (a-d) Same as Fig. 2.7a-d, except for lows in Track B passing through regions 1, 2, and 4, respectively.

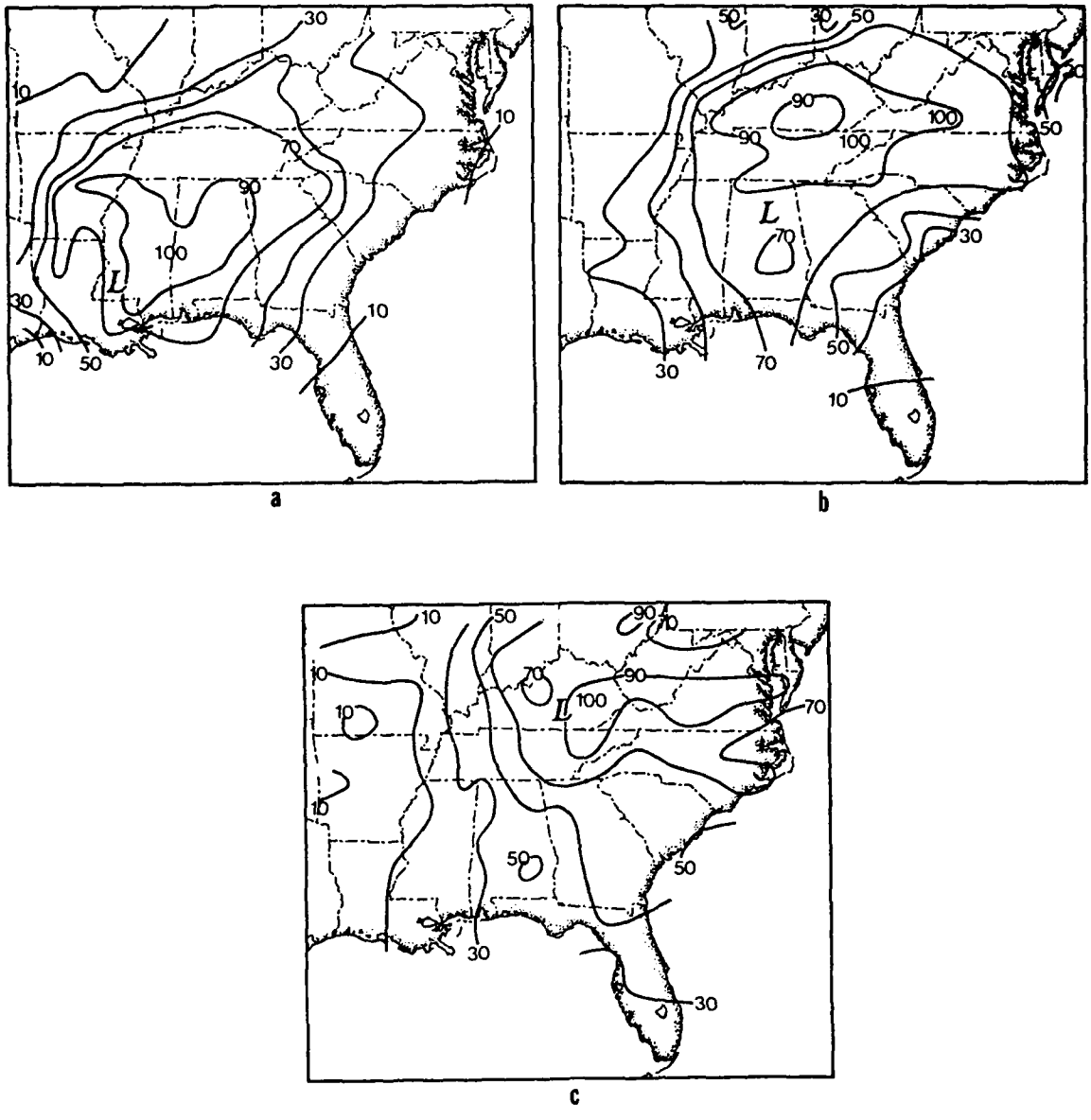

Figure 2.12 (a-c) Same as Fig. 2.11a-c, except contours are values of percent frequency of occurrence for precipitation totals ≥ 1 mm.

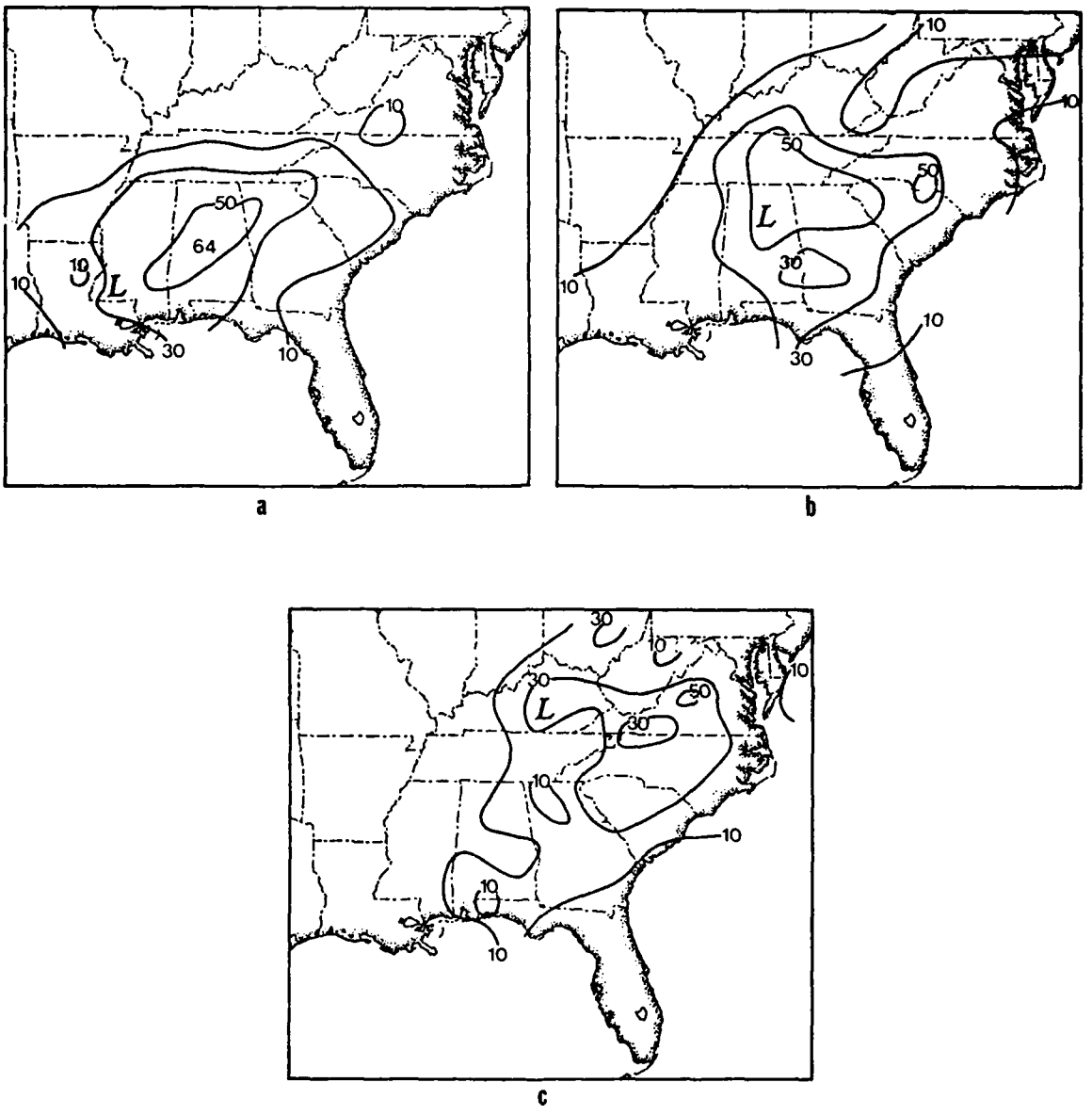

Figure 2.13 (a-c) Same as Fig. 2.12a-c for precipitation totals ≥ 10 mm.

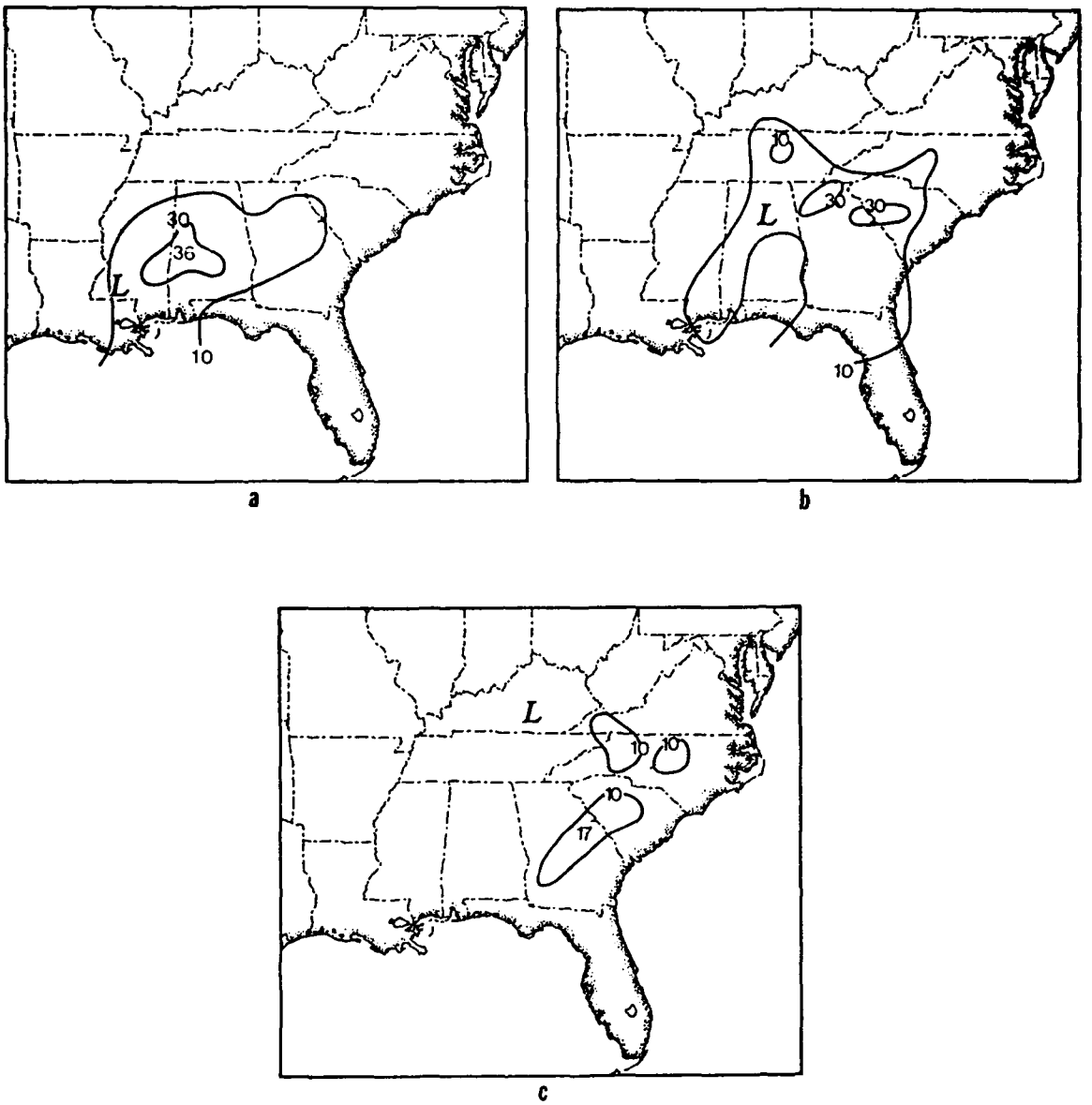

Figure 2.14 (a-c) Same as Fig. 2.12a-c for precipitation totals ≥ 20 mm.

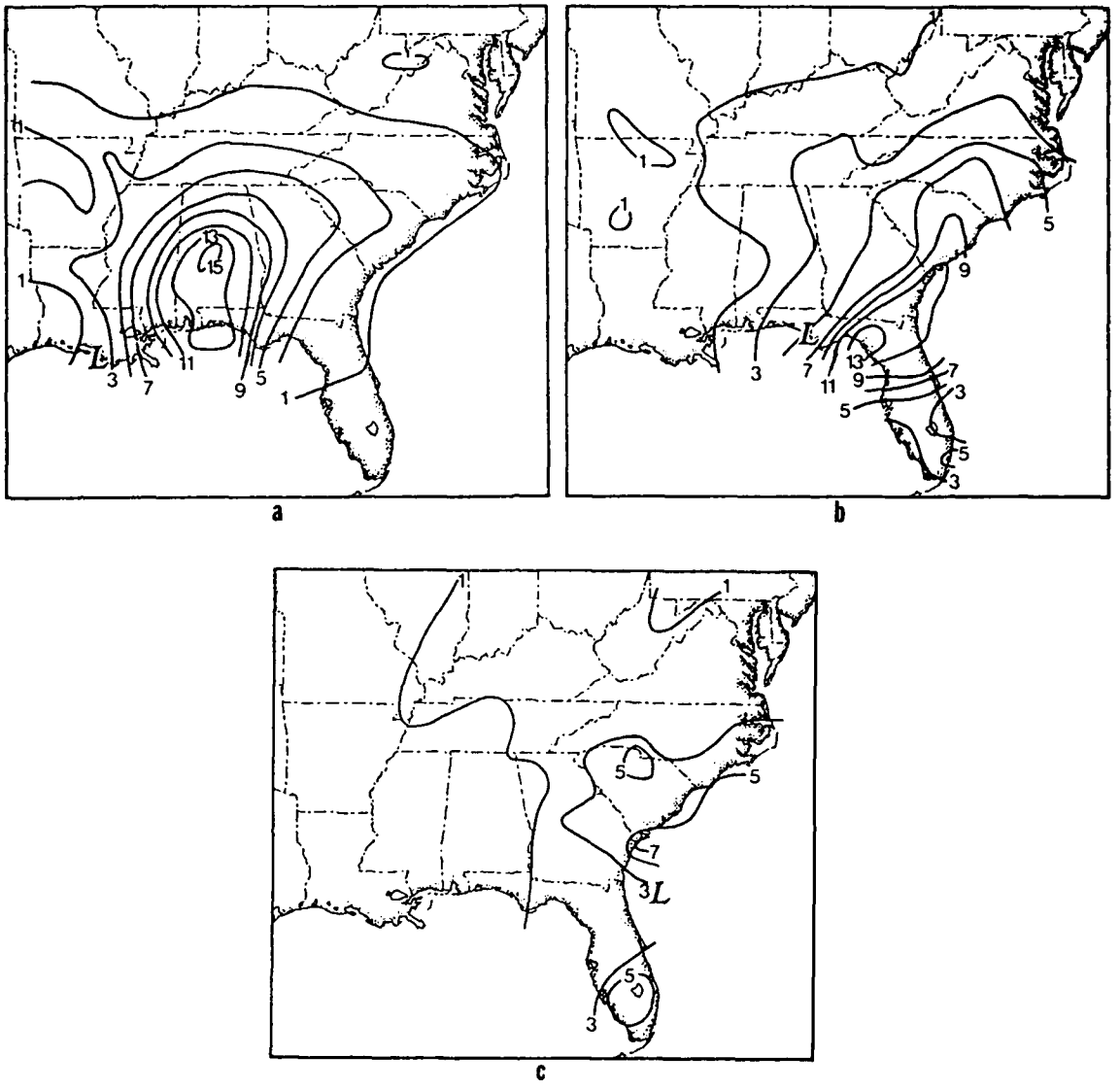

Figure 2.15 (a-c) Same as Fig. 2.7a-d, except for lows in Track C passing through regions 1, 2, and 3, respectively.

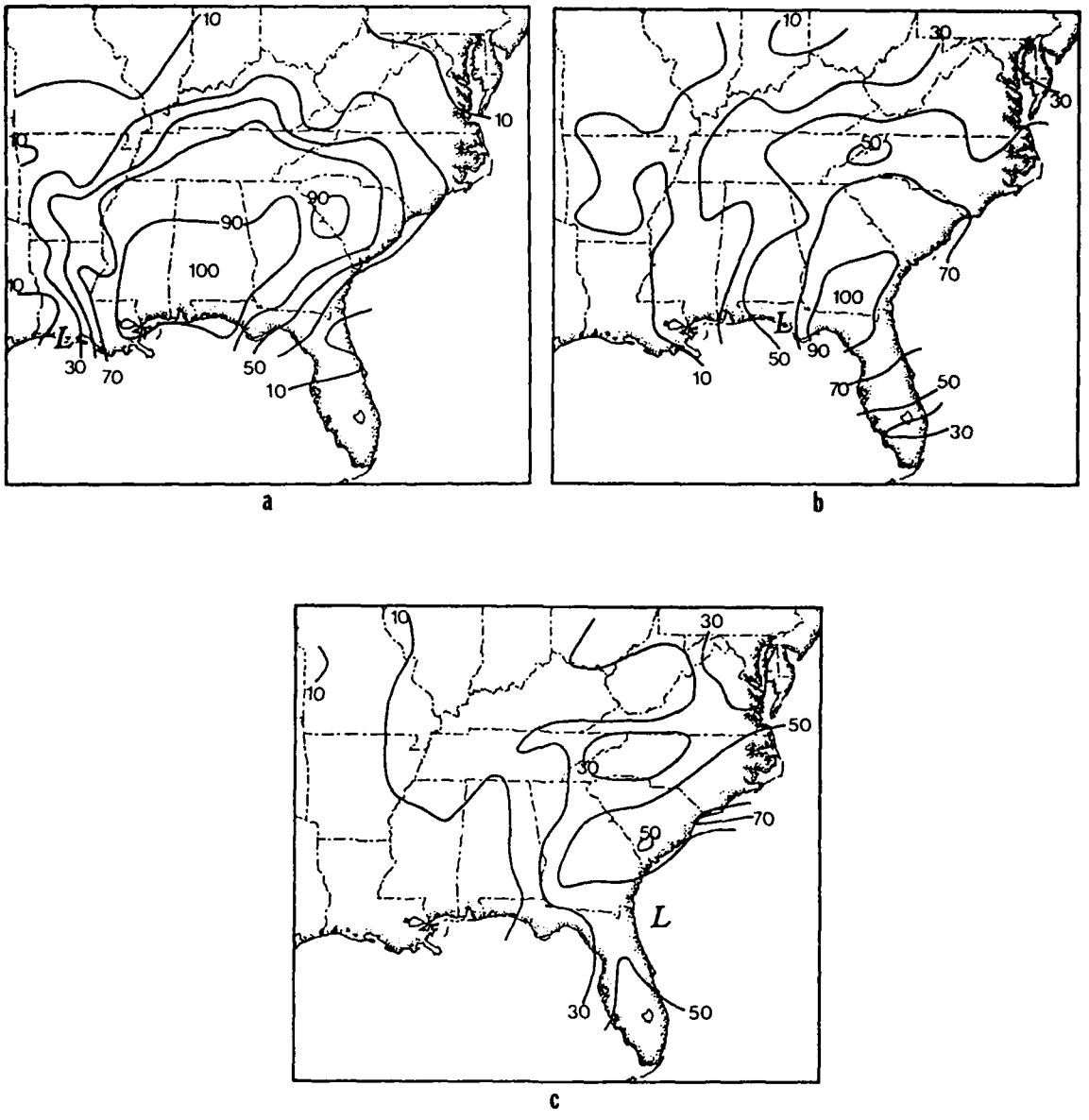

Figure 2.16 (a-c) Same as Fig. 2.15a-c, except contours are values of percent frequency of occurrence for precipitation totals ≥ 1 mm.

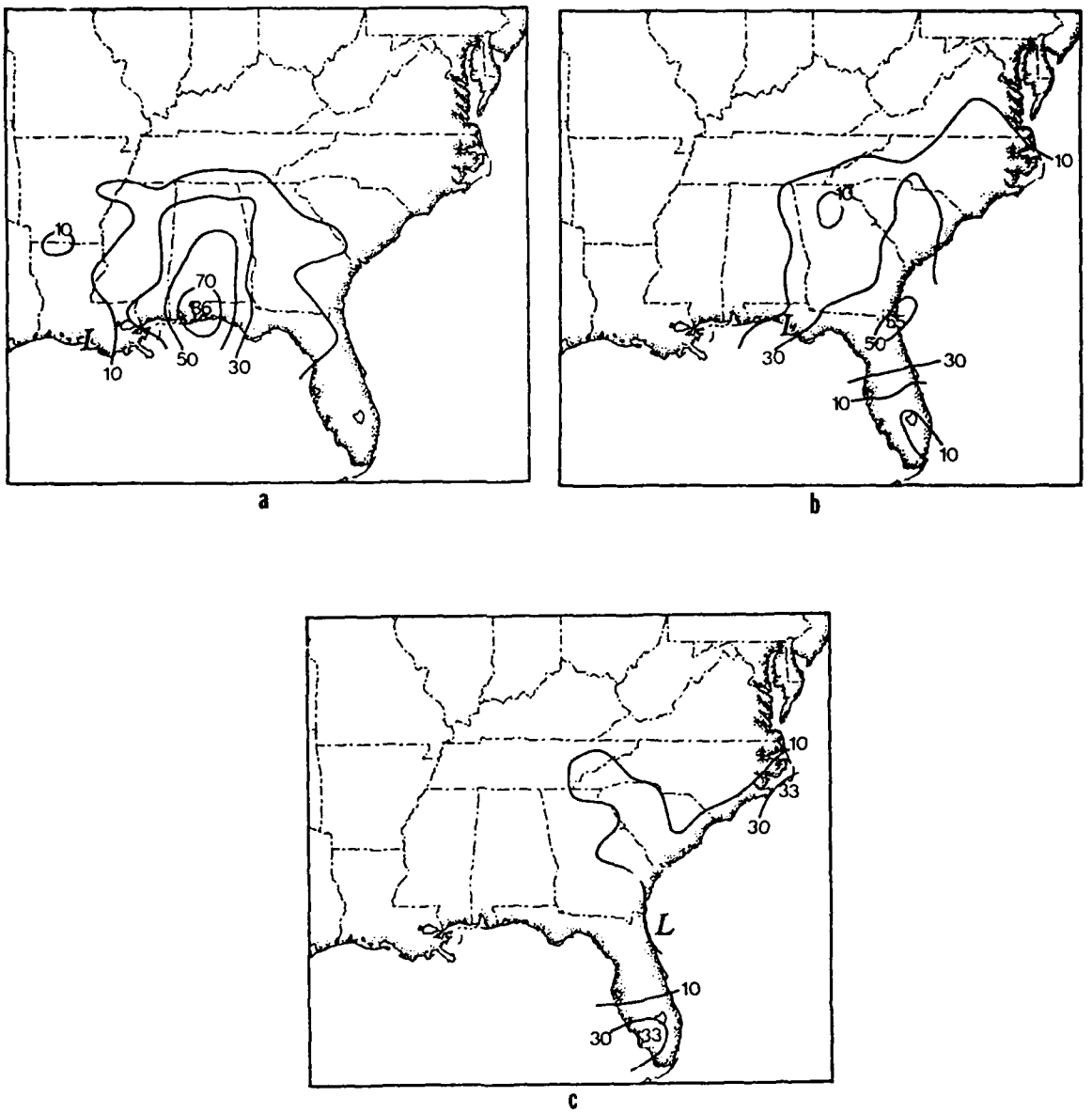

Figure 2.17 (a-c) Same as Fig. 2.16a-c for precipitation totals ≥ 10 mm.

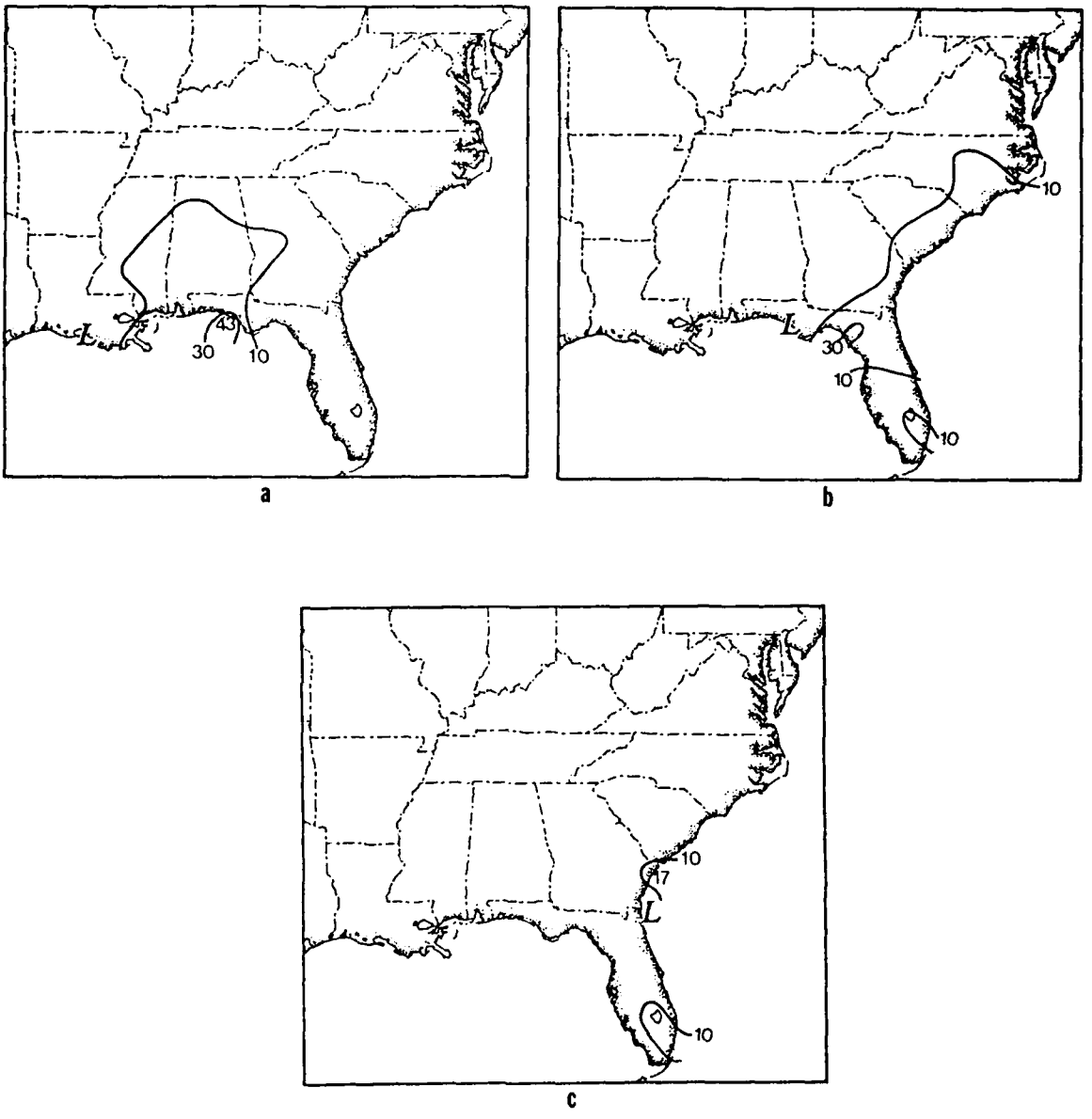

Figure 2.18 (a-c) Same as Fig. 2.16a-c for precipitation totals ≥ 20 mm.

2.4.2 Statistical Analysis

Table 2.4 presents a subdivision (by track and region) for the mean values of three different precipitation variables calculated from the raw data and values at the grid points in Fig. 2.5b. Data from all 66 lows (including those in Tracks D and E) were used for these calculations. Actual maximum recorded HPD station precipitation values (over 6 hours) were found to be highest for all storms in Region 2, for Track B storms in Regions 1 and 2, and for Track A storms in Region 3. The mean area of precipitation occurrence was calculated by averaging the number of grid points (Fig. 2.5b) recording at least 1 mm of precipitation for each storm in each region. Storms in Region 4 averaged over half the grid points experiencing precipitation. Track B storms dominate this category when compared to values for Tracks A and C in Regions 1 and 2. Track A storms in Region 3 provide more precipitation coverage than those in Track C. Total mean precipitation amounts were calculated by averaging each storms' grid point precipitation totals when tracked in each region. Results (by track and region) match those found for area of precipitation occurrence discussed above.

Multiple linear regression procedures were used to determine which independent variables significantly influenced the three variables described above. The list of independent variables consisted of the storm's central pressure (X_1), geostrophic relative vorticity (X_2), latitude (X_3), and londitude (X_4) recorded as described in Section 2.2. Dependent variables were actual maximum precipitation values (Y_1), precipitation coverage (or area) (Y_2), and total precipitation (Y_3) as described above and in Table 2.5a.

The first step in the regression process was to ensure that frequency distributions of the three dependent variables were as near to normal as possible. To do this, three options were tested: (1) No transfromation of the variable; (2) a transformation by taking the square root of the variable; and (3) by taking the natural log (ln) of the variable. Once the "best fit" normal distribution was found, each dependent variable was modeled with the independent variables for the given data. By process of elimination, independent variables were deleted from the models to achieve a regression equation which best estimated each dependent variable. Rationale for choosing which models performed best were threefold:

1) Significance (at approximately the 95% confidence level) of each independent variable via a standard "t-test."

TABLE 2.4

PRECIPITATION VARIABLES: REGIONAL MEANS

TRACK	REGION	MAX PRECIP VALUE (mm) (6-hour totals)	AREA OF PRECIP OCCURRENCE (# of grid pts recording precip)	TOTAL PRECIP (total of all grid pts) (mm)
ALL	1	41	75	553
ALL	2	42	87	694
ALL	3	32	71	439
ALL	4	37	103	702
ALL	5	18	45	209
A	1	33	63	439
B	1	54	89	759
C	1	38	87	530
A	2	38	78	570
B	2	53	112	1047
C	2	41	81	538
A	3	33	75	474
C	3	28	50	260
B	4	40	103	721
A	5	17	41	187

2) Significance (at approximately the 95% confidence level) of the model via a standard "F-test."

3) Lowest standard error of the estimate (each dependent variable) while maximizing the square of the correlation coefficient (r^2).

Here, r^2 is defined as a measure of how well the regression equation explains the variation in the data. Statistically,

r^2 = Sum of Squares (Regression)/Sum of Squares (Total).

As r^2 approaches 1, more confidence is placed in the regression equation as accounting for the observed variation.

Results from the regressions appear in Tables 2.5a and b. Regressions were accomplished on each of the three dependent variables in four categories related to the climatological storm tracks discussed earlier. The most important independent variables for calculating a particular dependent variable appear in Table 2.5a. Longitude is observed to be the most significant independent variable, appearing in all regression equations. Latitude, however, is the least significant variable. It is a factor in only two of the eleven equations. Pressure and vorticity are also important variables, appearing in seven and eight equations, respectively.

Table 2.5b contains the actual equations and important statistics for the tracks listed in Table 2.5a. The signs (+ or -) of the coefficients for each independent variable were examined to compare their positive or negative contributions to the dependent variables. Considering all the regression results, central pressures (as expected) correlated negatively with increasing precipitation activity in all three categories. One would expect vorticity increases (i.e., increasing storm intensity) to be positively correlated with the dependent variables, however, this was not the case. Storm latitude was not a significant factor often enough to show a definite relationship. Higher longitude values (or the further west a storm center was located) tended to correlate positively with higher values for the dependent variables. This is to be expected. Once lows tracked eastward, eventually reaching the Atlantic coast, the precipitation recording stations were located west of the heavier precipitation totals expected to be found over the ocean. It is interesting to note that eastward progression of storms in Track B (lower longitude values over land, not water) led to the two occurrences of an increase in dependent variable values. This can be explained by the fact that heavy precipitation generally occurred over land with eastward

TABLE 2.5a

MULTIPLE LINEAR REGRESSION RESULTS (PART 1)

Dependent Variables:

Y_1 = Maximum Precipitation Value (mm)

Y_2 = Area of Precipitation Coverage (# of grid points)

Y_3 = Total Precipitation (mm)

Independent Variables:

X_1 = Pressure (mb)

X_2 = Vorticity ($10^{-5}s^{-1}$)

X3 = Latitude (degrees)

X_4 = Longitude (degrees)

TRACK	DEPENDENT VARIABLE	MEAN	STANDARD DEVIATION	SIGNIFICANT INDEPENDENT VARIABLES
ALL	Y_1	34.3	1.5	X_1 X_4
	Y_2	73.3	2.3	X_1 X_2 X_3 X_4
	Y_3	507.6	25.7	X_1 X_2 X_4
A	Y_1	29.6	1.6	X_4
	Y_2	63.5	2.7	X_1 X_2 X_4
	Y_3	407.4	25.8	X_1 X_2 X_4
B	Y_1	48.6	4.0	NONE
	Y_2	101.1	5.4	X_2 X_4
	Y_3	832.6	80.5	X_3 X_4
C	Y_1	36.4	3.8	X_1 X_2 X_4
	Y_2	74.6	6.2	X_2 X_4
	Y_3	459.7	46.5	X_1 X_2 X_4

TABLE 2.5b

MULTIPLE LINEAR REGRESSION RESULTS (PART 2)

(Standard errors appear below each coefficient in the models)

TRACK	MODEL	r^2
ALL	$Y_1 = \{31 - .04(X_1) + .18(X_4)\}^2$ [15] [.02] [.02]	.28
	$Y_2 = 974 - 1.3(X_1) - .63(X_2) + 2.7(X_3) + 3.5(X_4)$ [372] [.36] [.23] [.82] [.43]	.30
	$Y_3 = \{362 - .41(X_1) - .16(X_2) + .85(X_4)\}^2$ [84] [.09] [.06] [.10]	.32
A	$Y_1 = \{-7.1 + .15(X_4)\}^2$ [2.1] [.03]	.25
	$Y_2 = 1107 - 1.2(X_1) - 1.0(X_2) + 2.0(X_4)$ [452] [.46] [.26] [.47]	.29
	$Y_3 = \{299 - .34(X_1) - .20(X_2) + .73(X_4)\}^2$ [119] [.12] [.07] [.12]	.32
B	Y_1 = BAD FIT: X's and Model INSIGNIFICANT	
	$Y_2 = 349 + .95(X_2) - 3.1(X_4)$ [140] [.47] [1.6]	.24
	$Y_3 = \{205 - 1.5(X_3) - 1.4(X_4)\}^2$ [68] [.69] [.57]	.18
C	$Y_1 = \exp\{55 - .06(X_1) - .02(X_2) + .05(X_4)\}$ [14] [.02] [.01] [.02]	.48
	$Y_2 = \{-5.4 - .11(X_2) + .18(X_4)\}^2$ [5.1] [.03] [.06]	.57
	$Y_3 = \exp\{27 - .03(X_1) - .03(X_2) + .07(X_4)\}$ [11] [.01] [.01] [.02]	.67

progression in this track.

The multiple linear regressions presented can provide forecasters with a "first-guess" estimate of precipitation data to be expected from a particular storm of the type included in this climatology. Given a forecasted latitude, longitude, central pressure, and vorticity, the precipitation variables can be estimated. Note, though, that the r^2 statistics are rather low for all tracks except C. Since the total variability may not be sufficiently explained by the model, these regressions should be used strictly as a starting point for precipitation forecasts. It is interesting to note that the NWS precipitation forecast models use twelve independent variables from two seperate forecasting models (LFM and Primitive Equation) to make their estimates (Zurndorfer and Bermowitz, 1976). If this model is unavailable or outdated, the regression equations discussed earlier can serve as a backup for initial precipitation total estimates.

2.4.3 Maximum Precipitation Location Analyses

An attempt has been made to relate the locations of actual precipitation maxima over land to storm centers. This is done using a standardized rectangular area divided into a network of 500 cells, each 1^{o} latitude by 1^{o} longitude (Fig. 2.19), designed to coincide with a similar grid used to extract contoured HPD totals as in Fig. 2.6. Maximim precipitation locations are compiled by geographic region. The blackened grid box represents the cyclone center; the vertical grid lines at the center were oriented along the local meridian. Actual values of 6 hour maximum precipitation were extracted from the objectively analyzed and contoured HPD charts, assigned one of three intensity categories (Light = 1, 0 - 25 mm; Moderate = 2, 26 - 50 mm; Heavy = 3, $\geq$ 51 mm), and plotted in Fig. 2.19 based on grid distance from storm center. Fig. 2.19 and Table 2.6 summarize these statistics. Since many of the cyclones tracking through Regions 1, 2, 3, and 5 were centered over the Gulf of Mexico or Atlantic Ocean, true analyses of maximum precipitation locations cannot be determined due to the lack of data over water. Region 4 is the only area where
precipitation was recorded in all quadrants surrounding the storm centers.

Maximum precipitation locations in Region 1 predominantly occur to the northeast of cyclone centers (Fig. 2.19a). Moderate intensities dominate, appearing throughout the observed occurrence region. A band of moderate to heavy precipitation is found approximately 400-500 km northeast to east of the origin. Light precipitation totals appear due north, at a range of from 150-900 km. Storms in Region 2 (Fig. 2.19b) display

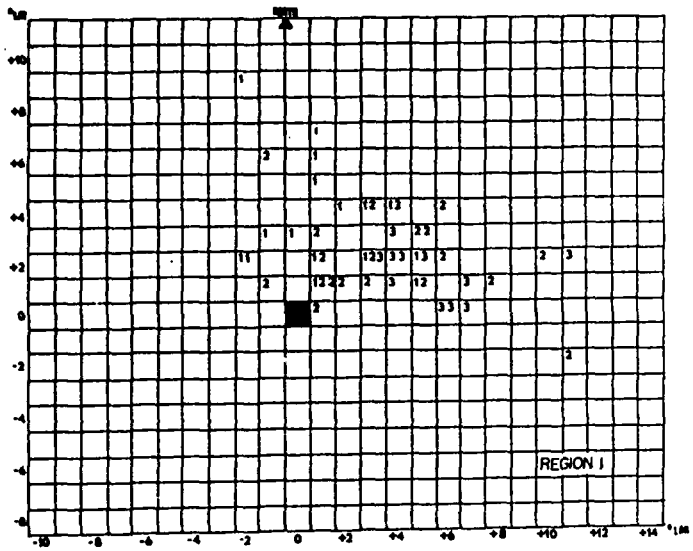

a

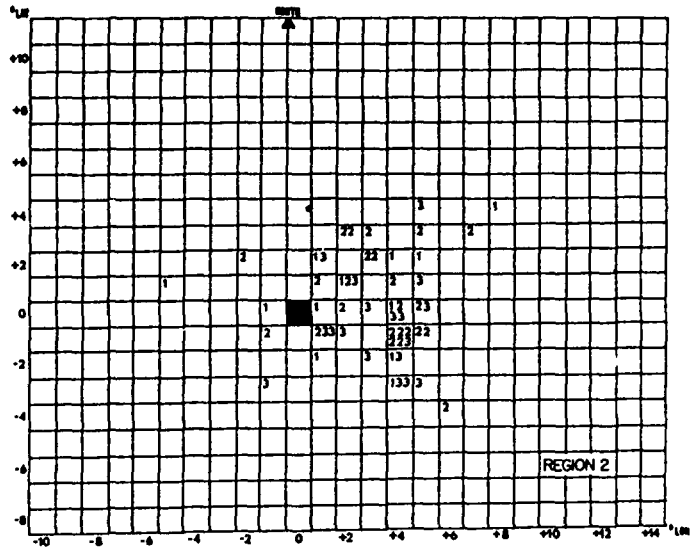

b

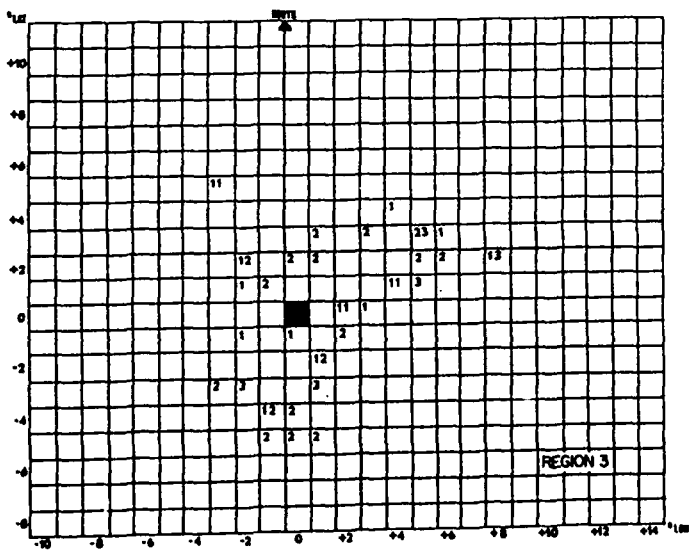

c

Figure 2.19 (a-c) Locations of individual storms' 6-hour precipitation maxima with respect to storm center (shaded block). (a) For Region 1 centers, (b) for Region 2, and (c) for Region 3. Intensity coding: 1 ≤ 25 mm; 2 = 26-50 mm; and 3 ≥ 51 mm.

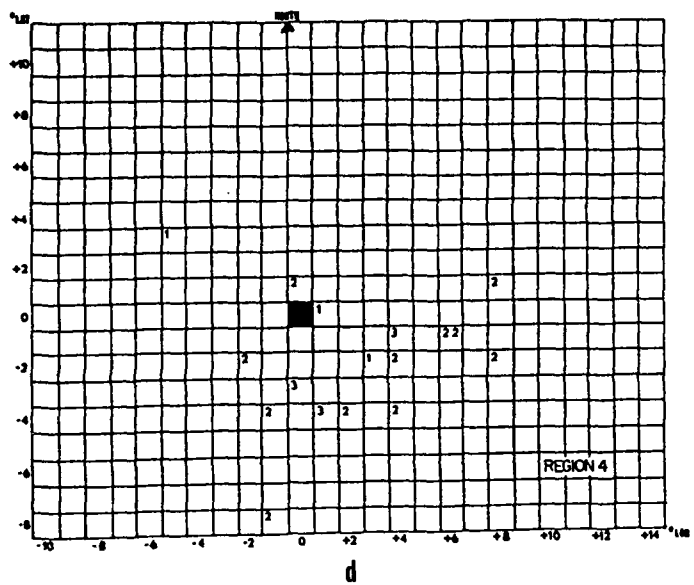

d

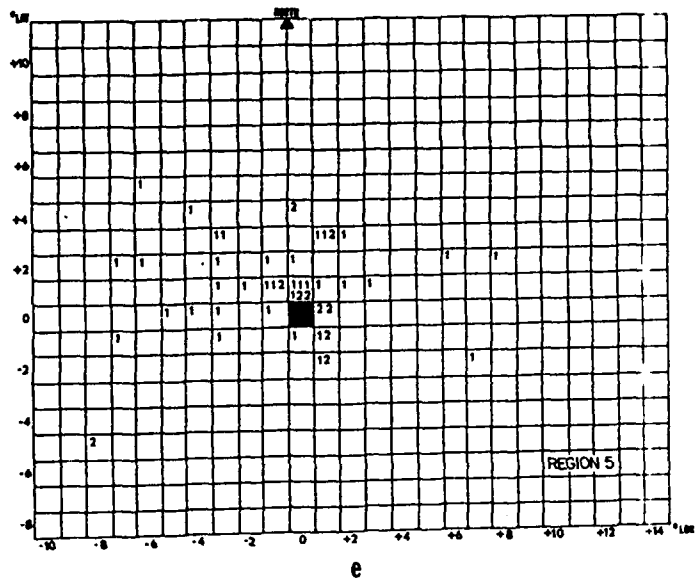

e

Figure 2.19 (d-e) Same as Fig. 2.19 (a-c), except for Regions 4 and 5, respectively.

TABLE 2.6

Maximum Precipitation Intensity Statistics (By Region)

REGION	INTENSITY CATEGORY	OCCURRENCES	% OF REGIONAL TOTAL	% OF TOTAL
	1	16	34	
1	2	19	40	
	3	12	26	
	1	12	23	
2	2	24	46	
	3	16	31	
	1	16	42	
3	2	17	45	
	3	5	13	
	1	3	18	
4	2	11	64	
	3	3	18	
	1	35	78	
5	2	10	22	
	3	0	0	
	1	82		41.5
ALL	2	81		40.5
	3	36		18

precipitation patterns shifting east and south of those in Region 1. Moderate intensities again dominate this region, with occurrences of heavier amounts surpassing the lighter totals by 8%. A moderate to heavy band of precipitation totals appears 350-600 km east to southeast of the origin, with a secondary band located approximately 100-250 km from east-southeast to northeast of the origin.

Light precipitation totals become more prevalent in Regions 3 and 5 as storm centers reach the Atlantic coast, and it is likely that the heaviest precipitation occurs off the coast in the warm sectors of storms where no data is available. A band of precipitation maxima is located northeast to south of the origin in Region 3 (Fig. 2.19c). This band coincides with the edge of the Atlantic coast from North Carolina to Georgia. Light to moderate totals far surpass the heavier amounts found in Regions 1 and 2, again due to the lack of data where heavier amounts would be expected to occur. Cyclones in Region 4 usually have reached their mature stage of development, and the flow pattern which helped push Gulf of Mexico moisture into the warm sector begins to weaken as the storms track further from this moisture source. This may explain the lack of heavy precipitation occurrences north of the origin (Fig. 2.19d). Light totals dominate and occur primarily north and west of storm centers in Region 5 (Fig. 2.19e), with a density maximum of light to moderate amounts occurring from northwest to southeast of the centers at a range of approximately 75-150 km.

2.4.4 Storm Track Precipitation Totals

The analytical and statistical findings discussed thus far have addressed precipitation distributions and storm totals across various regions of the southeast United States. These generalizations are useful on the synoptic scale, but local weather forecasters wish to know how much precipitation can be expected for their station and local area from cyclones following a particular track. Some pertinent information from the climatological study that may be helpful is obtained as follows. Speeds for each storm track from Table 2.3 were used to subdivide the legs in Fig. 2.4 into hourly increments. Figures 2.7, 2.11, and 2.15 were then used to determine hourly totals (contour values divided by six) for selected stations during each hourly increment. The appropriate precipitation distributions (by track and region) were overlayed onto the matching hourly increment tracks, and precipitation amounts were totaled for each station. As storms traveled from one geographic region to another, corresponding mean precipitation distribution charts were used so that the evolving precipitation field determined the total precipitation for the selected

stations.

The 14 stations for which these storm totals were determined are shown in Fig. 2.20a, and the contoured results (with precipitation totals listed for each station) appear in Figs. 2.20b-d. Track B cyclones produce the heaviest precipitation totals of the three tracks, and these totals appear across Mississippi, Alabama, and northern Georgia (Fig. 2.20c).

The tongue of maximum precipitation extending across the Appalachians into North Carolina and Virginia suggests that Miller's Type B cyclones that form along the Atlantic coast as discussed in Section 2.4.1 are responsible for this feature. Storms in Track C (Fig. 2.19d) produce higher precipitation totals than those in Track A due in part to the slower speeds of Track C cyclones and greater mean 6-hour precipitation totals (Fig. 2.15). The strong precipitation contour gradient from a maximum of 39.4 mm at Atlanta to 13.0 mm at Nashville indicates Gulf of Mexico moisture has not advected as far north as for Track B lows.

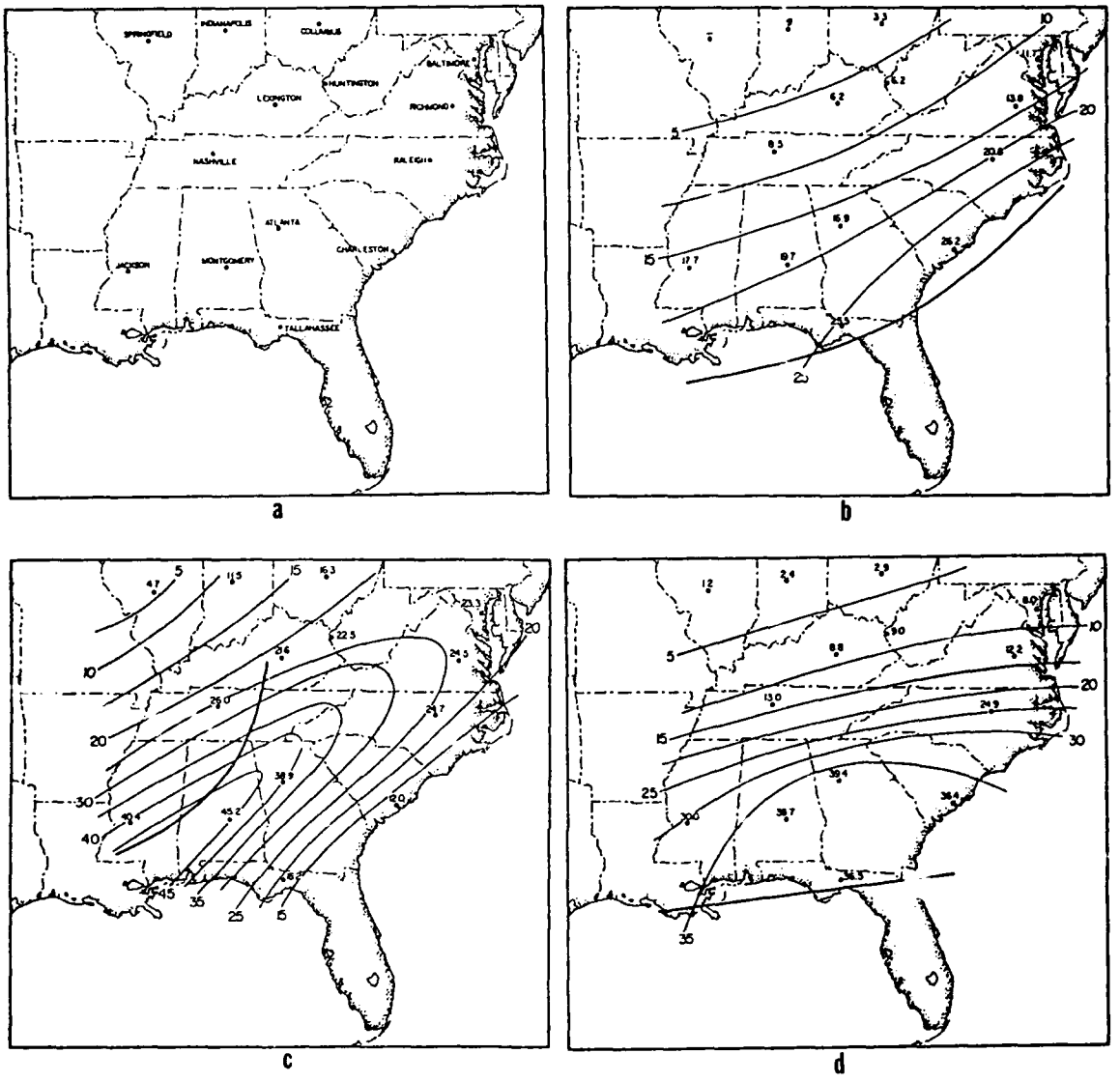

Figure 2.20 (a) Stations used for calculating precipitation totals along storm tracks. (b) Total precipitation contours (mm) for Track A lows. Track A indicated by heavy line. (c) Same as (b) for Track B lows. (d) Same as (b) for Track C lows.

3. CASE STUDY

3.1 GALE Project and Data

The field phase of the GALE project was conducted from 15 January to 15 March 1986. The objectives of GALE were to study mesoscale precipitation and air-sea interaction processes in East Coast winter storms, with their particular contributions to cyclogenesis (Dirks et al., 1988). The period of 10-11 February 1986 [Intensive Observing Period (IOP) 5] is one of the few cases during GALE in which a surface low develops over the coastal region of the Gulf of Mexico and moves across the southeast United States to the North Carolina coast. Study of this low provides a unique opportunity to examine the synoptic and mesoscale features affecting the precipitation distribution patterns for lows following paths close to Track A, discussed in Chapter 2. The data for this research consisted of a combination of standard observations with special observations at NWS and military stations and special sites operated specifically for the GALE field program. The GALE observing network consisted of soundings, surface measurements, ships, aircraft and radar operations, and satellite systems.

Fig. 3.1a depicts the general data-gathering region of interest. Two areas were of particular significance for this research. An inner GALE area in eastern North and South Carolina and adjacent coastal waters was approximately 500 km wide and extended 1000 km from the Georgia to Virginia borders. Portable-Automated Mesonet (PAM) II, Doppler radars, ships, buoys, most aircraft flights, and the Cross-chain Loran Atmospheric Sounding System (CLASS) rawinsonde sites were deployed in this area. The meso-α dynamic processes contributing to the precipitation distribution patterns for the IOP 5 surface low were studied using data from the inner area. The surrounding regional GALE area was 1,000 km wide (from the ridge of the Appalachians to 500 km offshore), and 1,500 km long (from Florida to New Jersey). Data from this region was designed to supplement the detailed data network found in the inner area.

An outline of the data-gathering facilities used in this research is provided below:

a) Surface measurements

The surface measurements were designed to provide surface data fields of standard meteorological variables within the inner GALE area with mesoscale resolution and to provide a complement to the data gathered through sounding operations. Routine standard measurements included air and dewpoint temperatures, barometric pressure, and wind speed and direction. Land-based stations also measured precipitation, and sea-based

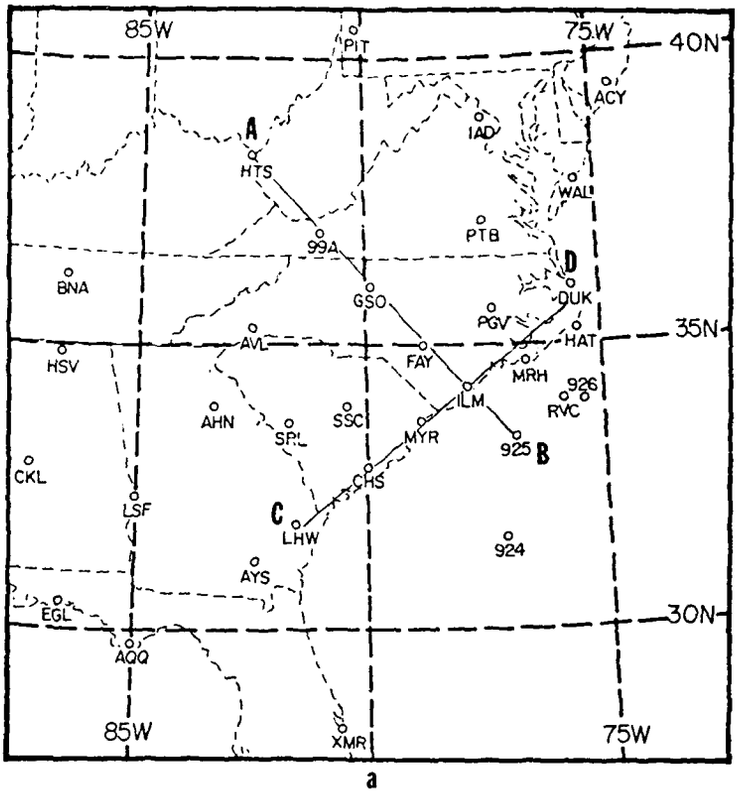

Figure 3.1 (a) Inner and Regional GALE Area rawinsonde network. The Inner Area extends from LHW-SRL in the southwest to WAL in the northeast. The Research Vessel Cape Hatteras (RVC) and dropwinsonde locations 924, 925, and 926 also shown. Cross-section lines A-B and C-D referred to in Figs. 3.16 and 3.17, respectively. (b) Location of surface observation sites, including the 50-station PAM-II network (numbered).

stations also measured sea surface temperature.

The 50-station PAM II network (Fig 3.1b), with an average spacing of 68 km, provided 5-minute meteorological surface observations over the eastern half of North and South Carolina and southeastern Virginia. Observations included air temperature, wet-bulb temperature, wind speed and direction, surface pressure, and precipitation amount. This network combined with the NWS routine observation sites aided significantly in locating surface features for this research. Deployment of the eight special GALE buoys (six North Carolina State University buoys, and two NOAA-E buoys) augmented observations in the data-sparse oceanic region of the inner GALE area.

b) Upper air measurements

The GALE sounding operations were designed to provide three-dimensional fields with time resolution adequate to resolve the structure and evolution of mesoscale weather systems in the GALE observational network. The land network consisted of CLASS and other specially placed rawinsonde systems with a spacing about one-third the standard U.S. network. In addition, soundings were obtained at two ship locations and by U.S. Air Force and GALE dropwinsonde flights off the coast of the Carolinas (Fig. 3.1b). The normal U.S. network would, on special request, join the GALE sounding network in providing 3-hourly soundings. GALE research aircraft would also supply in-flight data along planned tracks.

c) Other measurements

Radar and satellite data provided useful descriptions of the cloud and precipitation fields. The standard NWS network of 10 radars provided coverage of the regional and inner GALE areas. The meteorological satellites in operation during GALE were: GOES-6, NOAA-9, NOAA-6, DMSP F-6, DMSP F-7, and NIMBUS-7.

3.2 Barnes Objective Analysis

The analysis of meteorological fields, especially those to be used in computations, was aided by the Barnes (1964, 1973) objective analysis method. This widely-employed scheme accepts data from observation points and mathematically interpolates to any desired point in the geographic region. In particular, the scheme is used to obtain values at points in a two-dimensional grid array to be used in finite-difference calculations. If q represents any meteorological variable, the interpolated value is just the weighted mean ($\bar{q}$) of observations surrounding the point. That is,

$$\bar{q} = \frac{\sum_{i=1}^{N} w_i q_i}{\sum_{i=1}^{N} w_i}.$$

Here, N is the total number of stations influencing a given grid point. The observation weights (w) are inverse distance (d) dependent and are defined by

$$w = \exp(-d^2/k).$$

Here, k is the weight parameter and controls the rate at which the weight value decreases outward from the point of interpolation. Hence, k determines the degree of smoothing of the data field with small k providing little smoothing and large k for a greater smoothing.

The selection of k is therefore crucial to the structural detail remaining in the interpolated field. The choice of this parameter value must strike a balance between an attempt to retain as much detail as the observation network density allows, and filtering out sources of random error. Structural detail is limited by the minimum resolvable wavelength. The GALE PAM-II stations have a mean spacing of about 68 km, while the upper-air stations of the Inner GALE sounding (including NWS and CLASS) network have an average separation of about 180 km. These distances are about one-half those of the normal operational reporting networks. Theoretically, the Inner GALE networks can resolve features of twice the respective mean station separations, or about 140 km at the surface and 360 km aloft.

The weight parameter k is selected to reflect the degree of credibility given amplitudes of the minimally-resolved waves, that is, the signal to noise ratio of the observations at small wavelengths. The specific k values used in this application suppress the amplitudes of the two-station-spacing waves to only 10 percent of their original amplitude (that is, a response function of 0.1) in the belief that error does make a significant contribution to the amplitudes of the higher frequency features. Sources of "error" include turbulent fluctuations with periods of several minutes (especially near the ground), biases introduced by local topography and obstacles at observation sites (again, especially important for surface stations), and features on scales smaller than the station spacing (e.g. gravity waves). The appropriate k values are 2000 and 7500 km^2 for surface and upper-air analyses, respectively.

In spite of apparent strong smoothing, the interpolated fields still reflect features one would be inclined to accept if done subjectively by a skilled analyst. In particular, sharp discontinuities like frontal zones are well represented in wind and temperature fields. The Barnes scheme was applied specifically for calculating vorticity, divergence, and vertical motion fields within the mesoscale area of interest (Figs. 3.1a and b) and for the broader synoptic scale analyses.

3.3 Synoptic Overview

Moist southwesterly flow dominated the eastern half of the United States at 1200 GMT 10 February from 850 mb to 300 mb, with an 850 mb low centered over central Texas (not shown). A 300 mb jet streak extends from southwest Texas to eastern Massachusetts, with winds exceeding 65 ms^{-1} over Ohio (not shown). The 500 mb analysis shows cyclonic horizontal wind shear over southern South Carolina and the Georgia coast contributing to a weak vorticity maximum in this region (Fig. 3.2a). Another weak maximum is found over western Alabama. At the surface, a weak low pressure center off the North Carolina coast with a trough extending southwest towards the South Carolina coast produced light rain and fog (Fig. 3.2b). A weakening high pressure system centered over southeast Pennsylvania prevented precipitation from spreading north of South Carolina along the coast. Cold frontolysis occurred over the Appalachians, while weak cyclogenesis over western Florida generated convective activity over the warm front. Light snow was falling west of the weakening cold front as light rain, drizzle, and fog occurred north of the warm front.

By 0000 GMT 11 February, the 850 mb low (not shown) was centered over western Tennessee and had deepened 50 meters. Warm air advection was strongest at this level over the Appalachians of West Virginia and Tennessee, and weaker at 700 mb and 500 mb. A 300 mb jet maximum of 75 ms^{-1} was located over western New York or along a jet streak extending from western Mississippi to the Massachusetts coast (not shown). The 500 mb analysis shows three vorticity maxima at this time (Fig 3.3a). The maxima centered over southwest Oklahoma near the trough axis is associated with the surface low located in central Alabama (Fig. 3.3b). This low developed during the previous six hours and it is the storm of interest in this study. The two lows located in the Gulf of Mexico at 1200 GMT 10 February weakened and diminished. Thundershowers, light rain, and fog spread ahead of the cold front and along the stationary frontal boundary, and light rain, drizzle, and fog extends northward into southwest Virginia. An inverted trough (the

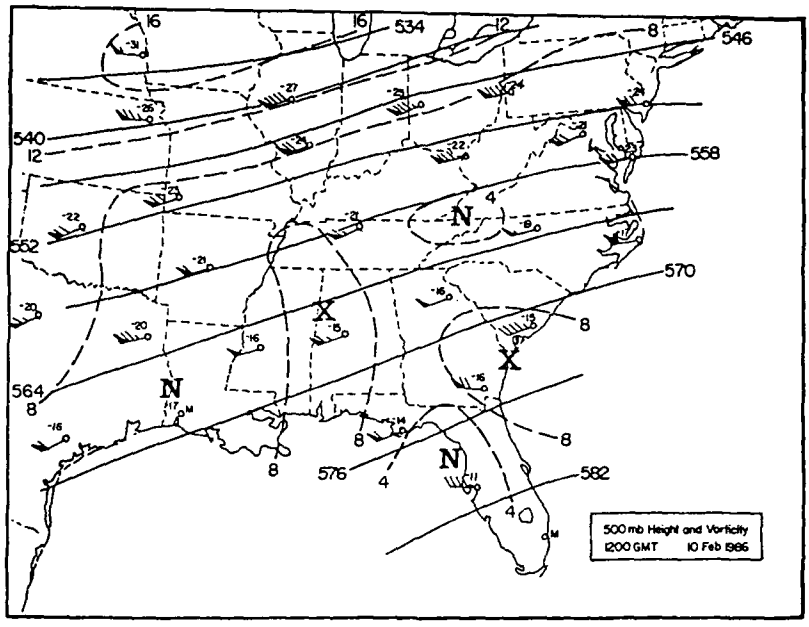

a

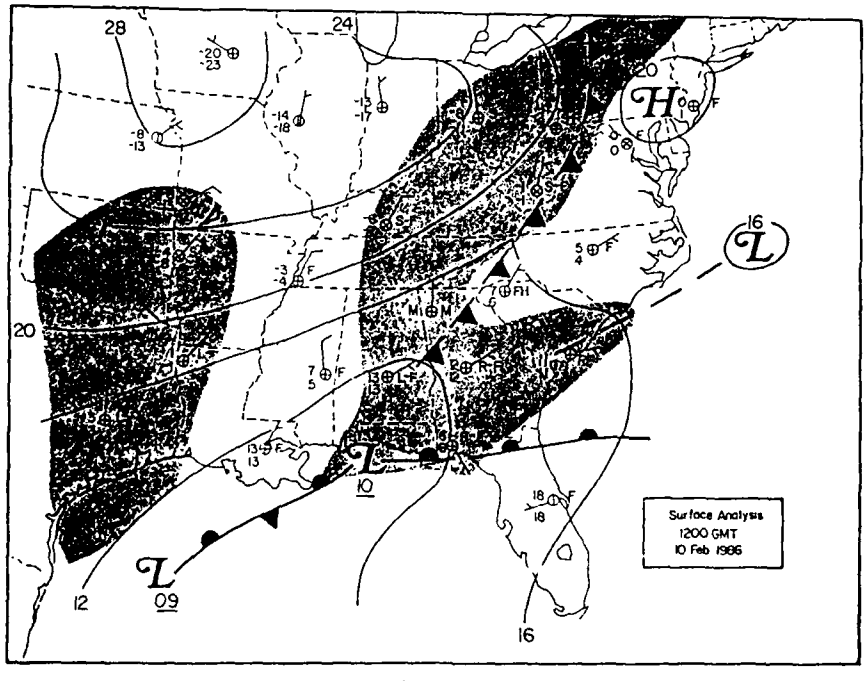

b

Figure 3.2 (a) 500-mb analysis for 1200 GMT 10 February 1986. Heights are solid (570=5700 m) and the "X" and "N" denote locations of vorticity maxima and minima ($x10^{-5}s^{-1}$) respectively. Station reports include temperature (^{o}C) and wind velocity (barb=$5ms^{-1}$; pennant=$25ms^{-1}$). (b) Surface frontal analysis for 1200 GMT 10 February 1986. Station reports include temperature and dewpoint (^{o}C), observed weather, cloud cover, and wind velocity (depicted as in (a)). Central pressure denoted by underlined value (10=1010 mb) if different from nearest isobar. Shading depicts area of precipitation.

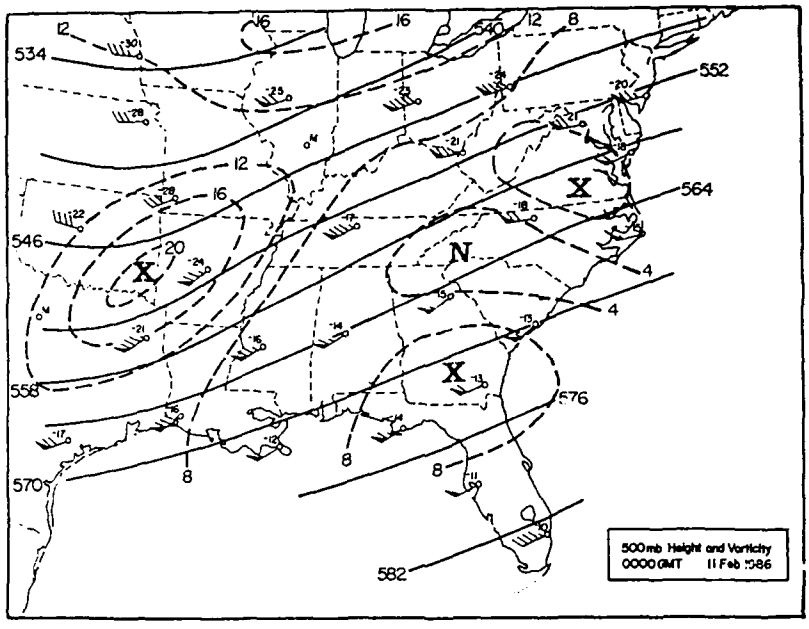

a

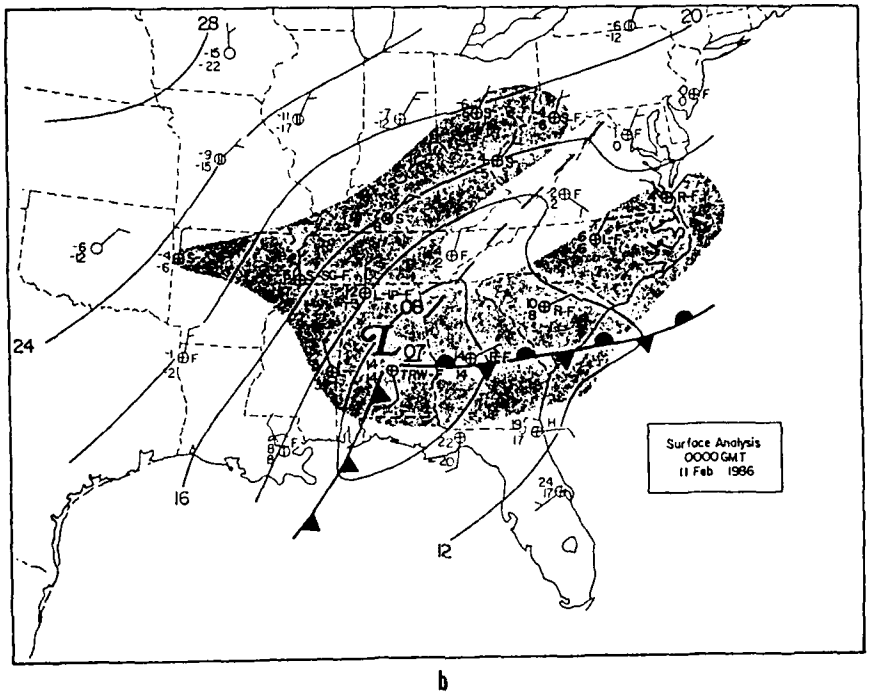

b

Figure 3.3 (a) and (b) Same as in Figs. 3.2 (a) and (b), respectively, except for 0000 GMT 11 February.

remains of the cold frontolysis line in Fig. 3.2b) extends from the low center, over the Appalachians, and into western Maryland, with light snow and freezing precipitation falling west of the trough. Though this synoptic picture appears to have the characteristics of cold-air damming along the lee of the Appalachians, note the warmer temperatures east of the mountains when compared with those to the west. Also, the section of the stationary front extending off the South Carolina coast does not exhibit the characteristics of a typical coastal front associated with cold-air damming.

The 500 mb trough axis shifts eastward, west of the Mississippi valley and the dominant vorticity maxima is centered over West Virginia at 1200 GMT 11 February (Fig. 3.4a). The 850 mb low has moved over southwestern Virginia with strong cold-air advection approaching western North Carolina, central South Carolina, and Georgia. The 300 mb jet maximum at 0000 GMT has advanced eastward off the New England coast, while a new 65 ms^{-1} maximum was located in southwesterly flow over Alabama (not shown). At the surface, high pressure builds towards the east from a Great Plains ridge (Fig. 3.4b). The surface low over Alabama at 0000 GMT has moved into southeastern North Carolina at this time, and cyclogenesis along the Virginia and northern North Carolina coast resulted in the development of a second low. Convective activity continued along and ahead of the cold front in Georgia and Florida, with mostly light rain, drizzle, and fog occurring in a broad band from the coastal regions of the Carolinas and Virginia to the Appalachians. Precipitation changes to snow from northern Virginia northward and west of the Appalachians behind the cold front.

Figures 3.5a to 3.5c depict the infrared satellite imagery for 1301 GMT 10 February, 0001 GMT and 1101 GMT 11 February, respectively. Widespread cloudiness is found along the frontal boundaries in the Gulf coastal states in Figs. 3.5a and b. Note the increase in convective activity by 0001 GMT 11 February (denoted by the colder cloud tops) surrounding the stationary front from the Florida panhandle to the South Carolina coast and the lower stratiform cloud coverage extending into Virginia. At 1101 GMT 11 February, clearing skies are seen behind the cold front (Fig 3.5c). Colder cloud tops are depicted over northeastern North Carolina between the two low pressure centers seen in the surface analysis of Fig. 3.4b.

3.4 Mesoscale Analysis

The mesoscale distribution of precipitation surrounding the surface cyclone was studied as it traveled from central Alabama to the North Carolina coast to determine how the

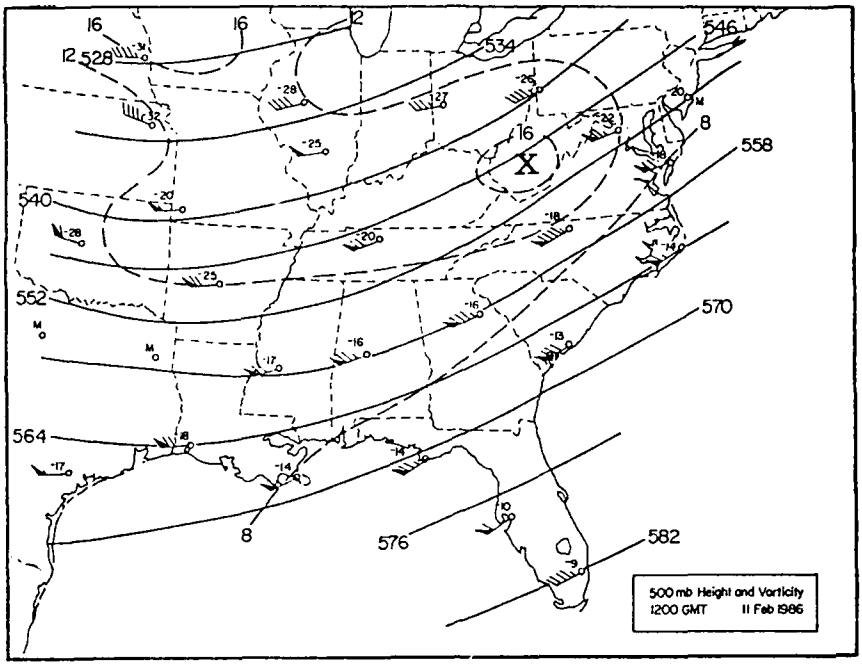

a

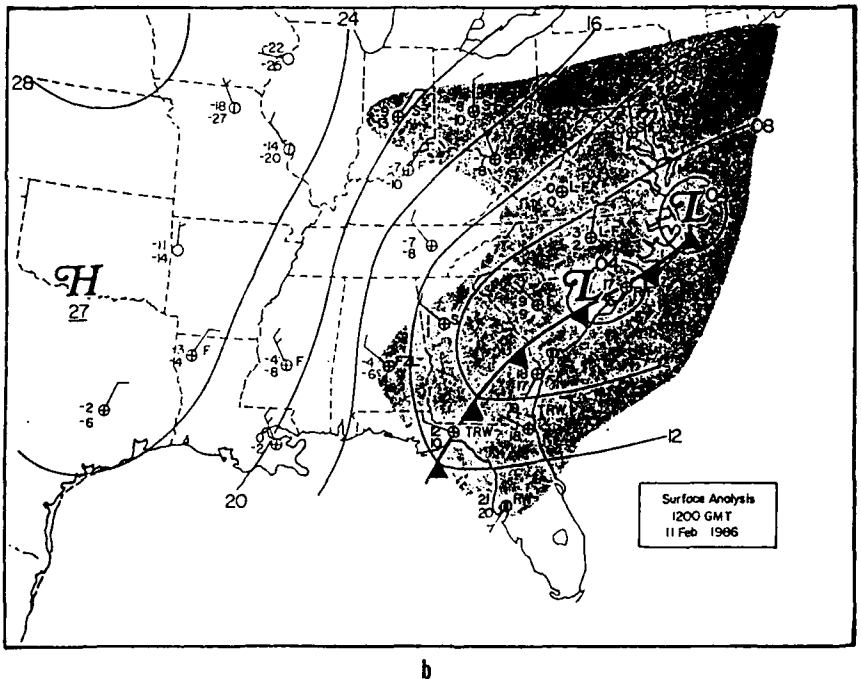

b

Figure 3.4 (a) and (b) Same as in Figs. 3.2 (a) and (b), respectively, except for 1200 GMT 11 February.

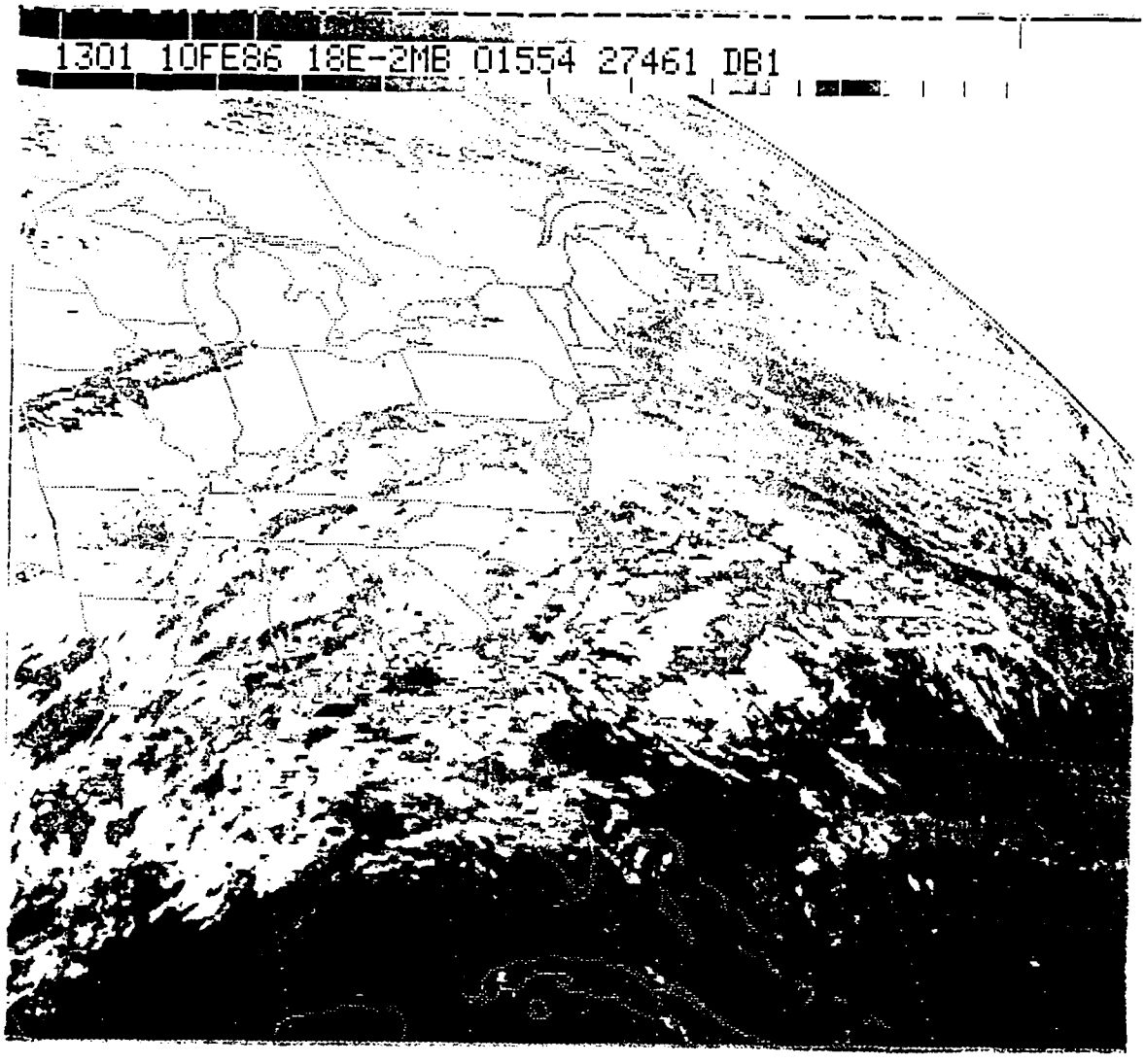

Figure 3.5 (a) Infrared satellite image at 1301 GMT 10 February 1986.

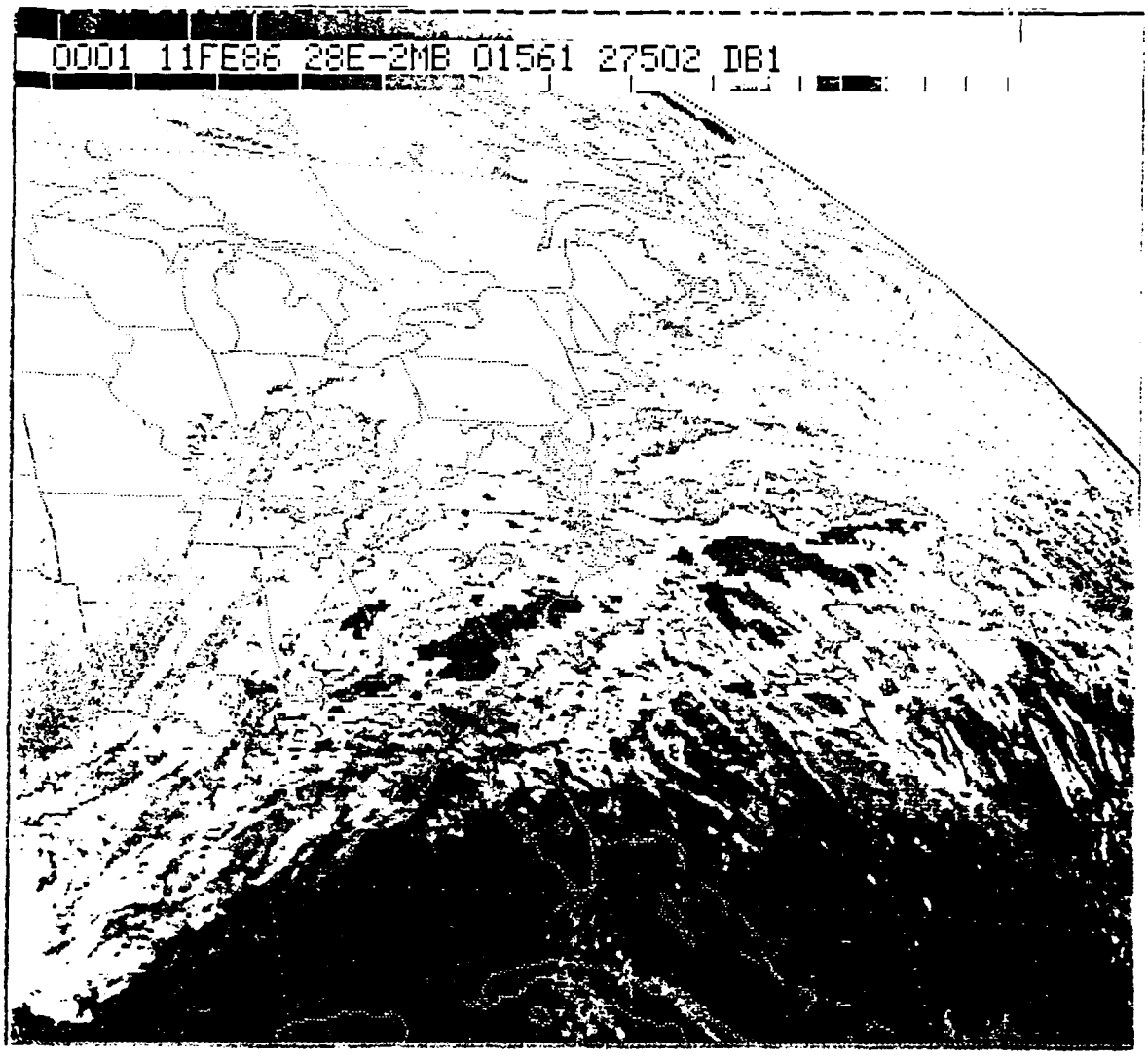

Figure 3.5 (b) Same as Fig. 3.5a, except for 0001 GMT 11 February.

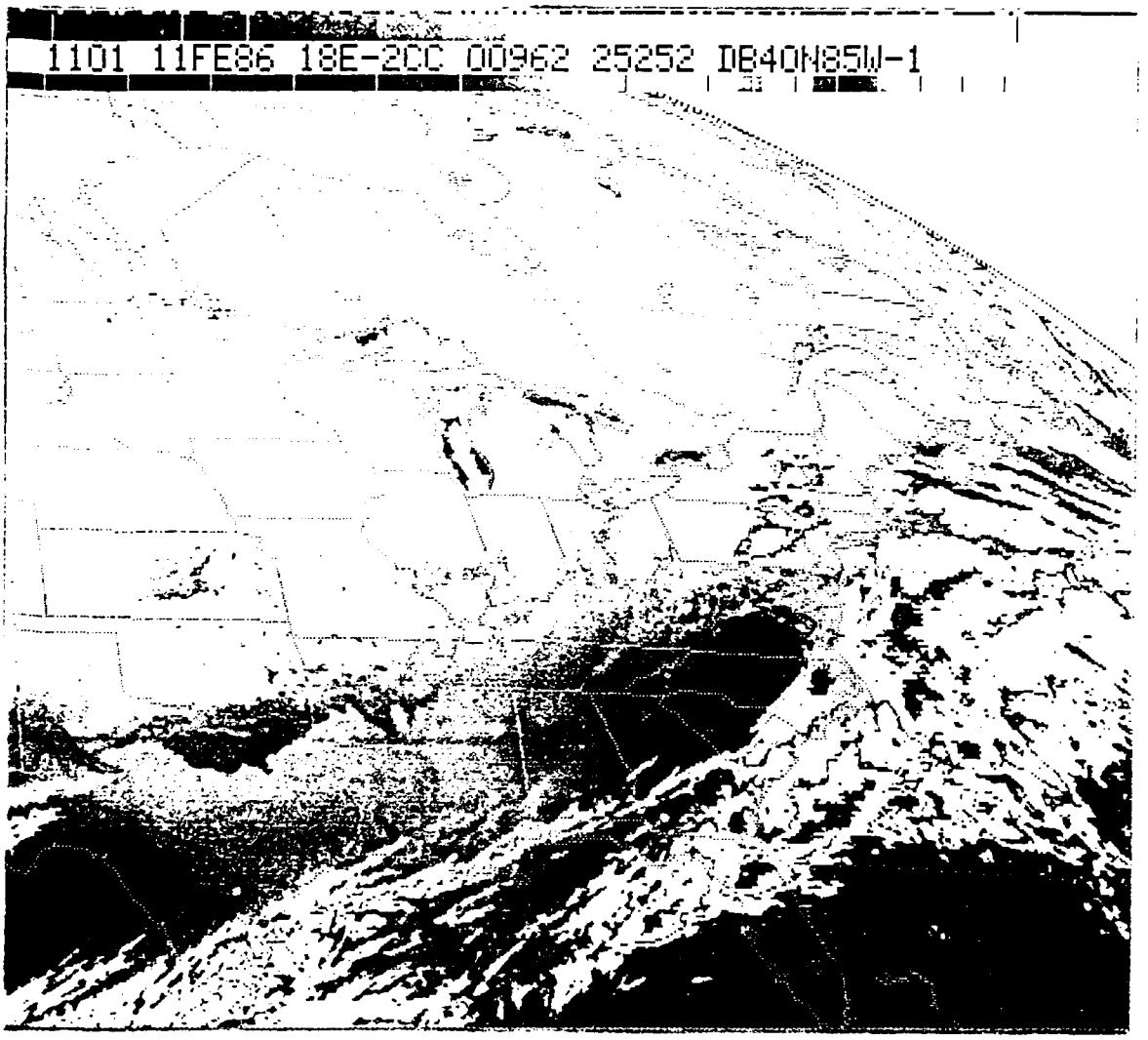

Figure 3.5 (c) Same as Fig. 3.5a, except for 1101 GMT 11 February.

circulation field related to the observed precipitation patterns. Maximum precipitation totals of more than 25 mm occurred across sections of Alabama, Georgia, and northern Florida for this storm, while totals generally were less than 15 mm across the PAM-II observation area. An attempt is made to explain why the Carolinas received lighter precipitation totals, considering the storm's track through the heart of the region.

3.4.1 500 mb and Surface Analyses

The inner and regional areas of upper-air data provide better data resolution of the pressure systems aloft than does the routine National Weather Service (NWS) sounding network. Soundings taken at 0300 GMT, 0600 GMT, and 0900 GMT 11 February provided the data for the 500 mb height and vorticity analyses shown in Figs. 3.6a to 3.8a. The general trend was for height falls during the 6-hour period (0300 GMT to 0900 GMT) as the main 500 mb trough axis approached the eastern United States. Winds at 500 mb generally increased in speed along the North and South Carolina coast until 0600 GMT, then tapered off by 5 to 10 ms^{-1} as the next speed maxima approaches from the west.

The spacing of CLASS locations (Fig. 3.1a) allows for mesoscale resolution of the vorticity field across the Carolinas. The 0000 GMT and 1200 GMT 11 February 500 mb charts (Figs. 3.3a and 3.4a) show a vorticity maxima moving with the long-wave 500 mb trough. However, the CLASS network detected a secondary (but important) vorticity maxima passing through North Carolina from south to north by 0900 GMT. This maxima was located over southern Georgia at 0000 GMT (Fig. 3.3a), peaked in intensity at 0600 GMT over southeastern North Carolina, and tracked to the eastern North Carolina/Virginia border by 0900 GMT. The maxima was a good precurser of the cyclogenesis which occurs between 0900 GMT and 1200 GMT 11 February (see Fig. 3.4b).

The surface cyclone approached and passed through North and South Carolina between 0300 GMT and 0900 GMT 11 February. At 0300, the storm was centered over western Alabama, and an inverted trough extended from the center northeastward along the Appalachians (Fig. 3.6b). A quasi-stationary front extended eastward from central Georgia to the central South Carolina coast, with convective activity in southern Georgia and northern Florida. Light rain, drizzle, and fog was reported to the north of the frontal boundary. Weakening high pressure off the New England coast kept winds northeasterly in the colder air east of the Appalachians and north of the front. By 0600 GMT (Fig 3.7b), a secondary surface low developed along the inverted trough line still located over the

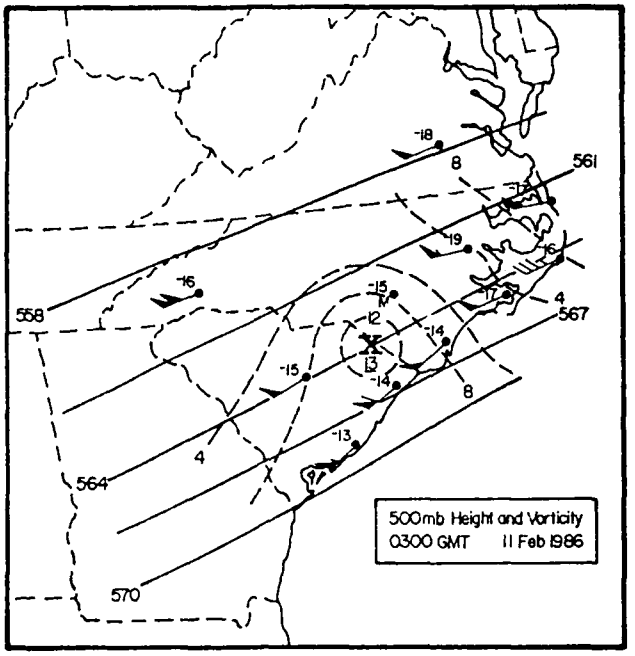

a

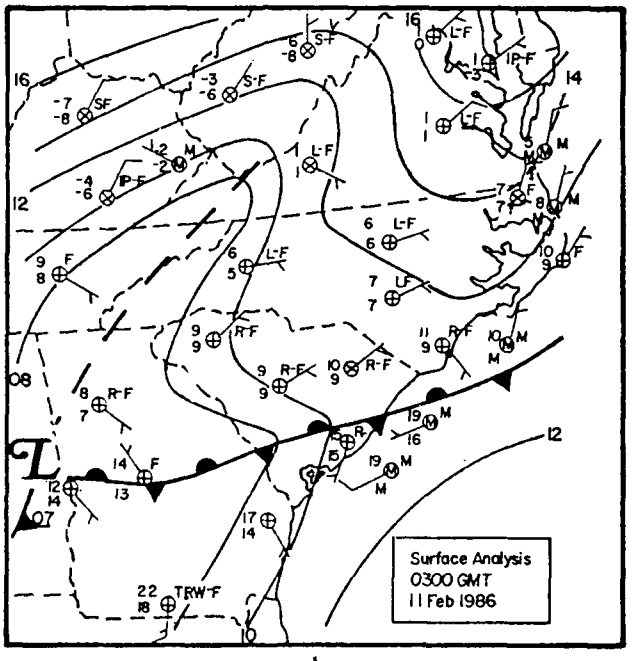

b

Figure 3.6 (a) and (b) Same as Figs. 3.2 (a) and (b), except for Inner and Regional GALE Area at 0300 GMT 11 February (precipitation shading omitted in (b)).

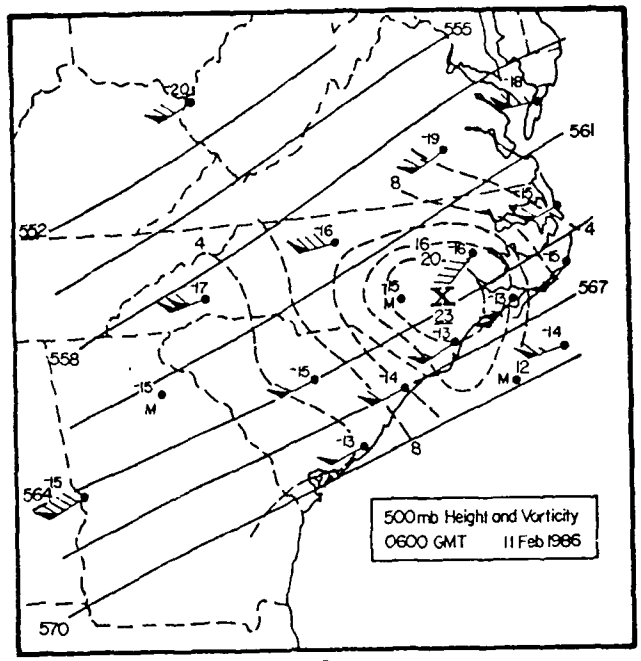

a

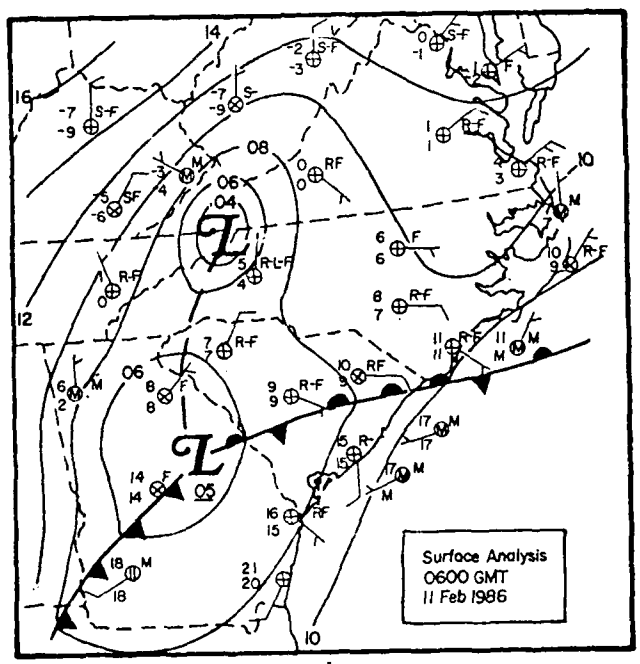

b

Figure 3.7 (a) and (b) Same as Figs. 3.6 (a) and (b), respectively, except for 0600 GMT 11 February.

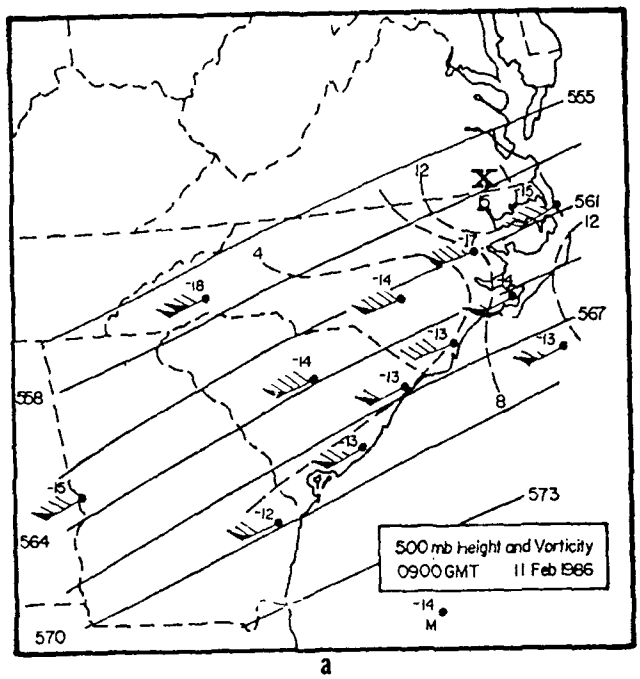

a

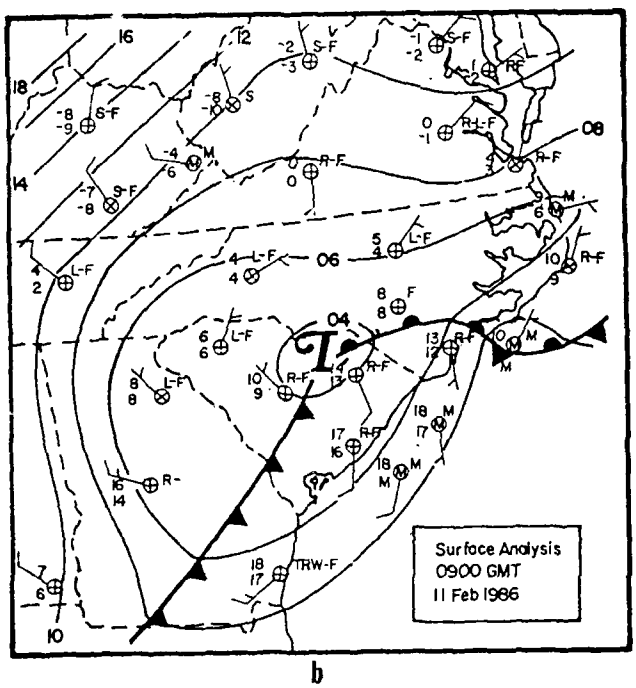

b

Figure 3.8 (a) and (b) Same as Figs. 3.6 (a) and (b), respectively, except for 0900 GMT 11 February.

Appalachians. This low filled by 0900 GMT 11 February. The quasi-stationary front developed characteristics of a warm-front from central South Carolina to the North and South Carolina coastal border. Steady rainfall occurred just north of the warm front. Light rain, drizzle, and fog continued to fall northward to central Virginia, changing to light snow and fog north of Washington, D.C. and west of the Appalachians.

The surface low advanced from eastern Georgia to north central South Carolina by 0900 GMT in Fig. 3.8b. Convective activity was observed ahead of the cold front in Georgia, and light rain and fog occurred in the warmer air mass located in eastern South Carolina and southeastern North Carolina. From 0300 GMT to 0900 GMT 11 February, the storm deepened by 3 mb with surface circulation becoming more cyclonic. A well-defined warm front existed eastward from the surface low to off the southeast North Carolina coast where it became stationary. Light rain, drizzle, and fog continued in the colder air north and west of the low, and light snow was falling west of the Appalachians eastward into northern Virginia at this time.

3.4.2 Evidence of the Gulf Conveyor Belt

A review of sounding data compiled from 0300 GMT to 0900 GMT 11 February within the inner and regional areas revealed the existence of a low-level jet between 900 mb and 700 mb. This jet was located approximately 100-300 km ahead of the surface cold front, approaching and eventually crossing, the quasi-stationary warm front. At 850 mb, the upper-level low center moved from southern Kentucky to southern West Virginia (Figs. 3.9a - 3.11a). Heights fell throughout the region with time, and the contour gradient tightened along the coast of the Carolinas at 0600 GMT and 0900 GMT (Figs. 3.10a and 3.11a). At 0000 GMT 11 February, the 850 mb jet (not shown) was found crossing the Florida panhandle heading into extreme southeastern Georgia. From 0300 GMT to 0900 GMT 11 February, this jet moves from south central Georgia to the Carolina coast, with warm air advection occurring along the jet axis.

Analyses of pressure, wind, and moisture on isentropic surfaces of 295^{o}K, 300^{o}K, and 305^{o}K aid in locating the level of this jet. The 300^{o}K surface revealed maximum wind speeds in excess of 35 ms^{-1} at 0600 GMT 11 February on both sides of the North and South Carolina coastal border (Fig 3.10b). Figs 3.9b to Fig. 3.11b shows that this low-level jet, or Gulf (of Mexico) Conveyor Belt (GCB), originated over central Georgia and moved off the Atlantic coast by 0900 GMT 11 February. These figures also display moist advection (defined here by higher mixing ratios) along the jet axis.

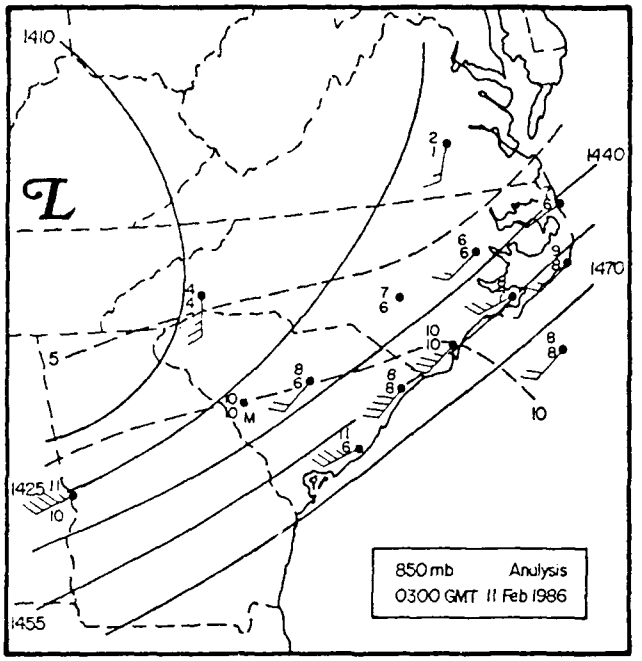

a

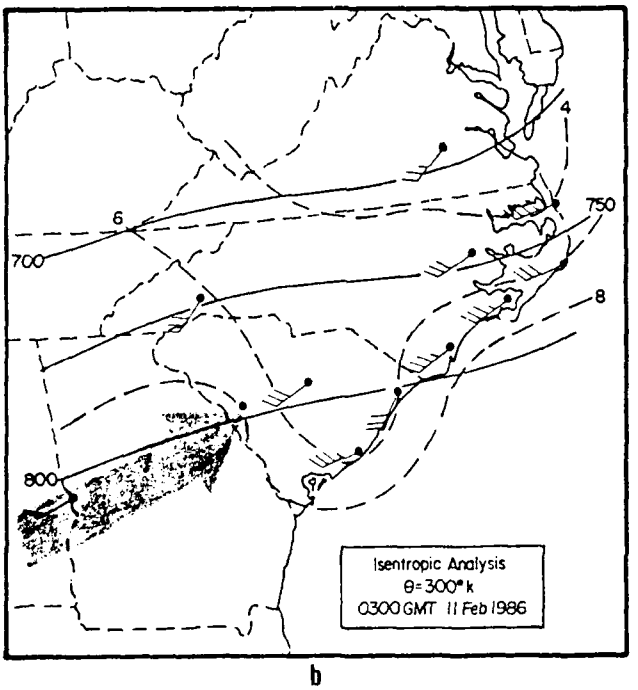

b

Figure 3.9 (a) 850-mb analysis for 0300 GMT 11 February 1986. Heights (*m*) are solid, and station reports include temperature and dewpoint (^{o}C) and wind velocity (barb=5ms^{-1}). Isotherms (^{o}C) are dashed. (b) Isentropic analyses of pressure, wind, and mixing ratio on the 300^{o}K surface at 0300 GMT 11 February: pressure (solid contours, mb); mixing ratio (dashed, gkg^{-1}); and wind (barb=5ms^{-1}, pennant=25ms^{-1}). Shaded arrow indicates axis of Gulf Conveyor Belt.

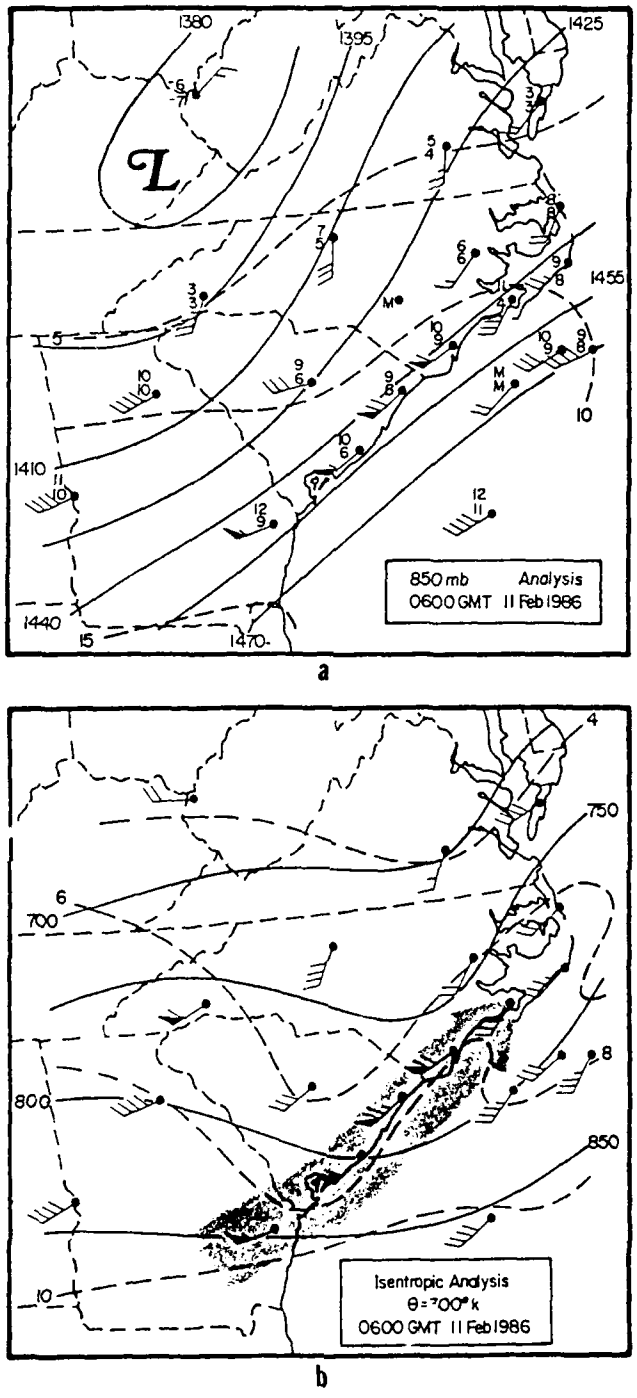

Figure 3.10 (a) and (b) Same as Figs. 3.9 (a) and (b), respectively, except for 0600 GMT 11 February.

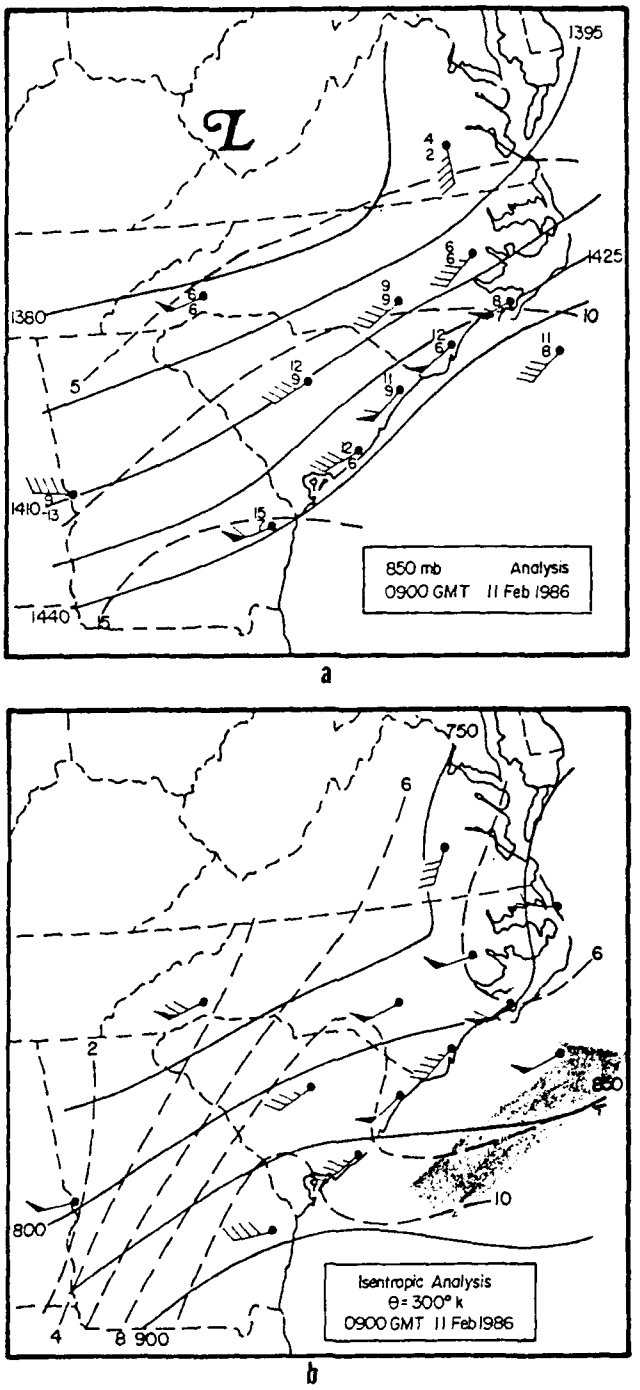

Figure 3.11 (a) and (b) Same as Figs. 3.9 (a) and (b), respectively, except for 0900 GMT 11 February.

Cross-isobaric flow along the jet axis (Figs. 3.9b and 3.10b) implies rising motion along the GCB until the northern edge of the jet streak is reached. An examination of precipitation patterns related to the location of the GCB follows.

3.4.3 Precipitation Distribution Analysis

HPD stations combined with hourly totals from the 50 PAM-II sites provide a dense network for depicting the precipitation patterns surrounding the storm as it passed across North and South Carolina. This network is shown in Fig. 3.12. Figures 3.13a-c show that maximum precipitation occurred in a narrow convective band stretching from southern Georgia into South Carolina from 0400 GMT to 0600 GMT 11 February (Figs. 3.13a-c). Note also how this band progressed eastward and northward, aligned with the GCB in Fig. 3.10b. Radar echoes at 0530 GMT (Fig. 3.13d) depict highest intensities over these areas of precipitation maxima. The infrared satellite imagery for 0600 GMT (Fig. 3.14) shows the convective area (cloud tops approximately 10.5 km) over southeastern Georgia into South Carolina with lower stratiform tops (at 7.5 to 9.0 km) over much of North Carolina. Note the band of higher cloud tops (9.0 km) from the Georgia thunderstorm northward to Cape Hatteras along the Gulf Conveyor Belt. After 0600 GMT, precipitation totals drastically decrease as the western edge of measurable precipitation advances eastward with the storm center and cold front (Figs. 3.15a-c). The 0830 GMT radar (Fig. 3.15d) shows highest echo intensities have moved off the coast, coinciding with the eastward movement of the GCB over the Atlantic Ocean in Fig. 3.11b.

3.4.4 Vertical Cross Sections

To illustrate the vertical atmospheric structure at the time the GCB is at its most pronounced along the Atlantic coast (0600 GMT 11 February), two cross-sections are presented. Soundings from Huntington, WV (HTS), Greensboro, NC (GSO), Fayetteville, NC (FAY), Wilmington, NC (ILM), and dropwindsonde location 925 were projected onto the cross-section line A-B shown in Fig. 3.1a. This line is oriented perpendicular to the GCB and passes through the quasi-stationary front off the coast at 0600 GMT. It is important to note that Fayetteville's wind readings (for the entire sounding) were inconsistent with winds at surrounding locations (Fig. 3.16). Also, station 99A was not reporting at this time. The other cross-section (C-D) is aligned parallel to the Atlantic coast and the GCB. This line passes through Fort Stewart, GA (LHW),

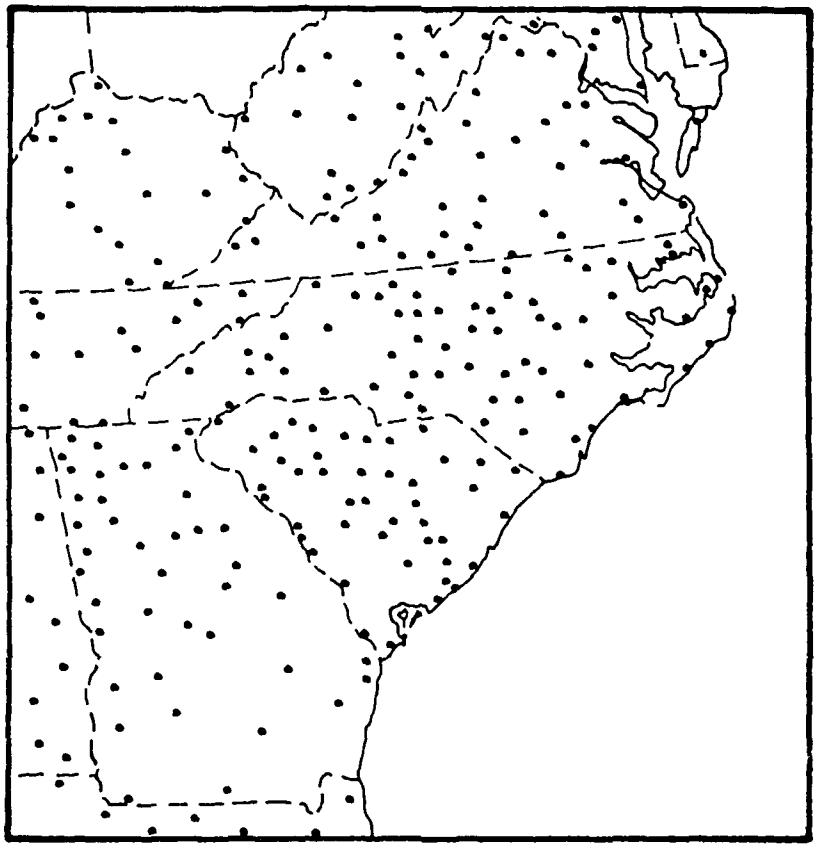

Figure 3.12 Hourly Precipitation Data stations including the 50-station PAM-II network.

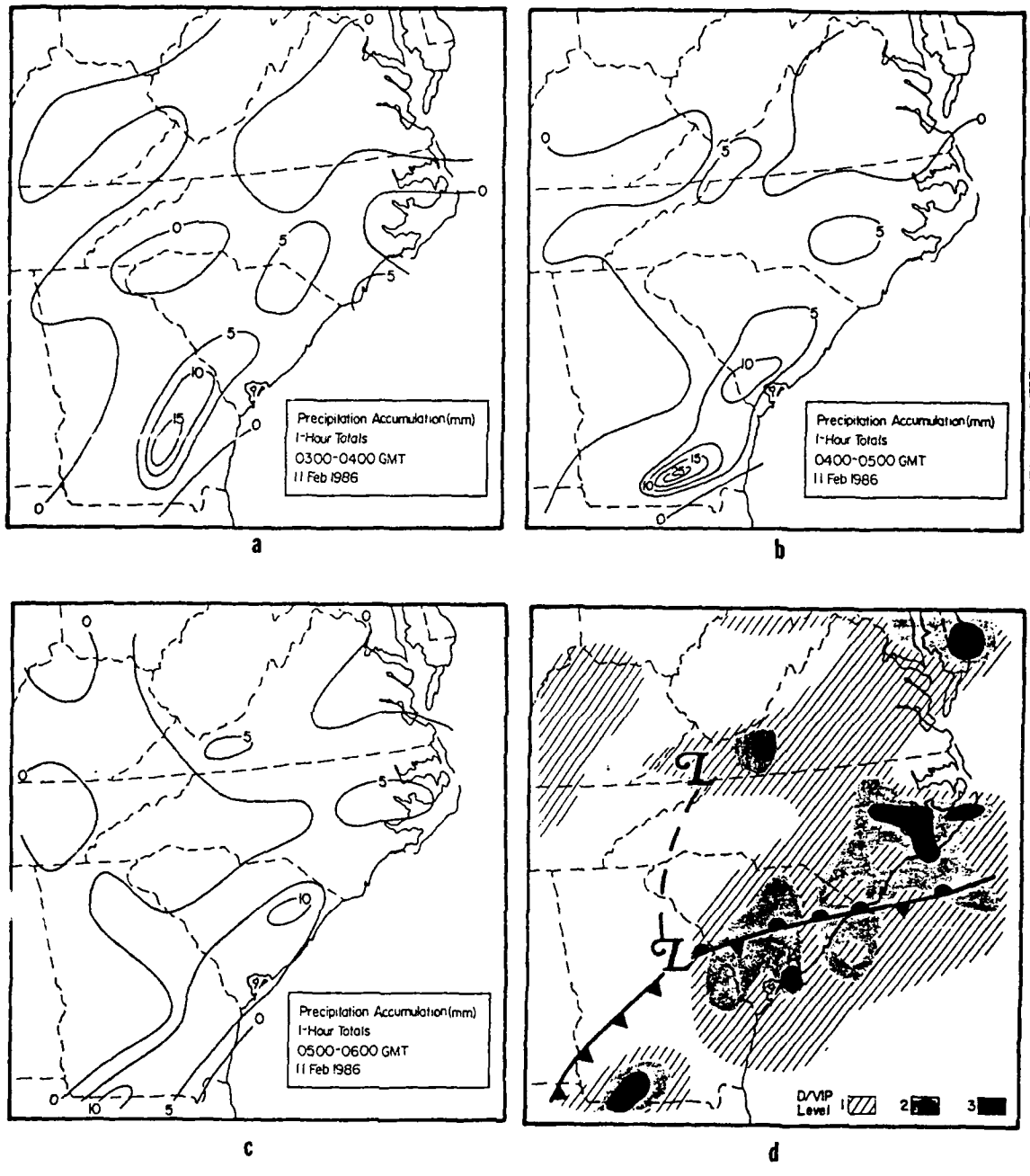

Figure 3.13 (a) Precipitation totals (mm) for the hour ending 0400 GMT 11 February 1986. (b) Same as (a) for hour ending 0500 GMT. (c) Same as (a) for hour ending 0600 GMT. (d) 0600 GMT 11 February 1986 surface frontal analysis with 0530 GMT radar intensities (D/VIP levels shaded) superimposed.

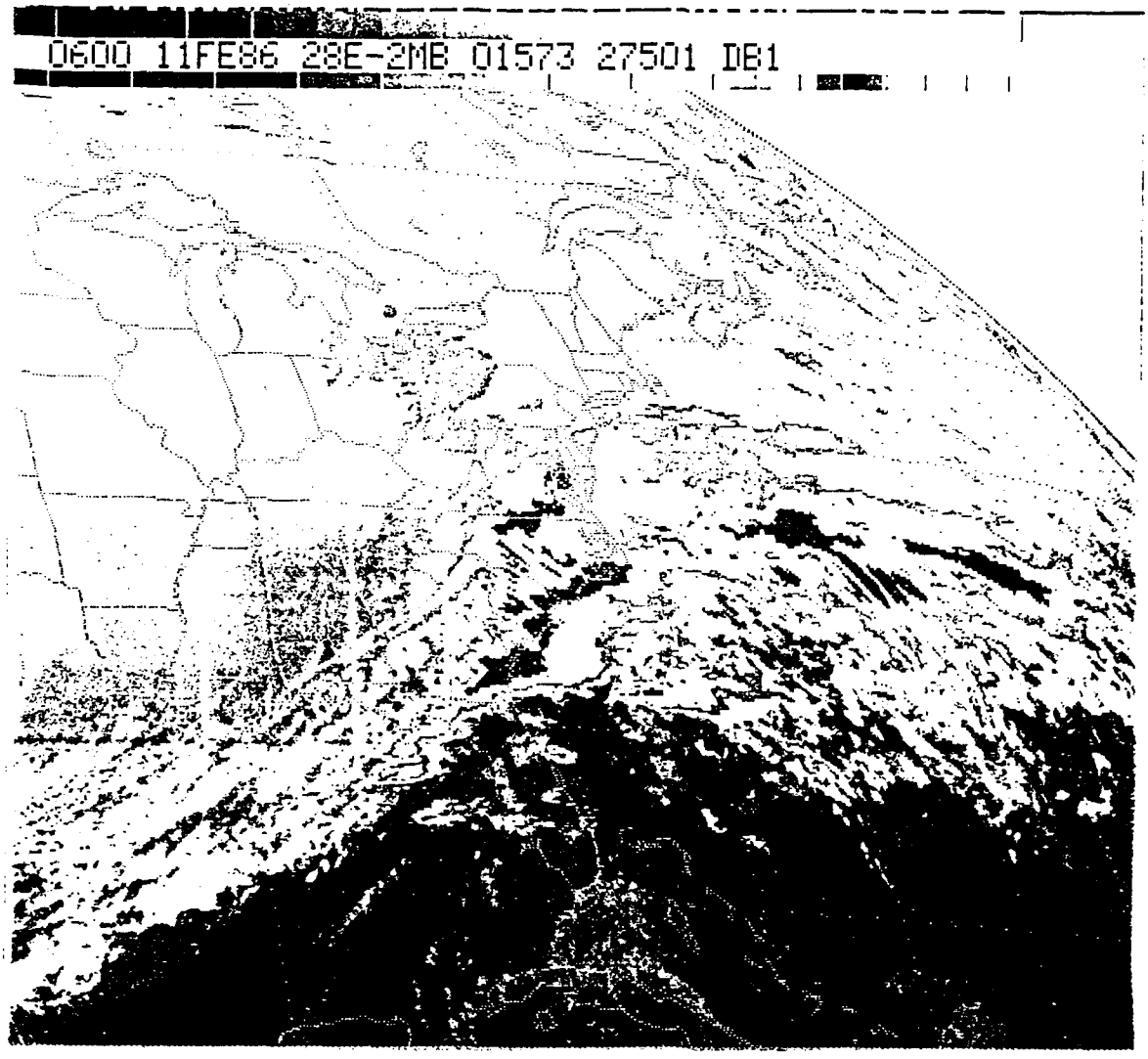

Figure 3.14 Same as Fig. 3.5a, except for 0600 GMT 11 February 1986.

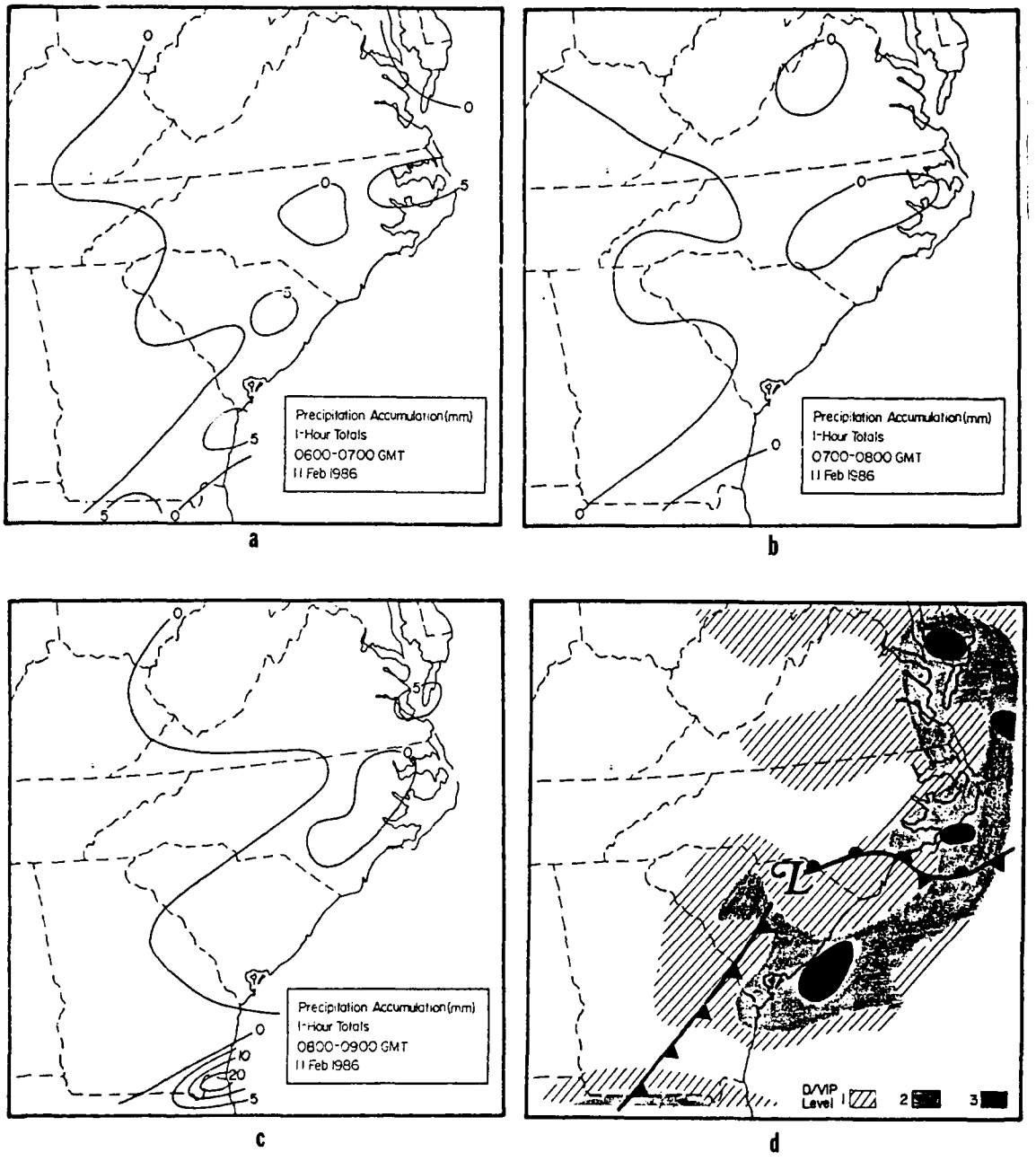

Figure 3.15 (a) Same as Fig. 3.13a, except for hour ending 0700 GMT. (b) same as (a), except for hour ending 0800 GMT. (c) Same as (a), except for hour ending 0900 GMT. (d) Same as Fig. 3.13d, except for 0900 GMT 11 February surface analysis and 0830 GMT radar intensities.

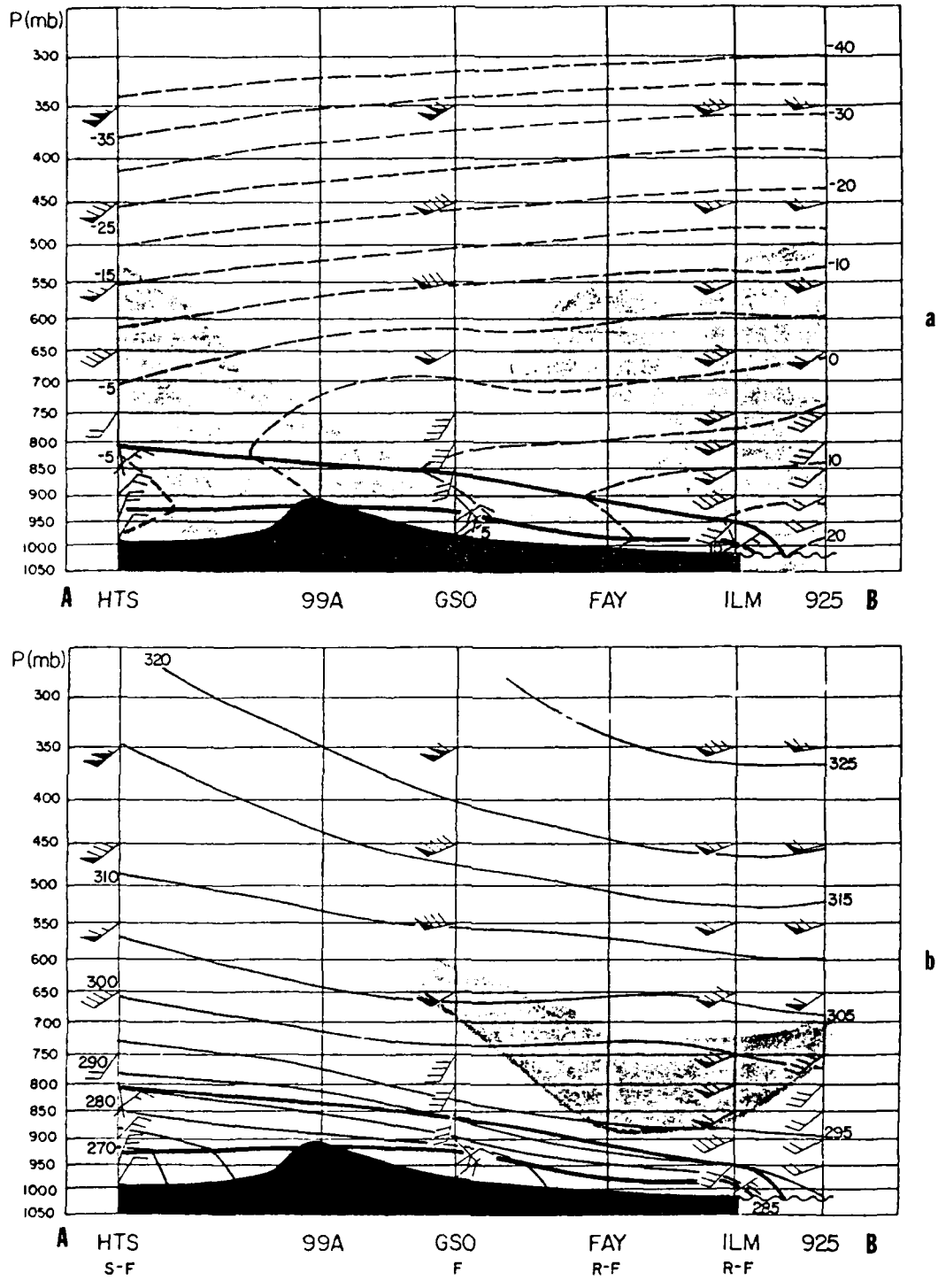

Figure 3.16 (a) Cross-section from Huntington, WV (HTS) to dropwinsonde 925 (see Fig. 3.1a for location) at 0600 GMT 11 February 1986. Dashed lines depict isotherms (^{o}C), shading indicates RH>90%, and wind vectors depicted with pennant=25ms^{-1}, barb=5ms^{-1}, half-barb=2.5ms^{-1}. Heavy solid lines indicate frontal boundaries. (b) Same cross-section as (a), except thin solid lines depict potential temperature (^{o}K) and shading indicates layer of potential instability. Observed weather (99A and 925 not reporting) is indicated below the station identifier.

Charleston, SC (CHS), Myrtle Beach, SC (MYR), Wilmington, NC (ILM), Morehead City, NC (MRH), and Duck, NC (DUK).

Analysis of temperature and relative humidity (RH) greater than or equal to 90% for the A-B cross-section appear in Fig. 3.16a. The frontal inversion is well-defined, and a relatively moist layer exists from the surface to 500 mb from FAY to 925 and over HTS. Potential temperature is analyzed in Fig. 3.16b. Above the stable frontal region, a less stable area of potential instability characterized by an upward decrease of equivalent potential temperature is seen from 925 inland to GSO. Note the stronger wind speeds from 900 mb to 700 mb over ILM compared to the surrounding stations, indicative of the GCB.

Fig. 3.17a depicts temperature and RH analyses along the coastal cross-section from C-D. Above the surface front, the atmosphere is saturated (RH $\geq$ 90%) to 500 mb from MYR to ILM, with a relatively drier layer from 880 mb to 760 mb over CHS and 930 mb to 800 mb over MRH. Wind maxima along the GCB can be seen rising along the cross-section in a 200 mb layer from LHW to ILM. Within this GCB area is a layer of potential instability (Fig. 3.17b), also rising with the GCB northward to ILM. Note that the precipitation falling at these stations is light rain, not showery activity that would be expected to characterize this region effected by the GCB. It is of interest to compare this case to others where layers of potential instability have led to convective precipitation. The goal is to determine why only light precipitation fell in this region.

Marks and Austin (1979) studied wintertime storms in New England to determine the effects of the coastal front on convective activity typical of these extratropical cyclones. Convective instability develops when an area of cool dry mid-tropospheric air overruns a layer of warm moist air moving northward over a warm frontal zone. The influx of the warm moist air is defined by Harrold's (1973) conveyor belt which is the source of moisture for the baroclinic circulation. In one of Marks and Austin's cases, soundings 100-200 km ahead of an approaching storm's warm front revealed a layer of stable warm moist air at 850 mb, approximately 200 mb (2.4 km) thick, corresponding to the conveyor belt. A shallow (50 mb) layer of convectively unstable air was located from 625 mb to 575 mb, at the base of a considerably drier and colder layer of mid-tropospheric origin. Precipitation totals for this case ranged from 20 to 35 mm across a wide area of eastern Massachusetts and Rhode Island. Similar vertical structure and precipitation totals were observed in the seven other cases studied by the authors.

Bosart (1973) suggests that convective activity along quasi-stationary fronts can be triggered when conditional instability is general along and/or across the frontal boundary, and surface convergence is coupled with only weakly favorable divergence aloft. In the

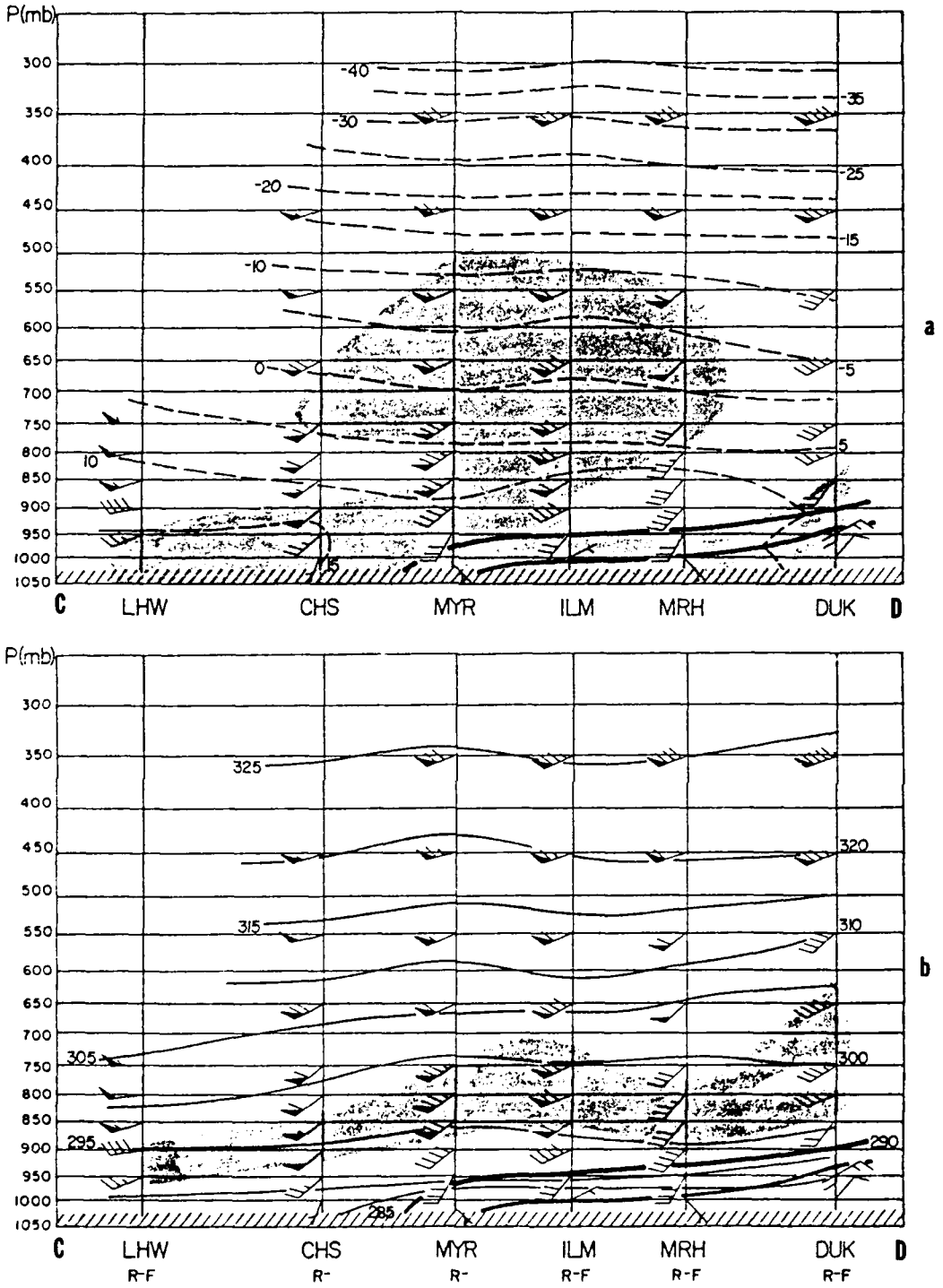

Figure 3.17 (a) and (b) Same as Figs. 3.16 (a) and (b), respectively, except for cross-section C-D.

two cases studied, Bosart found a 70 to 250 mb deep layer of convectively unstable air located parallel to and above the quasi-stationary warm frontal boundary east of a surface low, with relatively drier air above. Where convection produced hourly totals in excess of 8 mm, the convectively unstable layer was deepest, and the mean surface to 500 mb RH ranged from 50 to 70%.

From these findings, it can be concluded that key ingredients for convective activity along a quasi-stationary or warm front east of a surface low are a layer of convectively unstable air (originating in the warm conveyor belt) with relatively dry air above. From both cross-sections (Figs. 3.16 and 3.17) presented for this GALE case, mean surface to 500 mb RH's never decreased below 85%. The atmosphere was uniformly saturated and convective tendencies generated in parcels within the potentially unstable layer could not achieve enough buoyancy for strong convection to develop. Only two stations exhibited RH values less than 70% at 0600 GMT. MRH and DUK recorded values from 60% to 70% in layers from 900 mb to 800 mb and 650 mb to 600 mb, respectively. Note that Figs. 3.13c and 3.15a show the 5 mm precipitation maxima passing through this region, with the most intense radar echoes recorded (VIP 3) centered over eastern North Carolina at 0530 GMT (Fig. 3.13d). MRH recorded 5.3 mm of precipitation for the hour ending at 0600 GMT and DUK recorded 4.8 mm at 0700 GMT.

3.4.5 Divergence and Vertical Velocity Fields

Divergence and vertical velocity analyses across the PAM-II region are presented to examine the relationship of the surface flow field and the precipitation pattern, for the time surrounding the 0600 GMT 11 February observations. The divergence field was calculated using PAM-II wind data averaged over one hour and centered at 0600 GMT. These data were analyzed to grid points by the Barnes objective analysis scheme described earlier. The horizontal divergence is defined by:

$$\delta = \partial u / \partial x + \partial v / \partial y \ ,$$

where u and v are wind components in the x and y grid directions, respectively. The grid distance is about 34 km and centered differences are thus obtained over 68 km. The latter is comparable to the average separation between PAM-II stations. It should be mentioned that the data available to the Barnes program include the GALE buoy network and the

research vessel RVC. These over-water data are crucial to the meaningful computation of meteorological fields along the coast and the near-shore waters.

The vertical velocity field was calculated by vertical integration of the continuity equation (kinematic method) in isobaric coordinates, that is:

$$\omega_U = \omega_L + \bar{\delta}\Delta p .$$

Here, ω_U and ω_L are the vertical velocities at the upper and lower pressure levels Δp (>0) apart. The layer mean divergence δ is obtained as the simple average of the δ at the two levels. The integration commences at the ground level where

$$\omega_L = V_H \bullet \nabla p_S .$$

That is, only the terrain-induced ascent or descent is calculated as the lower boundary condition. The gradient of the terrain pressure (P_S) is determined from a Barnes analysis of U. S. Standard Atmosphere pressure altitudes at several surface stations, PAM-II and buoy locations, plus some bogus points along the crest of the Appalachians. The pressure topography thus obtained realistically represents the terrain over the computation domain.

The Inner GALE Area is gently sloped and the terrain ω is expected to be small. (Note that 1 microbar per second (μbs^{-1}) is approximately equal to 1 cms^{-1} in the lower troposphere.) Divergence and vertical velocity computations are presented at the surface, 970 mb, 850 mb, and 700 mb. The 970 mb level intersects the ground west of GSO, well beyond the western edge of the main body of the PAM-II network.

Divergence patterns superimposed on the 0600 GMT 11 February frontal analysis are presented from the surface to 700 mb in Figs. 3.18a to 3.21a. Similarly, vertical velocity is depicted superimposed on the 0700 GMT precipitation totals in Figs. 3.18b to 3.21b. Two areas of precipitation $\geq$ 5 mm are located over northeastern North Carolina and central South Carolina. Strong convergence in the vicinity of the eastern North Carolina area from the surface to 970 mb becomes divergent flow at 700 mb. Vertical velocities of 3-4 μbs^{-1} at 970 mb over this area slopes southward to the central coastal regions at 850 mb and towards ILM at 700 mb as values increase to 30 μbs^{-1} in the vicinity of the northern extent of the GCB. Divergence and vertical velocity depicted over the South Carolina pocket do not clearly explain the precipitation area at 0700 GMT. Radar

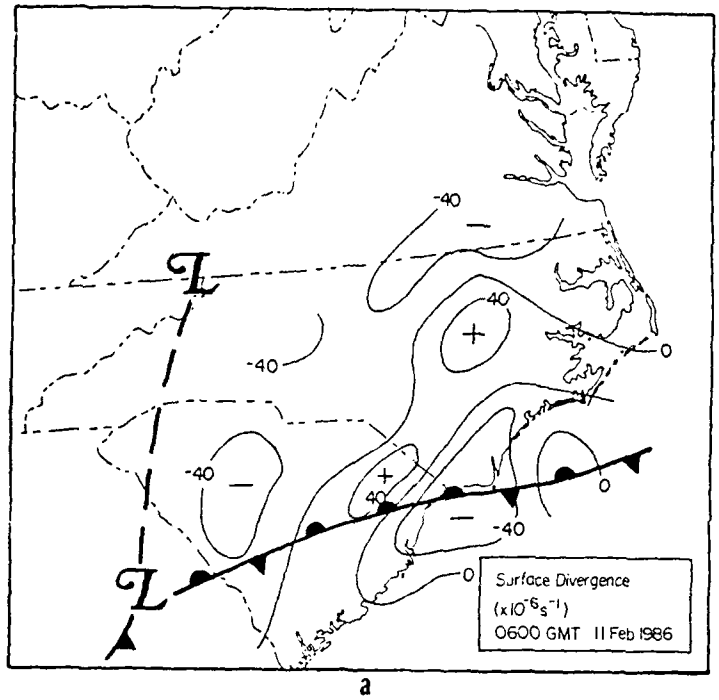

a

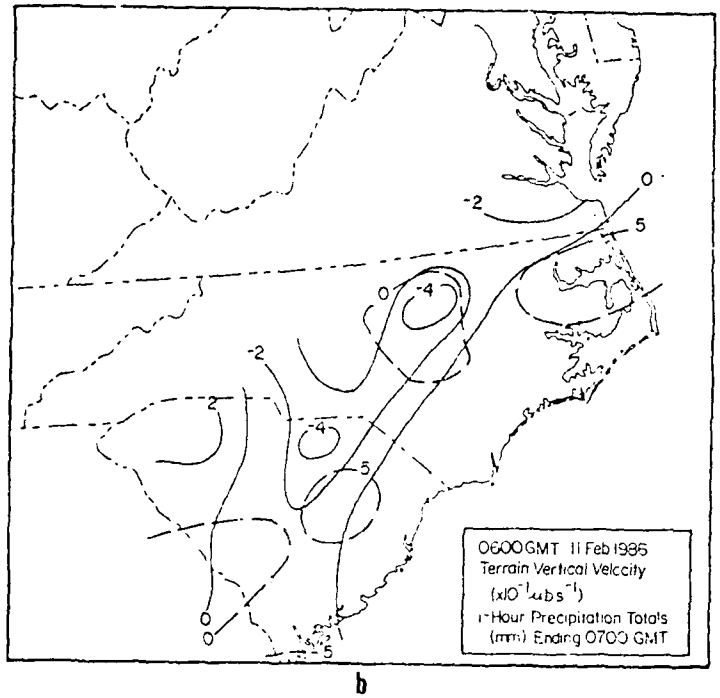

b

Figure 3.18 (a) Analysis of surface divergence using the PAM-II wind data averaged over one hour centered at 0600 GMT 11 February 1986. Divergence analyzed every $40x10^{-6}s^{-1}$. The 0600 GMT surface features are also shown. (b) Analysis of terrain vertical velocity (solid lines) centered at 0600 GMT (analyzed every $2x10^{-1}mbs^{-1}$). Precipitation totals (dashed lines) for the hour ending 0700 GMT analyzed every 5mm.

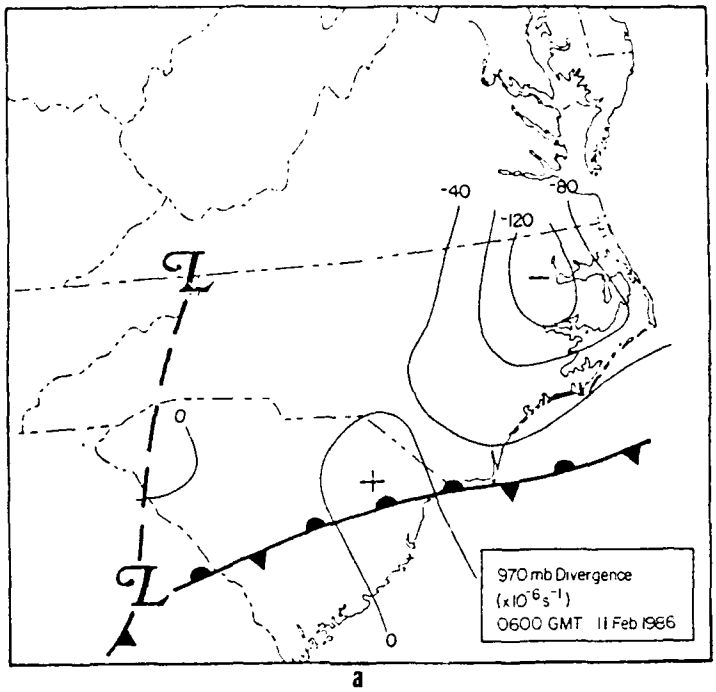

a

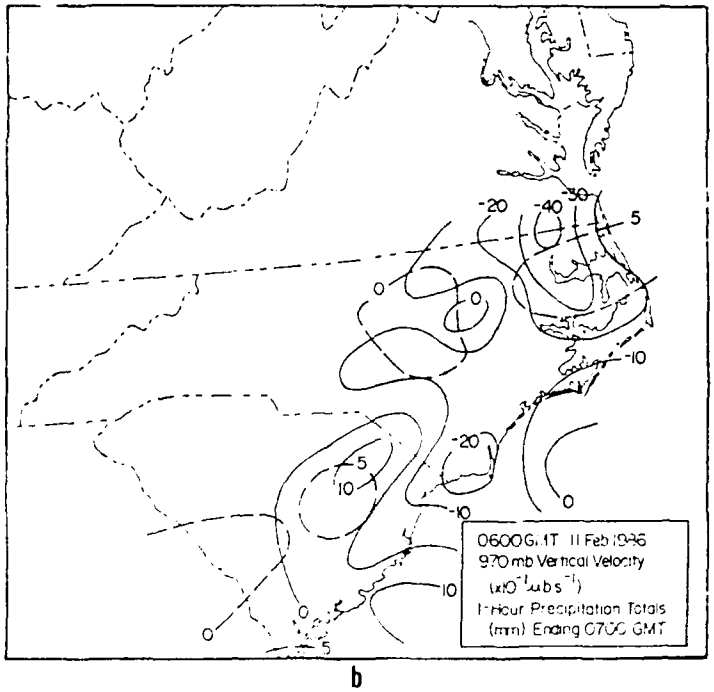

b

Figure 3.19 (a) and (b) Same as Figs. 3.18 (a) and (b), respectively, except for 970-mb (vertical velocity analyzed every $10 \times 10^{-1} \mu bs^{-1}$).

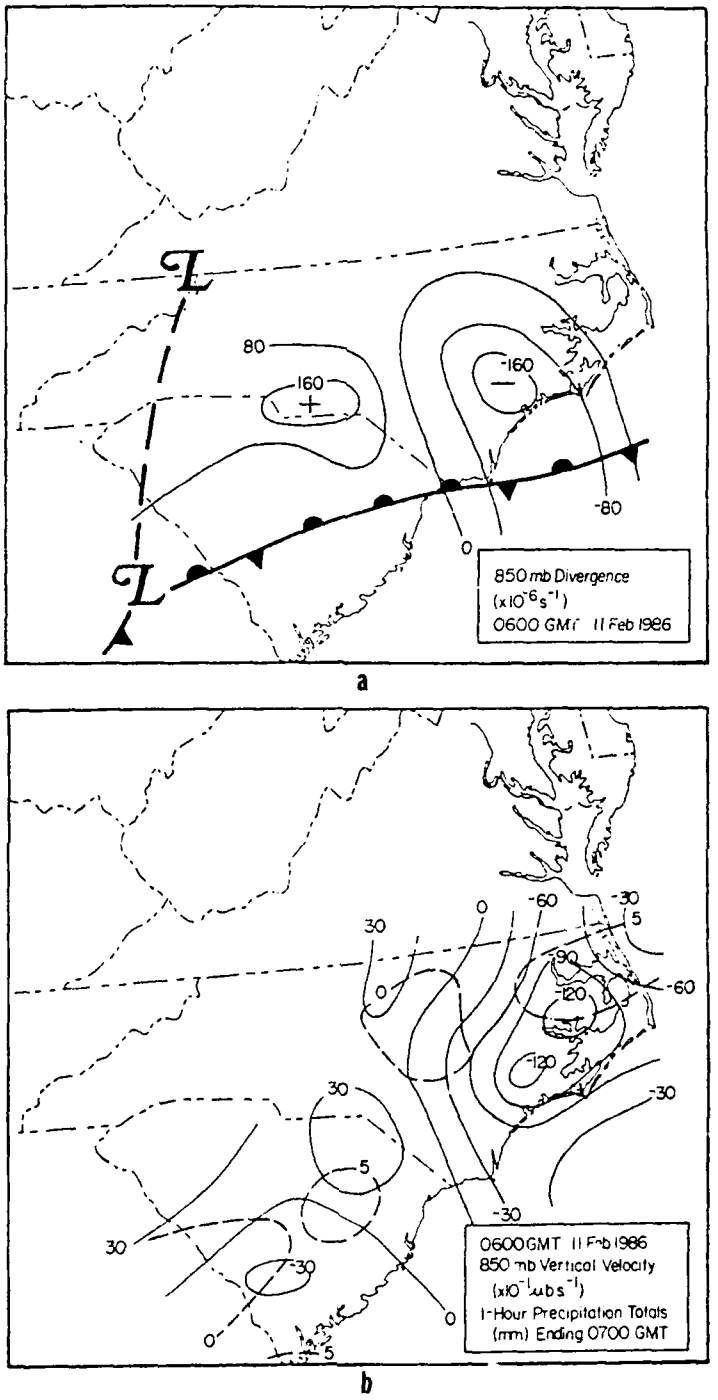

Figure 3.20 (a) and (b) Same as Figs. 3.18 (a) and (b), respectively, except for 850-mb (divergence analyzed every $80 \times 10^{-6} s^{-1}$ and vertical velocity every $30 \times 10^{-1} \mu bs^{-1}$).

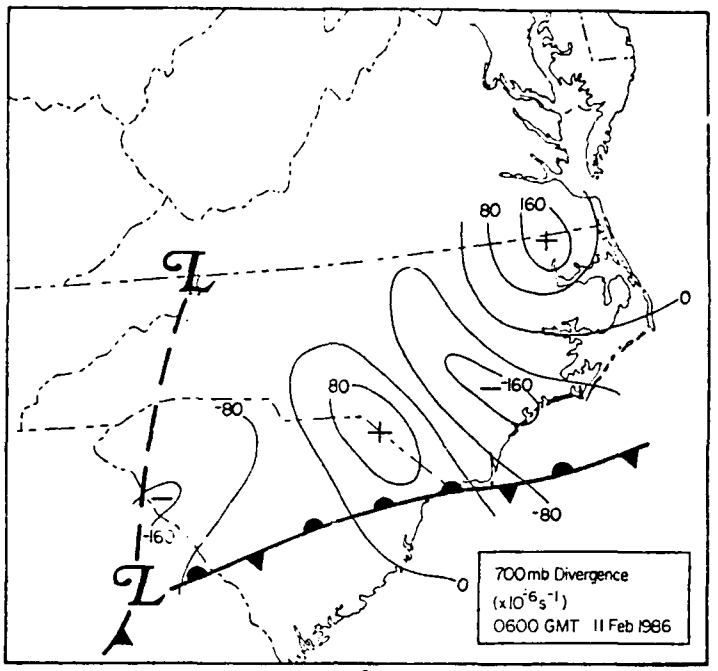

a

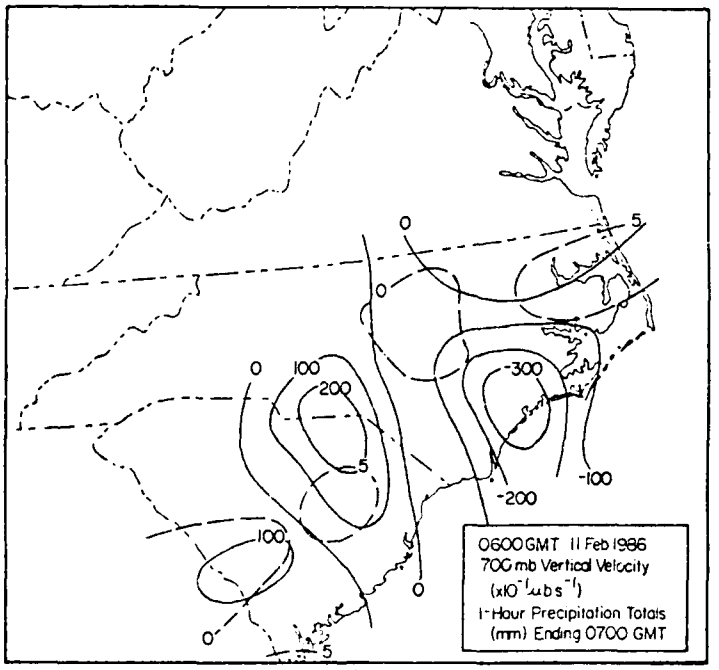

b

Figure 3.21 (a) and (b) Same as Figs. 3.18 (a) and (b), respectively, except for 700-mb (divergence analyzed every $80 \times 10^{-6} s^{-1}$ and vertical velocity every $100 \times 10^{-1} \mu bs^{-1}$).

echoes of VIP 2 at 0530 GMT (Fig 3.13d) imply localized low-level convergence and ascent. However, divergence patterns are relatively neutral to 970 mb and slightly divergent at 850 mb and 700 mb. Descent increases from 1 μbs^{-1} at 970 mb to 20 μbs^{-1} at 700 mb. These values would be expected to hinder the development of any local maxima of precipitation. One possible explanation for the South Carolina precipitation area would be the localized area of ascent from 970 mb to 700 mb over south-central South Carolina. This patch may have advanced to the northeast from 0600 to 0700 GMT, thus providing enough lift to produce the 5 mm precipitation pocket.

One other item of note is the eastward progression of the dry region located in central North Carolina at 0600 GMT (Fig. 3.15a) and advancing eastward to the coast by 0900 GMT. The radar depiction for 0830 GMT (Fig. 3.15d) shows the western edge of precipitation coinciding with the dry area. Vertical motion aloft supports this dry region with weak divergence and even convergence over the region from the surface to 700 mb. Though weak ascent is evidenced at the surface (-.4 μbs^{-1}), descent is seen from 970 mb to 700 mb.

Analysis of divergence and vertical velocity patterns are shown along the two cross-sections (at 0600 GMT 11 February) described earlier in Figs. 3.17 and 3.18. These patterns are derived by extracting values (at points corresponding to cross-section location) from divergence and vertical velocity charts compiled in 50-mb increments from the surface to 700 mb. Convergence and ascent (from jet streak forcing by the GCB) are strongest between ILM and MRH above 800 mb in Fig. 3.22 and between FAY and 925 in Fig. 3.23. Recall that this region is vertically above the northern tip of the GCB. The eastern edge of this area can be placed between ILM and MRH at 0530 (Fig. 3.13d) and east of MRH at 0830 GMT (Fig. 3.15d) where local radar intensities are strongest. It is proposed that the GCB triggerred this weak convective activity advanced to the northeast along the Carolina coast (by 0600 GMT) and eastward off the coast (0900 GMT). Recall that this convection was dampened due to the absence of a dryer layer above the GCB.

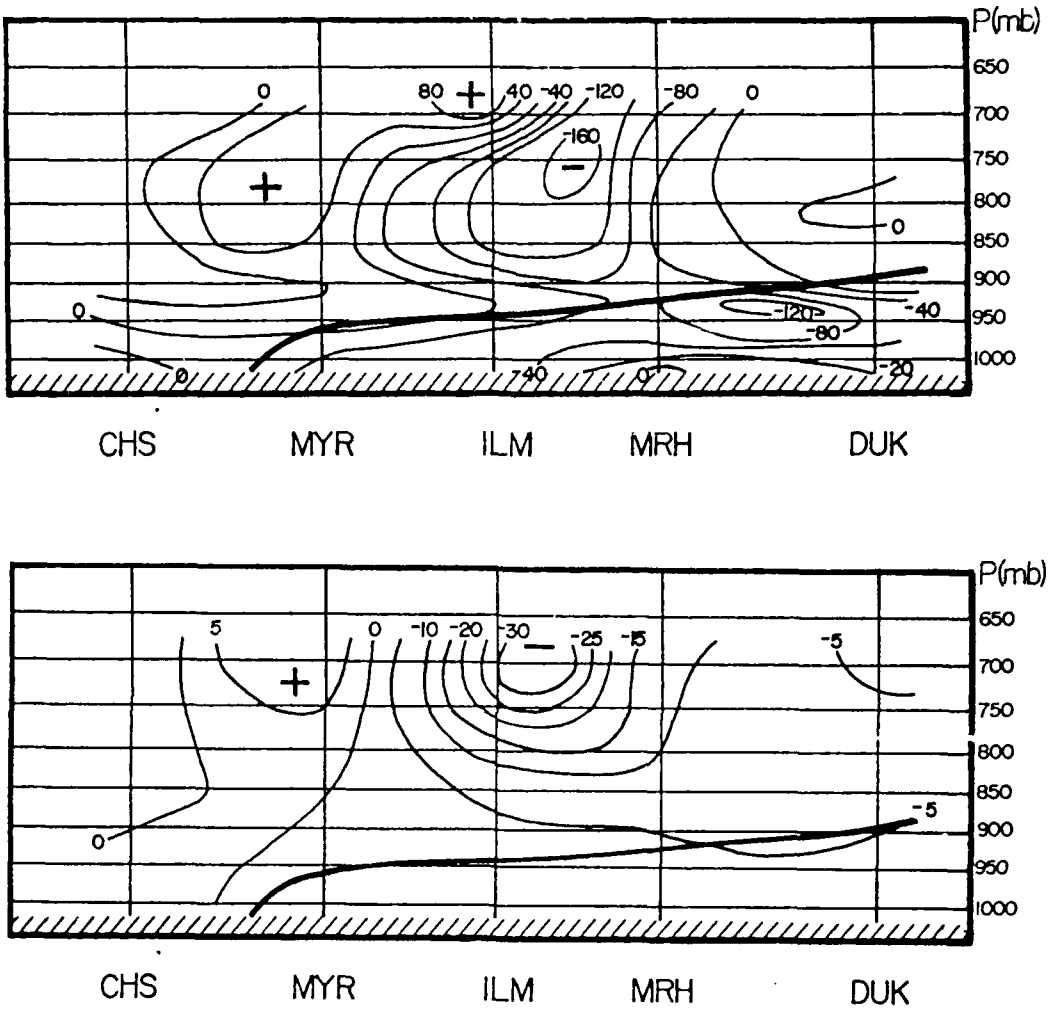

Figure 3.22 (a) Analysis of divergence for the cross-section of Fig. 3.17 from CHS-DUK. Divergence analyzed every $40 \times 10^{-6} s^{-1}$. Top of the frontal layer is shown. (b) Analysis of vertical velocity for the same cross-section as (a). Vertical velocity analyzed every $5 \times 10^{-1} mbs^{-1}$. Top of the frontal layer is shown.

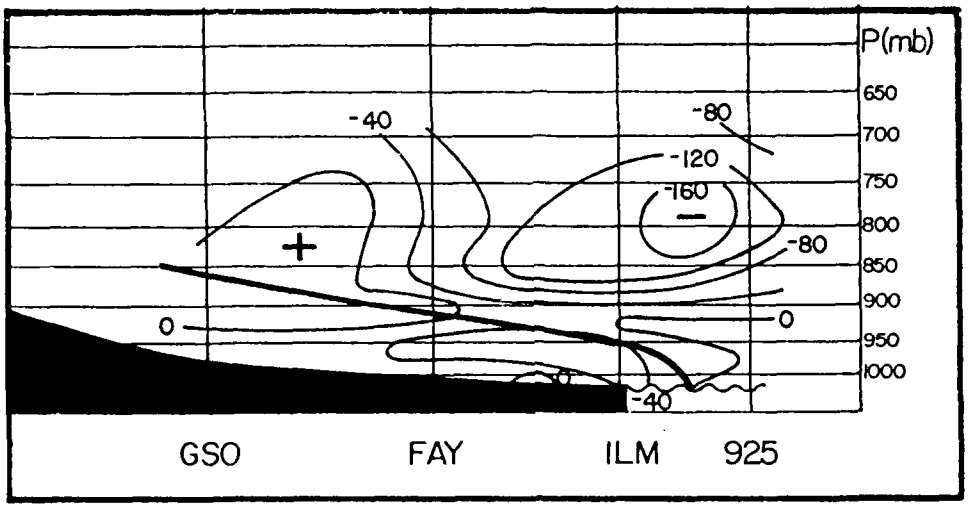

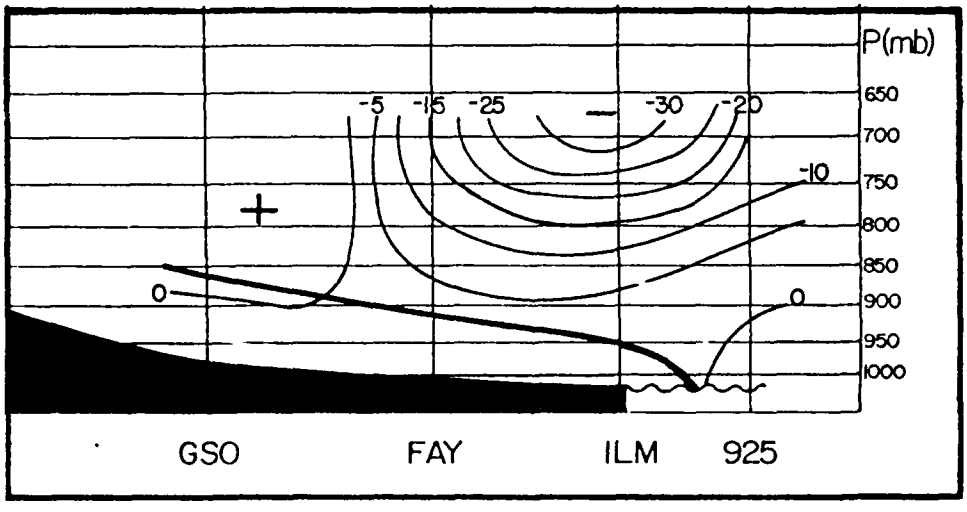

Figure 3.23 (a) and (b) Same as Figs. 3.22 (a) and (b), except for cross-section of Fig. 3.16 from GSO-925.

4. Summary and Conclusions

The evolution of precipitation patterns associated with wintertime lows in the southeast United States has been studied and analyzed with the help of precipitation composite charts. A 24-year climatology of heavy precipitation producing storms reveals general areas of cyclogenesis for these lows consistent with previous research. The Gulf Coast Region contained the most occurrences of cyclogenesis, outnumbering both the Atlantic Coast and Midwest Regions by a two-to-one margin. Only the 66 Gulf Coast Region lows were considered for further study because of the greater confidence in the statistics with the larger sample size.

The southeast U.S. was divided into five geographic regions to assist in following each storm center. Five common storm tracks were discovered, three of which were most dominant. Track A storms traveled from the Gulf of Mexico south of Louisiana, across the Florida panhandle, to the North Carolina coast. Track B storms were tracked from southwest Mississippi to the northeast, remaining west of the Appalachians in central Kentucky. Track C storms followed Track A across northern Florida to the Atlantic, then continued east off the Georgia coast. Pressure, geostrophic relative vorticity, latitude, and longitude at the storm center were recorded at selected locations along each storm's path. The intensity of lows tracking from the Gulf coastal states across northern Florida were found to weaken ($dq/dt<0$) while experiencing deepening ($dp/dt<0$). Maximum deepening rates occurred in Track B when storms traveled from the Gulf coast to northern Alabama.

Hourly Precipitation Data compiled at 316 observation sites across the southeast U.S. were totaled in 6-hour intervals (centered at a storm's observation time). These data were objectively analyzed and contoured. Values were extracted from the contour charts at specified grid points and compiled for all storms plotted in each geographic region along the tracks previously mentioned. Mean precipitation distribution charts and frequency of occurrence charts (for specified precipitation amounts) were compiled to investigate the evolving precipitation fields surrounding lows in Tracks A, B, and C. From the analyses of these fields, the impact of moisture sources (Gulf of Mexico and Atlantic Ocean) and local topography (specifically, the Appalachians) were suggested. The early stages of storms in Tracks A, B, and C drew moisture from the Gulf of Mexico into their warm sectors. As Track A lows crossed the Florida panhandle, a double maximum of precipitation totals in western Florida and eastern Georgia suggested that the Atlantic provided a second moisture source. The frequency of moderate to heavy precipitation was highest northeast of Track A storm centers until lows moved to the North Carolina coast.

The lack of precipitation data over the ocean were reflected in results from Tracks A and C.

While Track B storms experienced a gradual decrease in precipitation totals as they advanced further north, areas of light precipitation continued to cover most of the southeast United States. As lows in this track moved into Tennessee and Kentucky, upslope flow along the western Appalachians maximized precipitation totals and frequencies of occurrence between the storm centers and the mountains. These maxima were also found to exist to the lee side of the mountains. This may be explained by Atlantic moisture from Miller's (1946) Type B cyclones which developed along the Atlantic coast. These coastal storms force moist (upslope) flow north and west from the Atlantic towards the Appalachians. The central Gulf coast area tended to receive the most precipitation from Track C lows.

The three precipitation variables (maximum reported value, areal coverage, and areal totals for the 6-hour time periods) were compiled and averaged for all 66 lows studied (including those in Tracks D and E). Maximum reported totals were greatest for all storms when tracked from the northeastern Gulf of Mexico to northern Alabama, and for Track B lows across the Gulf coastal regions northward into Tennessee. Areal precipitation coverage and storm totals maximized again for Track B lows as they moved from the Gulf coast into Tennessee and West Virginia.

Multiple linear regression equations were compiled to determine which of the observed independent variables significantly affected the three precipitation variables. Longitude, pressure, and vorticity recorded at cyclone centers were found to be most significant. Decreasing central pressure and higher (more western) longitude values tended to correlate positively with higher precipitation amounts. However, higher surface vorticity values did not necessarily result in this same increase in precipitation. Storm latitude was not a significant factor often enough to draw conclusions about its relationship with precipitation.

The locations of reported 6-hour maximum precipitation totals (over land) were recorded with respect to all storm centers and compiled by geographic region. Moderate to heavy precipitation totals appeared north and east of storm centers along the Gulf coast, shifting to the southeast as systems traveled north (west of the Appalachians as in Track B). A possible explanation for this is a weakening of the Gulf of Mexico moisture flow pattern the further north the storms traveled. For lows tracking to the Atlantic coast, maximum amounts were found north and west of storm centers where it is likely that the heaviest precipitation occurred off the coast where no data were available.

Storm track speeds and 6-hour precipitation totals were combined in each

geographic region to reveal total precipitation distributions along Tracks A, B, and C. Track B cyclones produced the heaviest precipitation totals across Mississippi, Alabama, and northern Georgia. Precipitation totals in Track C exceeded those in Track A, and the Gulf of Mexico as a moisture source for all storms was found to be strongest from the Gulf coast northward to the southern Tennessee and North Carolina border.

Based on the climatology, the following conclusions can be drawn for winter storms in the southeast United States:

1) Most heavy precipitation producing storms form in the Gulf coastal regions and travel east-northeastward to the Atlantic coast.

2) The Gulf of Mexico provides most of the moisture supply for all storms tracking across the southeast United States, and heaviest totals over land are located north and east of the storm center in most cases.

3) Storms tracking west of the Appalachians tend to produce heavier precipitation totals (over land) across wider areas than those which track south and east of the mountains to the Atlantic coast.

4) The role of the Atlantic ocean as a moisture source is limited until storms start moving up the Atlantic coast.

5) The Appalachian Mountains tend to locally enhance precipitation from all storms, whether located west or east of the mountains (assuming that Miller's Type B cyclones develop).

6) Decreasing central storm pressure and higher longitude tend to correlate positively with precipitation totals for all storms. However, increasing vorticity correlates with decreasing precipitation for those lows traveling south and east of the Appalachians.

The GALE case study (IOP 5, 10-11 February 1986) provided a detailed look at the mesoscale precipitation distribution around a surface low similar in path to those of Track A in the climatology. In this case, a surface low developed over central Alabama at 0000 GMT 11 February and traveled rapidly east-northeastward into eastern North Carolina. Precipitation in the vicinity of the storm center and a quasi-stationary front east of the center consisted of light rain and fog throughout central Alabama, Georgia, and the Carolinas. Heavier convective activity remained well south of the storm center and the west-to-east frontal boundary. An attempt was made to explain why heavier precipitation remained south of the Carolinas when the storm center tracked through the heart of the PAM-II network.

Analysis of the 300°K surface revealed the existence of a low-level jet streak in excess of 35 ms^{-1}, originating along the Gulf coast and moving rapidly through central Georgia and the Carolinas (over the frontal region) to off the coast in just six hours. Along the axis of this jet streak was a tongue of relatively higher mixing ratios originating over the Gulf coastal states, adding evidence to the assumption that this was a moist (Gulf of Mexico) conveyor belt (GCB). Vertical cross-sections perpendicular and parallel to the GCB axis through the Carolinas revealed these winds and relative humidity maxima in a 200 mb layer rising above the top of the surface frontal boundary from eastern Georgia to the central North Carolina coast.

Within the GCB was a layer of potential instability rising towards station ILM. However, only light precipitation fell in this region along the coast, not convective precipitation usually responsible for more significant totals. Research by Marks and Austin (1979) and Bosart (1973) conclude that locally heavy convective activity along a quasi-stationary or warm front east of a surface low is dependent upon the presence of a layer of potential instability (aligned along the warm conveyor belt axis) and a relatively dry layer above. In this GALE case, most of the coastal Carolinas reported a uniformly saturated layer from the surface to 500 mb, thus hindering convective development from the potentially unstable layer. Only two stations reported relative humidity values less than 70% aloft (in shallow layers) above the GCB at 0600 GMT 11 February. Areas surrounding these locations recorded localized maxima in precipitation totals during the subsequent few hours. Radar observations confirmed this development of weak convective activity. Lower tropospheric divergence and vertical velocity fields across the inner GALE region further supported these findings.

The GALE case study led to the following conclusions for this storm:

1) The GCB supplied much of the moisture for the warm sector precipitation maximum.

2) Heavier precipitation totals depended on the combined presence of the GCB, a layer of convectively unstable air traveling with the GCB, and a relatively drier layer vertically above the GCB.

3) Precipitation totals for this case may also have been limited by the relatively higher speed of the surface low center as it traveled through the Carolinas (approximately 80 km/hr compared to a mean speed of 55 km/hr for storms in Track A). The GCB traveled with the speed of the surface storm and frontal systems, thus the moisture and potential instability had relatively little time to produce locally heavy precipitation amounts.

Appendix 1

List of surface low pressure systems included in the climatology:

YEAR	LOW #	TRACK	DATE(S)
1960	1	A	17-19 JAN
	2	A	13-14 FEB
1961	3	A	6-9 FEB
	4	B	21-22 FEB
	5	B	24-26 FEB
	6	C	30-31 MAR
1962	7	A	1-2 JAN
	8	B	5-6 JAN
	9	C	27-28 JAN
1963	10	A	18-20 FEB
	11	D	1-2 MAR
1964	12	C	16-17 JAN
	13	A	5-7 FEB
	14	A	18-19 FEB
	15	B	2-3 MAR
1965	16	B	24-25 FEB
	17	A	2-3 MAR
1966	18	A	5-6 JAN
	19	A	15-16 JAN
	20	A	25-27 JAN
	21	D	12-13 FEB
1967	(NONE)		
1968	22	C	10 JAN
	23	A	28-29 FEB
	25	D	11-13 MAR
	26	E	22-23 MAR
1969	27	A	14-17 FEB
	28	A	6-7 MAR
	29	E	16-19 MAR
1970	30	A	6-7 JAN
	31	A	17-18 FEB
	32	C	8-9 MAR
	33	A	21-23 MAR
1971	34	A	8-9 JAN
	35	A	8-9 FEB
	36	E	2-4 MAR

APPENDIX 1 (continued)

YEAR	LOW #	TRACK	DATE(S)
1972	37	A	1-2 FEB
1973	38	A	28-29 JAN
	39	A	9-11 FEB
	40	B	16-17 MAR
1974	41	A	15-17 FEB
	42	E	29-31 MAR
1975	43	E	13-14 MAR
1976	(NONE)		
1977	44	B	9-10 JAN
1978	45	A	12-14 JAN
	46	A	19-20 JAN
	47	B	25-26 JAN
	48	C	3-4 MAR
1979	49	B	1 JAN
	50	A	12-14 JAN
	51	B	20-21 JAN
	52	B	24-26 FEB
1980	53	E	22-23 JAN
1981	54	A	23 MAR
1982	55	D	3-4 FEB
	56	D	18-19 FEB
	57	C	26-27 FEB
	58	A	6-8 MAR
1983	59	A	2-3 JAN
	60	B	20-22 JAN
	61	C	21-22 JAN
	62	C	5-6 FEB
	63	A	10-11 FEB
	64	A	13-15 FEB
	65	A	1-2 MAR
	66	A	16-19 MAR

Appendix 2

Independent and dependent variables for surface lows included in the climatology:

LOW #	REGION	LATITUDE (°N)	LONGITUDE (°W)	PRESSURE (mb)	VORTICITY ($\times 10^{5} s^{-1}$)	6-HOUR MAX PRECIP RECORDED (mm)	AREA OF COVERAGE (# of grid pts.)	TOTAL 6-HR PRECIP (mm)
1	1	30.5	91.5	1009	9.1	38	79	547
	2	31	86	1010	9.1	19	46	177
	3	32	81.5	1011	11.8	18	54	167
	5	36	75.5	1006	2.7	4	30	59
2	2	27.5	87.5	996	43	38	86	795
	3	31.5	81.5	996	29.7	34	78	531
	5	36	76	995	22	12	61	247
3	1	28	91	1014	8.5	23	31	224
	2	28.5	86	1009	17.5	24	34	145
	3	30	80	1014	7.1	54	105	713
	5	35	76	1002	29.3	25	45	270
4	1	31.5	91	1013	7.2	75	61	628
	4	37.5	88	1005	18.4	39	73	579
5	1	32	91.5	1005	22.5	85	71	890
	2	34.5	87.5	1001	23	69	92	831
	4	37.5	84	985	42.5	28	119	801
6	1	32	91	1002	8.6	76	78	852
	2	33	87	997	11.5	63	102	1072
7	3	31.5	80.5	1010	25	27	52	340
	5	35.5	75	992	45.7	1	5	5
8	1	32	91	1006	29.8	25	92	552
	2	33	87	1003	22.6	90	130	1019
	4	36	83.5	1000	19.7	40	142	1130
9	1	30.5	90.5	1013	11.3	36	89	452
	2	32.5	86	1009	24	38	76	497
	3	32.5	82	1007	22	30	55	364
10	1	29	91	1002	30.1	49	50	652
	2	32	86	1001	20	37	98	851
	3	33	83	1001	20.8	36	99	801
	5	35.5	76.5	996	31.8	20	57	310
11	1	34	91	1005	27.1	22	71	411
	4	36.5	85	1001	21.2	25	114	618
	5	38	77	1001	12.6	8	33	69

LOW #	REGION	LATITUDE (°N)	LONGITUDE (°W)	PRESSURE (mb)	VORTICITY ($\times 10^5 s^{-1}$)	6-HOUR MAX PRECIP RECORDED (mm)	AREA OF COVERAGE (# of grid pts.)	TOTAL 6-HR. PRECIP (mm)
12	1	28.5	92	1004	35.9	36	39	257
	2	29.5	85	1002	36.9	24	55	289
	3	31	79	1005	23.9	20	44	203
13	1	29	91	1001	22.6	39	58	460
	2	29	86	1003	0.3	28	104	672
	3	32	82	999	12.4	35	123	962
	5	36	76	990	31.4	25	67	498
14	1	29	90	1001	28.9	30	77	863
	2	30.5	86	1001	14.5	55	94	1173
	3	32.5	82.5	998	19.9	44	102	921
	5	36	83	990	29.1	20	80	335
15	1	32	91	1005	21.8	78	72	1223
	2	34	87.5	1004	12.6	61	98	728
	4	37.5	83	1007	10	38	64	288
16	1	33.5	89	997	31.8	40	113	627
	2	34.5	87.5	990	42.1	36	124	916
	4	38	85	983	45.6	32	148	1040
17	1	28	90	1001	19.2	54	105	731
	2	31	86	1002	14.8	42	92	692
	3	33	79	1002	22	23	53	343
	5	33.5	72.5	1006	26.8	4	13	17
18	1	28.5	90	1014	7.5	31	97	735
	2	30.5	86	1014	9.1	31	120	814
	3	32.5	82	1013	7.3	38	86	490
	5	36.5	77	1005	23.5	27	79	363
19	2	29	86	997	43.9	35	54	494
	3	32	79	999	24.7	22	49	330
	5	34	73.5	996	34.8	13	35	127
20	2	27.5	85	1004	42	41	59	530
	3	30	79	1007	20.2	30	73	458
	5	35	74	984	63.1	24	45	204
21	1	31	91	1002	28.5	51	97	788
	2	34	86.5	998	25.8	54	97	1012
	4	36.5	83	986	37.5	58	117	1090
	5	38	78.5	986	28.5	23	73	447
22	1	30	91	1015	20.3	30	94	475
	2	31	86	1014	17.1	23	79	475

LOW #	REGION	LATITUDE (°N)	LONGITUDE (°W)	PRESSURE (mb)	VORTICITY ($x10^5 s^{-1}$)	6-HOUR MAX PRECIP RECORDED (mm)	AREA OF COVERAGE (# of grid pts.)	TOTAL 6-HR PRECIP (mm)
23	1	32	91	1012	14.2	20	34	150
	2	32	85.5	1004	29.8	20	53	176
	3	33	81	1003	19.5	10	42	124
	5	34.5	74.5	996	37.9	2	7	8
24	1	31	91	1004	32.7	22	60	395
	2	31.5	86	1002	32.7	23	67	291
	3	32.5	81.5	997	36.5	21	65	311
	5	35.5	74.5	987	43.6	17	78	274
25	1	32	92.5	994	44.7	61	96	936
	4	35.5	85	994	30.9	26	135	702
	5	37	76.5	995	17.8	25	57	254
26	2	32	86	1009	29.1	21	74	425
	5	37	79	1002	28.5	21	81	371
27	1	27.5	90.5	1000	46.9	28	70	403
	2	28.5	86	1002	30.1	58	74	6.52
	3	31	79	1002	29.6	17	61	150
	5	33.5	72.5	990	48.7	7	15	32
28	2	28	85.5	998	18.7	38	100	1024
	3	31.5	80.5	992	39.4	36	90	685
	5	35	76	986	26.5	36	58	442
29	1	27	90	1010	19.4	67	72	635
	2	33	86	1004	17.8	28	64	448
	5	35	77	998	30.3	29	30	152
30	1	27	90	1006	28.3	28	95	565
	2	28	86	1002	31.5	45	113	832
	3	32	80	1000	34.9	69	85	502
	5	35	75	992	47.4	6	39	85
31	3	31	80.5	1011	17.1	21	42	209
	5	33.5	72.5	1004	28.8	1	1	1
32	2	27	84	1000	35.3	41	36	344
	3	30	79	995	27.8	36	34	276
33	1	27.5	89	1006	29.5	45	83	657
	2	30.5	85.5	1006	16.7	36	79	511
	3	33	83	1004	14.6	44	75	646
	5	36	76.5	1000	22.7	15	37	92
37	1	28	91	1004	22.8	41	34	201
	2	29.5	85.5	1005	17.5	58	70	679
	3	31	80	1005	20.9	34	73	566
	5	35	75.5	999	44.6	36	36	207

LOW #	REGION	LATITUDE (°N)	LONGITUDE (°W)	PRESSURE (mb)	VORTICITY ($\times 10^{5} s^{-1}$)	6-HOUR MAX PRECIP RECORDED (mm)	AREA OF COVERAGE (# of grid pts.)	TOTAL 6-HR PRECIP (mm)
38	2	30.5	86	1006	20.5	49	92	927
	3	32	82	1005	15.7	30	101	463
	5	35.5	76	995	23.6	18	66	326
39	1	27	89	1007	19.7	16	46	219
	2	27.5	86	1002	20.1	35	43	390
	3	30	79	1000	27.5	26	50	267
	5	33.5	73	984	71.2	2	10	12
40	1	32.5	90.5	1003	18.8	93	98	998
	2	34.5	87.5	1001	18.6	69	120	1008
	4	37	84.5	995	20.1	76	123	882
41	1	31	91	1011	14.4	33	67	437
	2	32.5	85.5	1008	14.6	38	75	583
	3	33	82.5	1005	18.8	22	60	331
	5	35.5	76	983	60	17	15	56
42	5	36	76	995	31.8	22	88	387
43	1	30	90.5	1005	21	78	92	913
	2	32.5	87	1000	27.2	60	99	1216
	5	37.5	79	1002	25.1	28	91	535
44	1	30.5	91.5	1000	35.3	51	99	842
	2	34.5	88	998	25.6	36	113	841
	4	37.5	84.5	999	23.4	46	121	677
45	1	29	91	1014	19.7	13	72	164
	2	30	86	1011	10.7	28	100	393
	3	31.5	81	1007	17.5	23	84	473
	5	35.5	75.5	998	23.6	27	45	284
46	2	30.5	86	1004	29.6	64	91	911
	3	32.5	82.5	1001	20.9	79	100	957
	5	36	76	1000	28.2	13	73	303
47	1	32	91	1002	16.4	51	133	924
	2	33	86.5	994	15.7	13	74	297
	4	38	82.5	972	44.3	61	123	1161
48	1	28.5	91	1002	20.5	23	139	689
	2	29.5	86	1002	15.9	64	116	706
	3	30.5	79.5	995	21.6	42	32	253
49	2	34.5	83	1011	20.9	38	136	2742
	4	37.5	85	1011	18.4	55	125	780

LOW #	REGION	LATITUDE (°N)	LONGITUDE (°W)	PRESSURE (mb)	VORTICITY ($\times 10^{5} s^{-1}$)	6-HOUR MAX PRECIP RECORDED(mm)	AREA OF COVERAGE (# of grid pts.)	TOTAL 6-HR PRECIP (mm)
50	2	29	85.5	1006	16.3	20	73	340
	3	31.5	81	1008	12.4	22	80	247
	5	36	76.5	1004	12.4	10	89	202
51	1	31.5	91	996	10.9	58	130	988
	2	33	86.5	988	24	66	150	1584
	4	36.5	82.5	981	18.3	28	74	480
52	1	31	91	1008	14.8	20	34	315
	2	34.5	87.5	1000	37.9	51	85	504
	4	37	82	1000	17.4	26	84	730
53	1	31	91	1012	6.9	25	50	269
	2	33	87	1007	16.4	41	94	887
	5	35.5	76	997	12.7	41	52	435
54	5	23.5	74	988	37.8	5	5	6
55	2	35	88	1011	14.2	78	131	1373
	4	37	84	1010	18.3	46	126	831
	5	36	75.5	1009	19.1	5	60	111
56	1	32	92	1007	17.5	8	49	84
	4	36	86	1013	13.6	8	26	45
	5	37	76.5	1009	9.9	4	8	17
57	1	29	91	1014	21.3	23	85	509
	2	30	88	1014	21.5	18	94	432
58	1	29.5	90.5	1010	9.5	78	43	518
	2	31	86	1006	9.1	30	76	538
	3	32.5	83.5	1001	19.9	20	103	566
	5	35	76	1001	19	29	41	214
59	1	28.5	89	1016	10	31	58	322
	2	30	86	1014	12.8	34	60	291
	3	32	81.5	1014	6.5	23	44	124
	5	34	75.5	1009	20.9	2	5	6
60	1	30	89.5	999	39.4	23	78	365
	4	39	91	1010	8.8	5	37	104
61	2	28	84	1007	12.1	74	77	562
	3	29.5	79	1010	8.3	13	92	275
62	1	30	91	1009	15.5	42	83	479
	2	30.5	86	1007	21.3	20	101	462
	3	30.5	81	1006	19.4	28	45	191

LOW #	REGION	LATITUDE (°N)	LONGITUDE (°W)	PRESSURE (mb)	VORTICITY ($\times 10^{5} s^{-1}$)	6-HOUR MAX PRECIP RECORDED (mm)	AREA OF COVERAGE (# of grid pts.)	TOTAL 6-HR PRECIP (mm)
63	1	29	89	1000	28.9	25	54	315
	2	31	86	1002	15.6	30	97	633
	3	32.5	82	1003	17.8	74	64	522
	5	35	75.5	1001	37.9	74	36	391
64	3	30	81	1003	34.6	33	49	494
	5	34.5	76.5	996	33.2	20	36	214
65	5	34.5	75.5	991	27.2	12	22	93
66	1	28	91	990	15.2	19	53	225
	2	29	85.5	983	47.7	69	57	533
	3	31	80.5	990	21.7	23	101	536
	5	36	78	990	21.5	23	70	314

References

Austin, P. M. and R. A. Houze, Jr., 1972: Analysis of the structure of precipitation patterns in New England. J. Appl. Meteor., 11, 926-935.

Barnes, S. L., 1964: A technique for maximizing details in numerical weather map analysis. J. Appl. Meteor., 3, 396-409.

_____, 1973: Mesoscale objective analysis using weighted time-series observations. NOAA Technical Memorandum, ERL NSSL-62, Norman, OK., 60 pp.

Blevins, R. D., 1985: On the Evolution of Precipitation Associated with a Wintertime East Coast Cyclone - A GALE Preliminary Study. Masters Thesis, North Carolina State University. Raleigh, 104 pp.

Bosart, L. F., 1973: Detailed analyses of precipitation patterns associated with mesoscale features accompanying U.S. east coast cyclogenesis. Mon. Wea. Rev., 101, 1-12.

Browning, K. A., 1986: Conceptual models of precipitation systems. Wea. and Forecasting, 1, 23-41.

_____ and T. W. Harrold, 1969: Air motion and precipitation growth in a wave depression. Quart. J. Roy. Meteor. Soc., 95, 288-309.

_____ and C.W. Pardoe, 1973: Structure of low-level jet streams ahead of mid-latitude cold fronts. Quart. J. Roy. Meteor. Soc., 99, 619-638.

Carlson, T. N., 1980: Airflow through mid-latitude cyclones and the comma cloud pattern. Mon. Wea. Rev., 108, 1498-1509.

Climatological Data, National Summary, January, February, and March, 1960-1980: NOAA/EDIS, U.S. Department of Commerce.

Colucci, S. J., 1976: Winter cyclone frequencies over the eastern United States and adjacent western Atlantic. Bull. Amer. Meteor. Soc., 57, 548-553.

Dirks, R. A.; J. P. Kuettner; and J. A. Moore, 1988: Genesis of Atlantic Lows Experiment (GALE): An Overview. Bull. Amer. Meteor. Soc., 69, 148-160.

Harrold, T. W., 1973: Mechanisms influencing the distribution of precipitation within baroclinic disturbances. Quart. J. Roy. Meteor. Soc., 99, 232-251.

_____ and P. M. Austin, 1974: Structure of precipitation systems: a review, Journal de Researches Atmospheriques, 8, 41-53.

Houze, R. A.; P. V. Hobbs; K. R. Biswas; and W. M. Davis, 1976: Mesoscale rainbands in extratropical cyclones. Mon. Wea. Rev., 104, 868-878.

Jorgensen, D. L., 1967: A computer derived synoptic climatology of precipitation from winter storms. J. Appl. Meteor., 6, 226-234.

_____; W. H. Klein; and A. F. Korte, 1967: A synoptic climatology of winter precipitation from 700-mb lows for Intermountain areas of the West. J. Appl. Meteor., 6, 782-790.

Klein, W. H.; D. L. Jorgensen; and A. F. Korte, 1968: Relation between upper-air lows and winter precipitation in the western plateau states. Mon. Wea. Rev., 96, 162-168.

Korte, A. F.; D. L. Jorgensen; and W. H. Klein, Aug 1972: Synoptic climatological studies of precipitation in the plateau states from 850-, 700-, and 500- mb lows during spring. NOAA Technical Memorandum, NWS TDL-48, 130 pp.

Langs, N. A., 1986: Dynamic Climatology of Cyclones Over Eastern North Carolina: Regions of Mobile Cyclone Activity. Masters Thesis, North Carolina State Univesity. Raleigh, 101 pp.

Mariners Weather Log January, February, and March, 1981-1983: NOAA/EDIS, U. S. Department of Commerce.

Martin, D. N., 1986: Dynamic Climatology of Cyclones Over Eastern North America. Masters Thesis, North Carolina State University. Raleigh, 114 pp.

F. D. Marks, Jr. and P. M. Austin, 1979: Effects of the New England Coastal Front on the Distribution of Precipitation. Mon. Wea. Rev., 107, 53-67.

Miller, J. E., 1946: Cyclogenesis in the Atlantic coastal region of the United States. J. Meteor., 3, 31-44.

_____, 1955: Intensification of precipitation by differential advection. J. Meteor., 12, 472-477.

National Climatic Data Summary, January, February, and March, 1960-1980: NOAA/NESDIS, U. S. Department of Commerce.

Petterssen, S.; D. L. Bradbury; and K. Pedersen, 1962: The Norwegian cyclone models in relation to heat and cold sources. Geophysical Publications, Geophysica Norvegica, 24, 243-280.

Reitan, C.H., 1979: Trends in the frequencies of cyclone activity over North America. Mon. Wea. Rev., 107, 1684-1688.

Tasaka, I., 1980: Distribution of precipitation caused by passages of lows in winter in Japan, Tohoku University Science Reports, 7th Series, Geography, Vol. 30, 133-146.

Whittaker, L. M. and L. H. Horn, 1981: Geographical and seasonal distribution of North America cyclogenesis, 1958-1977. Mon. Wea. Rev., 109, 2312-2322.

Zishka, K. M. and P. J. Smith, 1980: Climatology of cyclones and anticyclones over North America and surrounding ocean environs for January and July, 1950-1977, Mon. Wea. Rev., 108, 387-401.

Zurndorfer, E. A. and R. J. Bermowitz, 1976: Determination of an optimum number of predictors for probability of precipitation amount forecasting. TDL Office Note 76-17, National Weather Service, National Oceanic and Atmospheric Administration, Department of Commerce, 7pp.